The formation of OH radicals from Criegee intermediates: a LIF-FAGE study from laboratory to ambient

Dissertation

zur Erlangung des Grades

„Doktor der Naturwissenschaften“

im Promotionsfach: Chemie

am Fachbereich Chemie, Pharmazie und Geowissenschaften

der Johannes Gutenberg-Universität

in Mainz

Anna Novelli

geb. in Torino

Mainz, 2015

Dekan:

1. Berichterstatter:
2. Berichterstatter:

Tag der mündlichen Prüfung: 28th of April 2015

D77

Zusammenfassung

Das Hydroxyl Radikal ist, auf globalem Maßstab, das bedeutendste Oxidant in der Atmosphäre. Es initiiert den Abbauprozess vieler, teilweise schädlicher, Spurengase und insbesondere den von flüchtigen Kohlenwasserstoffen (VOC). Die OH Konzentration ist somit ein gutes Maß für die augenblickliche Selbstreinigungskapazität der Atmosphäre. Messungen zu nächtlicher Zeit mit LIF-FAGE-Instrumenten *(engl.: laser-induced fluorescence - fluorescence assay by gas expansion)* haben Konzentrationen des Hydroxylradikals (OH) ergeben, die signifikant höher waren, als sich mit der bekannten Chemie erklären ließ. Um herauszufinden, ob ein solches Signal wirklich atmosphärisches OH ist oder von einer störenden Spezies stammt, die im Messinstrument OH produziert, wurde das LIF-FAGE-Instrument des Max-Planck-Instituts für Chemie (MPIC) im Rahmen dieser Doktorarbeit modifiziert und getestet. Dazu wurde ein so genannter Inlet Pre-Injector (IPI) entwickelt, mit dem in regelmäßigen Abständen ein OH-Fänger in die Umgebungsluft abgegeben werden kann, bevor das OH vom Instrument erfasst wird. Mit dieser Technik ist es möglich, ein Hintergrund-OH (OH_{bg}), d. h. ein im Instrument erzeugtes OH-Signal, vom gemessenen OH-Gesamtsignal (OH_{tot}) zu trennen. Die Differenz zwischen OH_{tot} und OH_{bg} ist die atmosphärische OH-Konzentration (OH_{atm}). Vergleichsmessungen mit der hier entwickelten Technik, dem IPI, in zwei verschiedenen Umgebungen mit Instrumenten basierend auf Massenspektrometrie mit chemischer Ionisation *(CIMS, engl.: chemical ionization mass spectrometry)* als alternativer Methode des OH-Nachweises, zeigten eine weitgehende Übereinstimmung. Eine umfassende Beschreibung des Systems zur Ermittlung der Ursache des OH_{bg} hat ergeben, dass es weder von einem Artefakt des Instruments noch von hinlänglich bekannten und beschriebenen LIF-FAGE-Interferenzen stammt. Zur Bestimmung der Spezies, die das OH_{bg}-Signal verursacht, wurden verschiedene Laborstudien durchgeführt. Die Arbeit im Rahmen dieser Doktorarbeit hat ergeben, dass das LIF-FAGE-Instrument leicht auf OH reagiert, das beim monomolekularen Zerfall stabilisierter Criegee-Intermediate (SCI) im Niederdruckbereich des Instruments gebildet wird. Criegee-Intermediate oder Carbonyloxide entstehen bei der Ozonolyse ungesättigter flüchtiger Kohlenwasserstoffverbindungen *(VOC, engl.: volatile organic compounds)* und können daher in der Umgebungsluft vorkommen. Anhand von Tests mit verschiedenen Verweilzeiten der SCI im Niederdruckbereich des Instruments in Verbindung mit einem detaillierten Modell

mit der neuesten SCI-Chemie wurde die monomolekulare Zerfallsgeschwindigkeit von 20 ± 10 s^{-1} für den *syn*-Acetaldehyd-Oxykonformer bestimmt. Der in Feldkampagnen gemessene OH_{bg}-Wert wurde dahingehend untersucht, ob SCI die Quelle des beobachteten Hintergrund-OH im Feld sein könnten. Das Budget für die SCI-Konzentration, das für die Kampagnen HUMPPA-COPEC 2010 und HOPE 2012 berechnet wurde, ergab eine SCI-Konzentration zwischen ca. 10^3 und 10^6 Molekülen pro cm^3. In der Kampagne HUMPPA-COPEC 2010 ergab die Schwefelsäurekonzentration, dass die OH-Oxidation von SO_2 allein die gemessene H_2SO_4-Konzentration nicht erklären konnte. In dieser Arbeit konnte gezeigt werden, dass das Hintergrund-OH mit dieser ungeklärten Produktionsrate von H_2SO_4 korreliert und somit die Oxidation von SO_2 durch SCI als mögliche Erklärung in Frage kommt. Ferner korreliert das Hintergrund-OH in der Kampagne HOPE 2012 mit dem Produkt aus Ozon und VOC und konnte mit SO_2 als SCI Fänger entfernt werden. Qualitativ zeigen wir somit, dass das in der Umgebungsluft gemessene Hintergrund-OH wahrscheinlich durch den monomolekularen Zerfall von SCI verursacht wird, doch sind weitere Studien notwendig, um die quantitativen Beziehung für diese Spezies und dem Hintergrund-OH in unserem Instrument zu bestimmen.

Summary

The hydroxyl radical (OH) is an important atmospheric oxidant initiating the degradation processes of many trace gases and in particular of volatile organic compounds (VOC). Measurements of the OH concentration in the atmosphere therefore give a good indication of the instantaneous oxidation capacity of a certain environment. Measurements performed with some LIF-FAGE instruments during night time showed elevated concentrations of OH radical which could not be explained by known chemistry. In order to understand if such a signal is really atmospheric OH or if it originates from some interfering species, within the framework of this thesis the Max Planck Institute for Chemistry (MPIC) LIF-FAGE instrument was modified and tested. An inlet pre-injector (IPI) was designed which allows the periodic injection of an OH scavenger within the ambient air before it is sampled by the instrument. With this technique it is possible to separate a background OH (OH_{bg}), an OH signal generated within the instrument, from the total OH (OH_{tot}) signal measured. The difference between OH_{tot} and OH_{bg} is the atmospheric OH concentration (OH_{atm}). Measurements performed with IPI in two different environments alongside an alternative method of OH detection (CIMS) showed good agreement. A full characterisation of the system to discover the cause of the OH_{bg} found it does not originate from an instrumental artefact nor from well known and characterised LIF-FAGE interferences. Several laboratory studies have been performed to identify the species causing the OH_{bg} signal. The work done in this thesis revealed that the LIF-FAGE is sensitive to OH formed from the unimolecular decomposition of stabilised Criegee intermediates (SCI) within the low pressure region of the instrument. Criegee intermediates, or carbonyl oxides, are formed from the ozonolysis of unsaturated VOC and therefore can be present in ambient air. Tests completed for different residence times of the SCI within the low pressure region of the instrument coupled with a detailed model including the most updated chemistry concerning SCI, were used to estimate the unimolecular decomposition rate of $20 \pm 10\ s^{-1}$ for the *syn*-acetaldehyde oxide conformer. The OH_{bg} measured during field campaigns was investigated to elucidate if SCI could be the source of the observed OH_{bg} in the field. The budget for the SCI concentration calculated for the HUMPPA-COPEC 2010 and HOPE 2012 campaigns found the SCI concentration to be between ~ 10^3 and ~ 10^6 molecules cm^{-3}. During the HUMPPA-COPEC 2010 the sulfuric acid concentration found that only OH oxidation of SO_2 could not explain the measured

concentration of H_2SO_4. The OH_{bg} correlates with this unexplained production rate of H_2SO_4 for which SCI were suggested to be the cause. Additionally, during the HOPE 2010 campaign the OH_{bg} correlates with the product of ozone and VOC and it could be scavenged with SO_2. Qualitatively, we thus show that the OH_{bg} measured in ambient is likely caused by the unimolecular decomposition of SCI, though additionally studies are necessary to obtain the quantitative calibration factor for this bulk species in our instrument.

Contents

1 Introduction

The trace gases that comprise less than 1 % of the composition of the atmosphere play a crucial role in the chemical properties of the atmosphere despite their very low concentrations. Their abundance in the troposphere has changed remarkably over the last two centuries and technological improvements have enabled the identification and quantification of many of these gases for concentrations smaller than 1 x 10^5 molecules cm^{-3} (Seinfeld and Pandis, 2006). The impact that trace gases can have in the atmosphere on humans depends on how large their emissions are and on how quickly they can be removed from the atmosphere. Removal processes can be physical, wet and dry deposition, or driven by chemical reactions. In the gas phase, during daytime, the most important oxidant in the troposphere is the hydroxyl radical (OH). Other important known oxidants are ozone (O_3), acting both during day and night time and nitrate radical (NO_3) that, due to his photolabile nature, can play an important role during night time. While in the liquid phase, like in clouds, fog or rain, hydrogen peroxide (H_2O_2) is the dominant oxidant. These chemical species are all connected to each other through formation and destruction paths and they all affect the abundance of trace gases in particular environments. Recently, Criegee intermediates, or carbonyl oxides (Criegee, 1975), have been suggested as having an important role in the oxidation of certain trace gases such as SO_2 (Mauldin III et al., 2012; Welz et al., 2012) and NO_2 (Ouyang et al., 2013).

1.1 Criegee intermediates

Criegee intermediates are formed from the gas-phase ozonolysis of unsaturated compounds (Criegee, 1975). The addition of ozone across the double bond forms a primary ozonide (POZ), which immediately decomposes forming a Criegee intermediate and a carbonyl compound (Figure 1.1). The CI formed by ozonolysis have a different energy distributions and can be divided in two categories (Kroll et al., 2001; Chuong et al., 2004; Epstein and Donahue, 2010; Drozd and Donahue, 2011; Drozd et al., 2011): CI that are formed with a

(near)-thermal energy content, called stabilized CI (SCI); chemically activated CI with a high energy content that in the atmosphere have an extremely short lifetime and will either undergo unimolecular decomposition or get stabilized by collision forming SCI. The stabilised Criegee intermediate (SCI) can react with atmospheric trace gases and can also decompose unimolecularly. Recent studies performed in different laboratories (Berndt et al., 2012; Welz et al., 2012; Ouyang et al., 2013; Ahrens et al., 2014; Buras et al., 2014; Liu et al., 2014b; Sheps et al., 2014; Stone et al., 2014; Welz et al., 2014) reveal how SCI can react fast with sulphur dioxide (SO_2), nitrogen dioxide (NO_2) and organic acids. Although the importance of these reaction paths in the atmosphere has yet to be proved, Mauldin III et al. (2012) inferred SCI to be the missing oxidant of SO_2 needed to close the sulfuric acid (H_2SO_4) budget in a Boreal forest. Though, currently no direct or reliable indirect measurement of their steady state concentration in the atmosphere was performed.

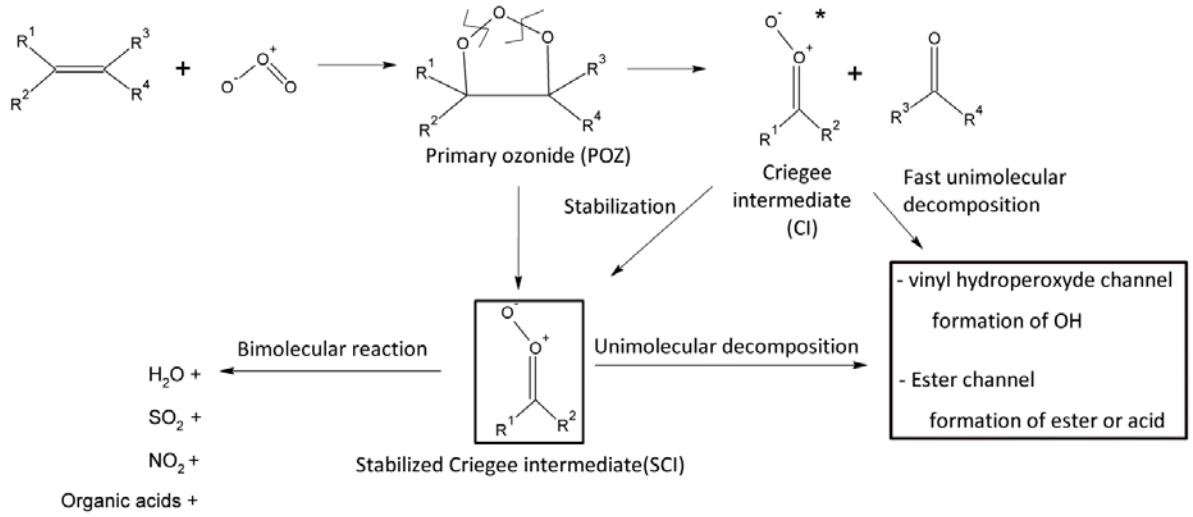

Figure 1.1. General reaction scheme for the ozonolysis of an unsaturated compound.

1.2 The hydroxyl radical

The main primary hydroxyl radical source in the lower troposphere during summer time is the photolysis of ozone with formation of $O(^1D)$. The excited oxygen reacts quickly with water vapor with the formation of two OH radicals (Levy, 1974). During night time, winter or indoor, the main primary source of OH radicals appear to be ozonolysis of unsaturated compounds (Johnson and Marston, 2008). Other primary sources are photolysis of nitrous

acid (HONO) and of H_2O_2. Another important source for OH is the reaction of O_3 and NO with the hydroperoxyl radical (HO_2). HO_2 is mainly formed during many destruction paths for OH, such as the reaction with carbon monoxide (CO) or volatile organic compounds (VOC), closing a fast cycle between OH and HO_2. Figure 1.2 is a simplified scheme that summaries the relationship between the OH and HO_2 radicals that are known together with the name of HO_x radicals.

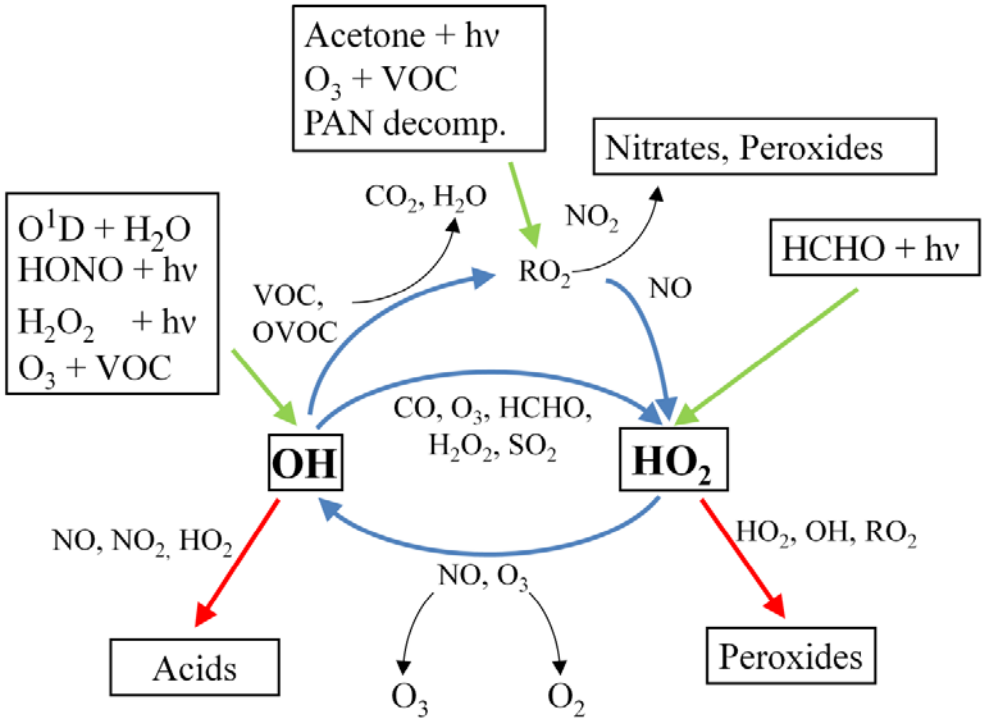

Figure 1.2. Schematic overview of the HOx radical photochemistry in the troposphere. Radical production (green), recycling (blue), and loss (red) pathways are indicated by bold arrows. Some reactions are simplified.

OH radicals react very quickly, < 1 x 10^{-11} cm^3 $molecule^{-1}$ s^{-1}, (Atkinson et al., 2004), with a large number of trace gases and especially with unsaturated VOC. The OH radical has a global average concentration in the troposphere of ~ 4 x 10^6 molecules cm^{-3} (Seinfeld and Pandis, 2006). The average concentration of OH is among the smallest for the measurable trace gases and its short lifetime, less than one second, makes absolute concentration

measurements very challenging and measurement techniques more likely to be affected by interference signals.

1.3 OH measurements techniques

The OH radical has been measured in the field with one of three techniques: differential optical absorption spectroscopy (DOAS) via direct absorption by OH (Perner et al., 1987), chemical ionization mass spectrometry (CIMS) via the detection of H_2SO_4 after the oxidation of SO_2 by atmospheric OH (Eisele and Tanner, 1991), and by laser-induced fluorescence of the OH molecules method based on the fluorescence assay by gas expansion technique (LIF-FAGE) via the detection of the fluorescence of OH radical after laser excitation (Hard et al., 1984). DOAS measures OH concentration by taking advantage of the Beer-Lambert law and therefore the accuracy depends on the cross section of OH while precision and detection limit on the path length. It does not require calibration and overcomes the problem of wall losses. Its downsides are a lower sensitivity, a poor spatial and time resolution and a complicated mechanical setup that makes it impossible until now to be used on aircraft measurements (Heard and Pilling, 2003). CIMS and LIF-FAGE are mechanically easier to use and have been widely applied in the last 20 years on both ground and aircraft campaigns and several times in comparison (Stone et al., 2012). The CIMS measures OH indirectly after conversion into H_2SO_4 via reaction with SO_2 added to the system. The H_2SO_4 is then ionized at atmospheric pressure with NO_3^- ions and the ratio $H_2SO_4^-$/ NO_3^- is measured by a mass spectrometer. It requires a calibration and a system of inlet and vacuum pumps. It has a low detection limit but requires minimal wall losses in the inlet and the injection of an OH scavenger, usually propane, to remove the OH formed via reaction of HO_2 with NO or ozone or formed via secondary chemistry. The more widely-used instrument for the detection of OH, both on the ground and on aircraft is the LIF-FAGE (Stone et al., 2012). The LIF instrument detects OH directly via measuring the fluorescence of the OH after excitation with a laser at 308 nm. It requires a system of inlet and vacuum pumps and a calibration. Several comparison campaigns, both on ground (Hofzumahaus et al., 1998; Schlosser et al., 2009) and aircraft (Eisele et al., 2001; Ren et al., 2012), have been performed between these

different instruments in order to test the relative reliability of the different techniques and in the main show good agreement.

1.3.1 LIF-FAGE instrument in use at the Max Planck Institute for Chemistry

The LIF-FAGE instrument in use at the Max Planck Institute for Chemistry (Kubistin, 2009; Martinez et al., 2010), also called HORUS (*H*ydrOxyl Radical Measurement Unit based on fluorescence Spectroscopy) is based on the GTHOS (Ground-based Tropospheric Hydrogen Oxides Sensor) in use at the Penn State University and described in details by Faloona et al. (2004). Both instruments reported the detection of a large OH signal during night time (Faloona et al., 2001; Kubistin, 2009) that was not explainable by the measured ancillary data. The HORUS instrument additionally measured a not expected large OH concentration during daytime over the tropical forest (Kubistin et al., 2010), concentrations that were also observed by a different group (Whalley et al., 2011). This led to the discovery of new chemical paths (Dillon and Crowley, 2008; Peeters et al., 2009; da Silva, 2010b, a, c; Crounse et al., 2011) and the development of alternative chemical mechanisms (Lelieveld et al., 2008; Hofzumahaus et al., 2009; Peeters et al., 2009; Peeters and Müller, 2010; Taraborrelli et al., 2012). Despite large uncertainties on the real efficiency of the OH recycling processes (Fuchs et al., 2013; Peeters et al., 2014; Rivera-Rios et al., 2014), the new paths discovered and described could account for the large OH measured in those isoprene rich environment during the day. Still, no clear explanation was found for the large OH observed during night time.

1.4 Thesis objectives

Focus of the current research is the investigation of the OH signals measured by the LIF-FAGE instrument in use at the MPIC in order to understand if the large OH signal observed especially during night time is atmospheric OH of it is generate from the instrument or from some interferences (Chapter 2). Following the discovery that our LIF-FAGE instrument is sensitive to the detection of an OH generated from an interference species, laboratory studies were performed to understand if SCI could be the cause for such OH signal (Chapter 3). Additionally, this non-atmospheric OH signal measured in ambient was analyzed to understand if it could be caused in the field as well by decomposition of SCI and if it could give an indication for the concentration of SCI in the atmosphere (Chapter 4). Additionally, a careful model to assess the fate of SCI in different environments (Chapter 3) together with a budget for the SCI steady state concentration was performed using available data from two different field campaigns (Chapter 4).

2 Characterisation of an inlet pre-injector laser induced fluorescence instrument for the measurement of atmospheric hydroxyl radicals

A. Novelli[1], K. Hens[1], C. Tatum Ernest[1], D. Kubistin[1,3], E. Regelin[1], T. Elste[2], C. Plass-Dülmer[2], M. Martinez[1], J. Lelieveld[1] and H. Harder[1]

[1] {Atmospheric Chemistry Dept., Max Planck Institute for Chemistry, 55128 Mainz, Germany}

[2]{German Weather Service, Meteorological Observatory Hohenpeissenberg (MOHp), Albin-Schwaiger-Weg 10, 83282 Hohenpeissenberg, Germany}

[3]{ University of Wollongong, School of Chemistry, Wollongong, NSW, Australia}

Manuscript published in Atmospheric Chemistry and Physics

Abstract. Atmospheric measurements of hydroxyl radicals (OH) are challenging due to a high reactivity and consequently low concentration. The importance of OH as an atmospheric oxidant has motivated a sustained effort leading to the development of a number of highly sensitive analytical techniques. Recent work has indicated that the laser-induced fluorescence of the OH molecules method based on the fluorescence assay by gas expansion technique (LIF-FAGE) for the measurement of atmospheric OH in some environments may be influenced by artificial OH generated within the instrument, and a chemical method to remove this interference was implemented in a LIF-FAGE system by Mao et al. (2012). While it is not clear if other LIF-FAGE instruments suffer from the same interference, we

have applied this method to our LIF-FAGE HORUS (Hydroxyl Radical Measurement Unit based on fluorescence Spectroscopy) system, and developed and deployed an inlet pre-injector (IPI) to determine the chemical zero level in the instrument via scavenging the ambient OH radical.

We describe and characterise this technique in addition to its application at field sites in forested locations in Finland, Spain, and Germany. Ambient measurements show that OH generated within the HORUS instrument is a non-negligible fraction of the total OH signal, which can comprise 30% to 80% during daytime and 60% to 100% during the night. The contribution of the background OH varied greatly between measurement sites and was likely related to the type and concentration of volatile organic compounds (VOCs) present at each particular location. Two inter-comparisons in contrasting environments between the HORUS instrument and two different chemical ionisation mass spectrometers (CIMS) are described to demonstrate the efficacy of IPI and the necessity of the chemical zeroing method for our LIF-FAGE instrument in such environments.

2.1 Introduction

The hydroxyl radical, OH, plays a central role in the chemistry of the troposphere, where it acts as the main daytime oxidizing agent, initiating the photochemical degradation of many chemical species emitted by natural and anthropogenic sources. In the lower troposphere the primary OH radical formation is dominated by photolysis of ozone and subsequent reaction of the excited oxygen atom with water vapour (Levy, 1971). Minor primary sources are the photolysis of nitrous acid and hydrogen peroxide and ozonolysis of unsaturated carbon compounds. Once formed, the OH radical reacts rapidly with many atmospheric trace gas species converting a large fraction of the volatile organic matter (Levy, 1974). The ambient measurement of OH is therefore a good test of proposed chemical mechanisms postulating the importance of chemical species and/or processes in the atmosphere. The OH radical is usually measured in the field with one of three techniques: differential optical absorption spectroscopy (DOAS) (Perner et al., 1987) via absorption of light by OH, chemical ionization mass spectrometry (CIMS) (Eisele and Tanner, 1991) via the detection of H_2SO_4 after the oxidation of SO_2 by atmospheric OH, and laser-induced fluorescence (LIF-FAGE) (Hard et

al., 1984) via the detection of OH radical fluorescence after laser excitation. Several comparison campaigns have been performed, both on ground (Hofzumahaus et al., 1998; Schlosser et al., 2007) and aircraft (Eisele et al., 2001; Ren et al., 2012), to test the consistency and performance of the different techniques and have generally shown good agreement. However, a number of recent measurements performed by LIF-FAGE instruments in VOC rich environments have shown considerably higher values of OH radicals than can be accounted for by well established chemical mechanisms (Faloona et al., 2001; Lelieveld et al., 2008; Ren et al., 2008; Hofzumahaus et al., 2009; Kubistin, 2009; Whalley et al., 2011). These model-measurement disagreements have prompted the discovery of new chemical paths (Dillon and Crowley, 2008; Peeters et al., 2009; da Silva, 2010b, a, c; Crounse et al., 2011) and the development of alternative chemical mechanisms to account for the discrepancies (Lelieveld et al., 2008; Hofzumahaus et al., 2009; Peeters et al., 2009; Peeters and Müller, 2010; Taraborrelli et al., 2012). At least in part, the disagreement between models and measurements could be related to the measurement technique. LIF instruments can suffer from a number of well characterised interferences, such as OH generated by the laser pulse from species like ozone, acetone, or H_2O_2, as well as spectral interferences from, for example, naphthalene and SO_2. When present, these can be corrected for (Holland and Hessling, 1995; Martinez et al., 2004; Ren et al., 2004; Kubistin, 2009). Recent work by Mao et al. (2012) suggested that, at least in some LIF-FAGE designs and possibly depending on the characteristics of the environment, a process not currently accounted for may generate OH within the low pressure side of the instrument. The authors report the measurement of OH radicals in a Ponderosa pine plantation in the California Sierra Nevada Mountains with the deployment of a chemical zero level system in parallel with the traditional FAGE method. In this paper, we describe the characterisation and application of such a chemical zero system (inlet pre-injector, IPI) to the HORUS instrument, following the design of Mao et al (2012), to address the possible role of internally-formed OH in our system. In addition, we also describe how the atmospheric OH concentration is determined with the new modification of the instrument in three field measurements that include two comparisons of the Mainz IPI-LIF-FAGE instrument with CIMS measurements of OH in chemically distinct environments.

2.2 Methodology

2.2.1 Mainz LIF-FAGE description

The LIF-FAGE instrument (HORUS) in use at the Max Planck Institute for Chemistry, Mainz, is based on the design of GTHOS (Ground Tropospheric Hydrogen Oxide Sensor) described by Faloona et al. (2004) and is described in detail by Martinez et al. (2010). The instrument consists of three parts: the inlet and detection system, the laser system, and the vacuum system (Fig. 2.1).

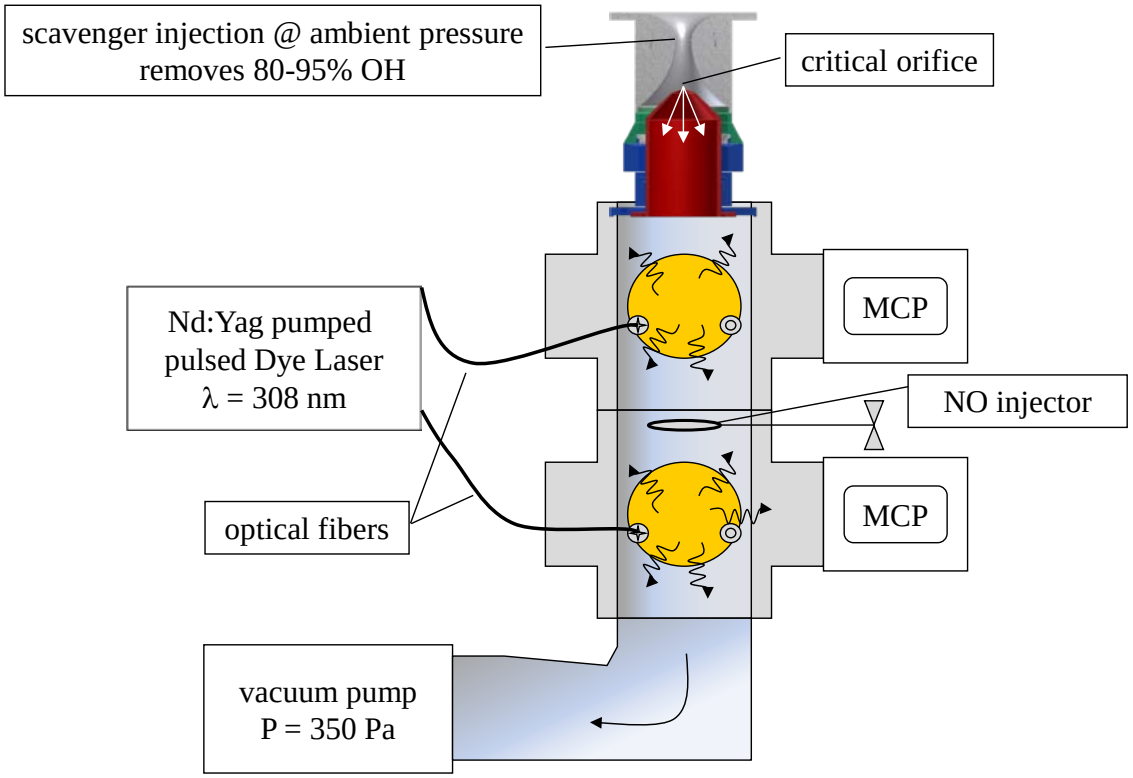

Figure 2.1. HORUS instrument setup scheme with IPI. The ambient air is sampled through IPI where an OH scavenger is added periodically and is then sampled by the instrument inlet through a critical orifice. In the first cell, OH is excited by a laser pulse at around 308 nm and the fluorescence is detected by an MCP. Directly in front of the second cell a mixture of NO with nitrogen is injected and HO_2 is detected after conversion into OH. The total pressure inside the instrument is maintained around 350 Pa.

The air is drawn at ~ 7 L min^{-1} through a critical orifice (1 mm diameter) and OH is selectively excited by pulsed UV light at around 308 nm on resonance with the $Q_1(2)$ transition line ($A^2\Sigma^+ - X^2\Pi$, $v'=0$ $v''=0$). The laser pulse is directed into a multipass "White Cell" (White, 1942) crossing the detection volume 32 times to increase the sensitivity. The

fluorescence signal from the excited hydroxyl radicals is detected at low pressure (~300-500 Pa). As the fluorescence is detected at similar wavelengths as the excitation, a time-gated photon counting technique using micro-channel plate detectors (MCP) is used. The UV light for excitation of the hydroxyl radicals is provided by a Nd:YAG pumped, pulsed, tunable dye laser system (Wennberg et al., 1994; Martinez et al., 2010) operated at a pulse repetition frequency of 3 kHz. The instrument has two consecutive detection cells: in the first cell OH radicals are detected, and in the second cell hydroperoxyl radicals (HO_2) are detected via the conversion of HO_2 to OH by the addition of NO. The calibration of the instrument is achieved via production of a known amount of OH and HO_2 from the photolysis of water at 185 nm using a mercury lamp. A more detailed description of the instrument calibration is reported by Martinez et al. (2010). The fluorescence background signal of the instrument is measured by tuning the excitation laser on (online signal, Sig^{on}) and off (offline signal, Sig^{off}) resonance with the OH transition line at 308 nm (Fig. 2.2a).

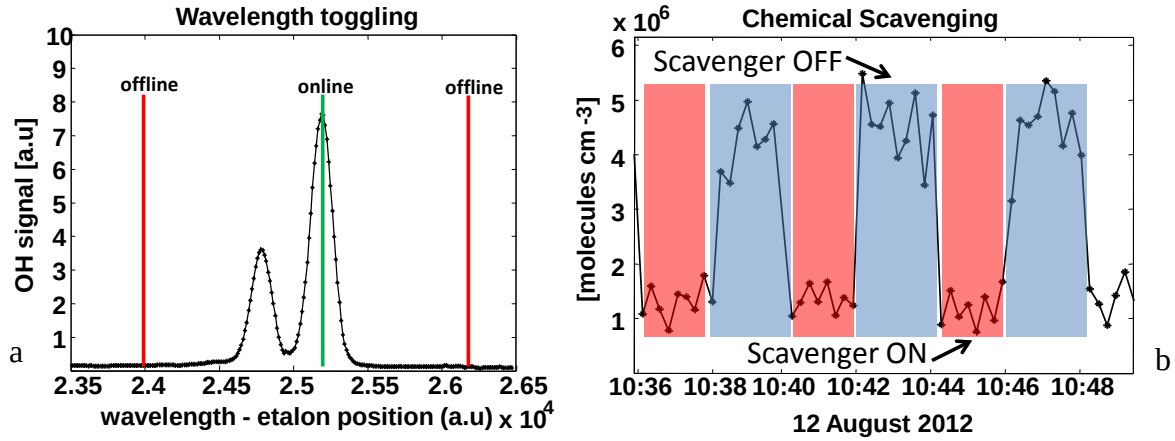

Figure 2.2. a, the HORUS instrumental fluorescence background signal is detected by tuning the excitation laser on (green line) and off resonance (red lines) with the OH line at 308 nm; b, the background OH signal is obtained by injecting an OH scavenger periodically in front of the inlet (red shaded area). The blue shaded area represents the total OH signal. The atmospheric OH is obtained from the difference between the two.

The spectra of the measured atmospheric OH is compared with the one obtained from a reference cell in order to rule out possible fluorescence signal due to species that fluoresce at similar wavelengths (such as naphthalene and SO_2). During all three measurement campaigns described in this paper, the HORUS instrument was equipped with a 14 cm inlet resulting in a residence time of the air between the pinhole and the detection cell of 2.5 ms(Novelli et al., 2014b). Laser power and pressure at the cell were, respectively, ~ 4 mW and ~ 310 Pa during

the campaigns in Finland and Spain and ~ 9 mW and 380 Pa during the campaign in Germany.

2.2.2 Inlet Pre-Injector (IPI)

Figure 2.3 shows a schematic cross-section of IPI currently in use as part of the HORUS instrument. The purpose of IPI is the addition of an OH scavenger to remove the atmospheric OH before it is sampled by the inlet to account for an OH signal generated within the instrument.

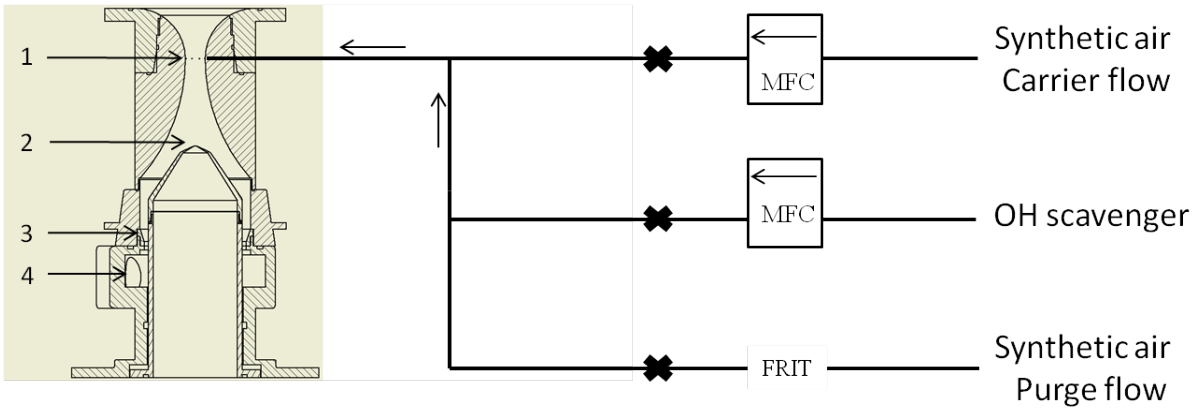

Figure 2.3. Inlet pre injector (IPI) scheme. The injection of the scavenger is achieved via eight 0.5 mm holes (Label 1) positioned 5 cm above the pinhole of the inlet (Label 2). The scavenger is carried through IPI with ~ 4000 sccm of synthetic air. The residence time in IPI after the injection of the scavenger is ~ 4 ± 0.5 ms to scavenge between 80% and 95% of the atmospheric OH, depending on the scavenger concentration. Label 3 indicates the position of a metallic grid. Label 4 shows the connection to the blower that samples the air through IPI.

Before the introduction of IPI, the atmospheric OH concentration was obtained by multiplying the OH fluorescence signal (OHF), obtained from the difference between fluorescence online and fluorescence offline signals, by the total instrument sensitivity (S). The total instrument sensitivity depends on many parameters such as laser power, efficiency of the detector, temperature and, humidity (Martinez et al., 2004) and is determined by performing calibrations on a regular basis.

$$OHF = (Sig^{on} - Sig^{off}) \qquad \textit{(Equation 2-1)}$$

$$OH = S \times OHF \qquad \textit{(Equation 2-2)}$$

With IPI (Fig. 2.2b), the instrument is also cycled every 2 minutes between injection of the scavenger (background OH fluorescence signal, OHF_{bg}) and no injection (total OH fluorescence signal, OHF_{tot}). The atmospheric OH concentration (OH_{atm}) is then obtained by multiplying the difference between the total OH fluorescence signal and the background OH fluorescence signal by the instrument sensitivity and by a factor (F) accounting for scavenging efficiency and radical losses introduced by IPI.

$$OH_{atm} = (S \times (OHF_{tot} - OHF_{bg})) \times F \qquad \textit{(Equation 2-3)}$$

To compare the derived atmospheric OH concentration with the respective total and background signals and to describe the error in concentration of atmospheric OH that would have been made without the use of IPI, we apply the same OH calibration factor to both OH fluorescence signals, OHF_{bg} and OHF_{tot}, and we refer to them as the background OH signal (OH_{bg}) and the total OH signal (OH_{tot}). The units of these variables are therefore molecules cm^{-3} OH equivalent and no inference is drawn as to the actual concentration of the interfering species.

As mentioned above, the detection of atmospheric OH using LIF-FAGE with an additional scavenger was employed following the method described by (Mao et al., 2012). The setup of the OH scavenger injection and its operation differ between the two LIF-FAGE instruments. The main differences between the two injection systems are the internal shape and the amount of air sampled, leading to differences in radical wall losses and in the scavenging efficiency. The hyperbolic internal shape of IPI (max. cross section = 35 mm, min. cross section = 6 mm) (Fig. 2.3) was chosen based on Eisele et al. (1997) to sample air that has little contact with walls and high velocity where the inner diameter is smaller to provide rapid turbulent mixing of atmospheric air and added scavenger. A blower (SCL 20DH from FPZ, Italy) is directly connected to IPI (Fig. 2.3, label 4) pulling air with a flow rate between 150 and 280 L min^{-1}. The flow velocity is monitored using a differential pressure sensor calibrated against a gas meter. An aluminium perforated mesh with square holes is located around the instrument inlet between the nozzle and the connection to the blower sampling the air through IPI (Fig. 2.3, labels 3 and 4). As the mesh texture is very thin and located above the blower connection, the resistance to the air is strong enough to break the flow pattern that would be strongly pointing towards the direction of the pulling position of the blower, allowing a more homogenous flow and mixing. The OH scavenger is injected via eight 0.5

mm diameter holes (Fig. 2.3, label 1) into the centre of the flow of air sampled by IPI, 5 cm above the pinhole of the inlet (Fig. 2.3, label 2). Assuming plug flow, the estimated residence time of the ambient air in IPI from the injection of the scavenger to the instrument inlet when pulling 150 L min^{-1} of air, is ~ 4 ms. To improve the mixing between the scavenger and the sampled air, the injection happens at the minimum cross-section of IPI and to achieve a good penetration of the scavenger into the sample flow, the scavenger is injected into IPI with a carrier flow of synthetic air. The carrier air flow (~ 4000 sccm) is maintained at all times to keep the conditions in IPI constant. The HORUS inlet samples approximately 7 L min^{-1} of air directly from the centre of the flow.

There are several critical parameters involved in the deployment of this chemical scavenger methodology such as the identity and concentration of scavenger, the IPI sampling flow and therefore the residence time within IPI, and the synthetic air carrier flow. The choice of scavenger and concentration is very important. The OH scavenger must react quickly with OH but slowly with other oxidants like ozone and NO_3, it should not be toxic and not have a high absorptivity at the laser excitation wavelength. Its concentration should be high enough to affect the removal of a known and substantial proportion, > 90%, of atmospheric OH but should not be in excess to prevent the risk that excess scavenger will react with the internally generated OH. The flow rate of ambient air through IPI must be fast to minimize losses of HO_x (OH and HO_2) onto the walls and the residence time of OH within IPI has to be an optimal compromise between being short compared to the atmospheric lifetime of OH and allowing sufficient time for the scavenger to react. The carrier flow must be high enough to favour efficient mixing between the scavenger and the atmospheric air and to flush the lines when no injection of scavenger takes place. Figure 2.3 shows the schematic layout of the IPI during the HOPE 2012 campaign. The flow of the scavenger is controlled with a mass flow controller (MFC). After the MFC the scavenger line combines with the carrier gas line where it gets mixed. The mixture then reaches IPI where it is injected into the sampled atmospheric air. In both parts of the injection cycle, i.e., scavenger on and scavenger off, the same amount of air is sampled through IPI and the flow of carrier air is maintained constant. To remove residual scavenger from IPI lines when switching to a period with no injection, the lines are purged with synthetic air at a flow of approximately 5000 sccm for 5 s. The current IPI cycle results in a minimum time resolution for the measurement of atmospheric OH of one data point over 4 minutes consisting of cycles of 2 minutes of injection of the OH scavenger and 2

minutes with no injection of the OH scavenger. Table 2.1 shows IPI parameters for three measurement campaigns.

Campaign	IPI flow Residence time	Scavenger / Flow	Carrier flow (Syn. Air)	Measured scavenging efficiency
HUMPPA COPEC 2010 & DOMINO HO_x	280 L min^{-1} ~ 2.5 ms	Propene / 20 sccm	4000 sccm	> 95 %
HOPE 2012	150 L min^{-1} ~ 4 ms	Propane / 5 - 30 sccm Propene / 2 – 8 sccm	2700 – 4300 sccm	60 – 95 %

Table 2.1. IPI parameters for the three measurement campaigns.

Details of the three measurement sites are given in the next section. During both HUMPPA-COPEC 2010 and DOMINO HO_x the prototype IPI version was in use. The main difference between the prototype version and the final design in current use, shown in figure 2.3, is the method of scavenger injection. The prototype IPI version injected the scavenger through eight 1/16 inch stainless steel tubes inserted into the centre of the IPI airstream. During these two campaigns the IPI parameters were the same. Propene (Aldrich 295663-330G, 99+% purity) was used as an OH scavenger with a flow of 20 sccm and was carried to IPI with 4000 sccm of synthetic air (Westfalen AG). Total IPI sample flow was ~ 280 L min^{-1} leading to a concentration of propene of 6.4 x 10^{14} molecules cm^{-3}. The residence time between the injection of the scavenger and the instrument inlet was ~ 2.5 ms, short compared to the lifetime of OH in those environments (on average ~ 80 ms) (Nölscher et al., 2012; Sinha et al., 2012). Under these conditions, more than 95% of the atmospheric OH was scavenged within IPI. During HOPE 2012 the current version of IPI was used (Fig. 2.3). The current version was designed with a simplified layout to reduce the number of connections and improve ease of use. Two OH scavengers were tested during the campaign. The main scavenger used was propane (Air Liquide 3.5, 99.95% purity) applied with an average flow of 17 sccm, a carrier flow of synthetic air of 4000 sccm and a sample flow within IPI of ~

150 L min^{-1} (propane concentration ~ 2.5 x 10^{15} molecules cm^{-3}). Pulling a smaller flow of atmospheric air through IPI led to a residence time after the injection of the scavenger of ~ 4 ms, that was still short compared to the average OH lifetime at the site (on average ~ 300 ms) and that allowed the use of a smaller concentration of scavenger preventing excessive titration of OH in the low pressure side of the instrument. With this concentration of propane, the lifetime of OH was 0.3 ms and a scavenging efficiency of ~ 90% was achieved. Propene was also used for some measurement cycles, for purposes of comparison, every few hours.

2.2.3 Measurement sites

We present measurements from three measurement sites represented by various meteorological and physicochemical characteristics. The HUMPPA-COPEC 2010 (Hyytiälä United Measurements of Photochemistry and Particles in Air – Comprehensive Organic Precursor Emission and Concentration study) campaign took place during the summer of 2010 at the SMEAR II station in Hyytiälä, Finland (61° 51’ N, 24°17’ E, 181 m a.s.l.) in a boreal forest dominated by Scots Pine (*Pinus Silvestris L.*). Continuous measurements of several trace gases and meteorological parameters as well as particle size distribution and composition (Junninen et al., 2009) were available. For the first part of the campaign the HORUS instrument measured side-by-side with an OH CIMS operated by the University of Helsinki (Petäjä et al., 2009). During the inter-comparison, the HORUS detection axis (Fig. 2.1) was located next to a white container where the main body of the CIMS instrument was at a distance of less than a meter from the CIMS inlet and with the sampling position at the same height. Container and instruments were located in a clearing surrounded by a pine forest. More specific information about the meteorology observed during the comparison period are given in Hens et al. (2014). The instrumentation and the meteorological conditions during the campaign are described by Williams et al. (2011). The DOMINO HO_x campaign took place in November 2010 in El Arenosillo, in south western Spain (37° 1’ N, 6° 7’ W, 40 m a.s.l.) at the same site as the DOMINO (Diel Oxidants Mechanisms In relation to Nitrogen Oxide) campaign in 2008 described in Crowley et al. (2011). The site is located in a forested area (Stone pines, *Pinus pinea*, 5–10 m in height) close to the South Atlantic Ocean shore and

12 km from the city of Huelva and associated petrochemical industry. The HOPE 2012 (Hohenpeißenberg Photochemistry Experiment) campaign was conducted during the summer 2012 at the Meteorological Observatory in Hohenpeissenberg, Bavaria (47° 48' N, 11° 2' E). The observatory is operated by the German Weather Service (DWD) and is located at an altitude of 985 m a.s.l. about 300 m above the surrounding terrain, which consists mainly of meadows and forests. During the entire campaign the HORUS instrument measured side-by-side with the OH CIMS operated by the German Weather Service (DWD) (Berresheim et al., 2000). HORUS detection axis and inlet (Fig.2.1) were located on the roof of the building at less than one meter distance from the inlet of the CIMS. The CIMS main body is located in the room below the roof and its inlet is at ~ 20 cm height from the ground. Nothing was positioned around the two instruments that were both located on the same corner of the roof opening toward a pine forest. More information about the site and the routine measurements can be found in Handisides et al. (2003).

Both CIMS instruments used during HUMPPA-COPEC 2010 and HOPE 2012 campaigns are based on the instrument described by Berresheim et al. (2000) and in both systems a titration with propane is required in order to measure atmospheric OH. The accuracy of both instruments is determined by the accuracy of the calibration system that includes both instrumental uncertainty and interferences caused by ambient parameters. The accuracy of the CIMS operated by the University of Helsinki is 32% (1σ) (Hens et al., 2014)and the accuracy of the DWD-CIMS is 30% (1σ). The precision of the instruments considered counting statistics, potential wind and chemical interferences caused by NO, NO_2, CO and hydrocarbons. The precision of the DWD-CIMS instrument is 26% (1σ, 30 s data) while the precision for the CIMS operated by the University of Helsinki is based on 30 minutes average data and their variability, calculated for every single point; for a typical OH concentration of 1×10^6 molecules cm^{-3} the precision was 5×10^5 molecules cm^{-3} (Hens et al., 2014).

2.3 Results and discussion

2.3.1 IPI characterisation

The addition of IPI to HORUS has a significant effect on the performance of the instrument with respect to losses of radicals in the inlet system. To account for the perturbation of the atmospheric OH measurement caused by the use of IPI, a number of tests were completed to assess the effects of changing instrumental parameters. Total radical loss on the IPI system, the variation of this loss with the atmospheric air sampled and with scavenger carrier flow, and the efficiency of OH removal by the scavenger were tested during the different campaigns in which HORUS was in use with IPI. The tests described below were performed during the HOPE 2012 campaign with the current version of IPI (Fig. 2.3). Titrations of atmospheric OH within IPI using different scavengers were completed with a stable source of OH radicals. The total radical loss in IPI was performed using ambient air as no artificial OH source is currently available due to the very high flow rates of zero air required. These tests were repeated and monitored through the entire campaign to obtain robust results. Tests were performed during daytime, between 10:00 and 16:00 (LT), and night time after 20:00 (LT) to distinguish the effect of IPI with high radical load, i.e., during the day, from situations where interferences might dominate the total signal, i.e., during the night.

Figures 2.4a and 2.4b show the average results of the radical loss tests checked by routinely measuring with and without IPI mounted on the inlet, conducted multiple times during the day and the night, respectively, with a sampled flow of ~ 150 L min^{-1} and a carrier gas of 4000 sccm. The average total OH signal loss was 27% during the day and 7% during the night. The error bars for every single point represent the variability of the data (1σ) during a single test. As the measurement characterising the losses of the total OH signal were completed during daytime when the ratio of atmospheric OH to background OH was highest, most of the variability is caused by the ambient variability of OH.

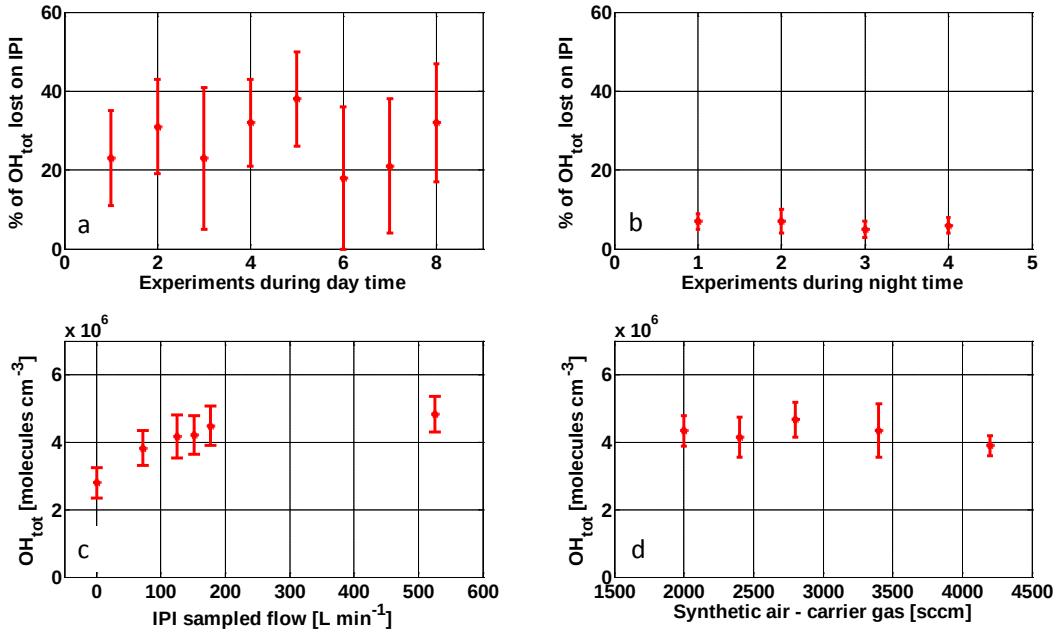

Figure 2.4. a and b, represent the loss of the total OH signal observed by measuring with and without IPI mounted on top of the inlet for day (a) and night (b) time; c, total OH signal measured while varying the sample flow through IPI; d, total OH signal measured with a constant IPI sampling flow of ~ 150 L min^{-1} and adding between 2000 and 4300 sccm of carrier gas flow. The results shown here were obtained during the HOPE 2012 campaign.

Figure 2.4c shows the loss of the total OH signal while changing sample flow through IPI with no carrier air and scavenger. The minimum loss, 20%, occurs at sample flows larger than 500 L min^{-1} while at the flow in use during the campaign, 150 L min^{-1}, the loss observed was ~ 30%. Figure 2.4d shows the losses of the total OH signal in IPI with the variation of the additional carrier flow used to mix the scavenger with the sampled atmospheric air while sampling 150 L min^{-1} of air. No dependency on the carrier flow rate between 1000 and 5000 sccm and no additional loss of OH compared to the loss due to the sampling of 150 L min^{-1} of air were observed indicating that the major cause of losses is due to contact with surfaces. The measured losses during day time, on average 27%, are the losses of the total OH signal and therefore the sum of the losses of atmospheric OH and losses of the species causing the background OH. During night time an average loss of 7% was measured from the total OH signal; since the atmospheric OH signal was below the limit of detection of the instrument (4 x 10^5 molecules cm^{-3}, 4 minute data) during the tests described, the loss is assumed to be entirely due to the species causing the background OH (L_{bg}). The loss of atmospheric OH (L_{OH}) is equal to the atmospheric OH signal measured with IPI mounted on the top of the

inlet (OH_{atm}^{IPI}) divided by the atmospheric OH signal measured without IPI mounted on the top of the inlet (OH_{atm}^{NoIPI}).

$$L_{OH} = \frac{OH_{atm}^{IPI}}{OH_{atm}^{NoIPI}} \qquad \textit{(Equation 2-4)}$$

The value of atmospheric OH without IPI mounted on the top of the inlet is impossible to measure but, by assuming that L_{bg} is constant, the loss on the atmospheric OH signal can be calculated using the equation below

$$L_{OH} = \frac{(OH_{tot}^{IPI} - OH_{bg}^{IPI})}{OH_{tot}^{NoIPI} - \left(\frac{OH_{bg}^{IPI}}{L_{bg}}\right)} \qquad \textit{(Equation 2-5)}$$

OH_{tot}^{IPI} and OH_{bg}^{IPI} are the total OH signal and the background OH signal, respectively, measured by the instrument with IPI mounted on the inlet and therefore affected by losses and their difference is the atmospheric OH affected by losses, OH_{atm}^{IPI}. OH_{tot}^{NoIPI} is the total OH signal measured during the tests without IPI on top of the inlet and therefore not affected by losses. Figure 2.5 shows an example of a test during which IPI was physically removed from the top of the instrument inlet (shaded area). IPI can be removed easily in less than 2 minutes and, on average, we measured without IPI during one period for 30 minutes and measurements were repeated routinely every 4 days during the HOPE 2012 campaign. Referring to equation 2.5, for one IPI on and off test the numerator, the atmospheric OH signal affected by losses, is the result of the interpolation of the measured atmospheric OH signal 12 minutes before and after the removal of IPI. In the denominator, the total OH measured when IPI was not on the inlet is the average of the signal measured when IPI was not on the top of the inlet.

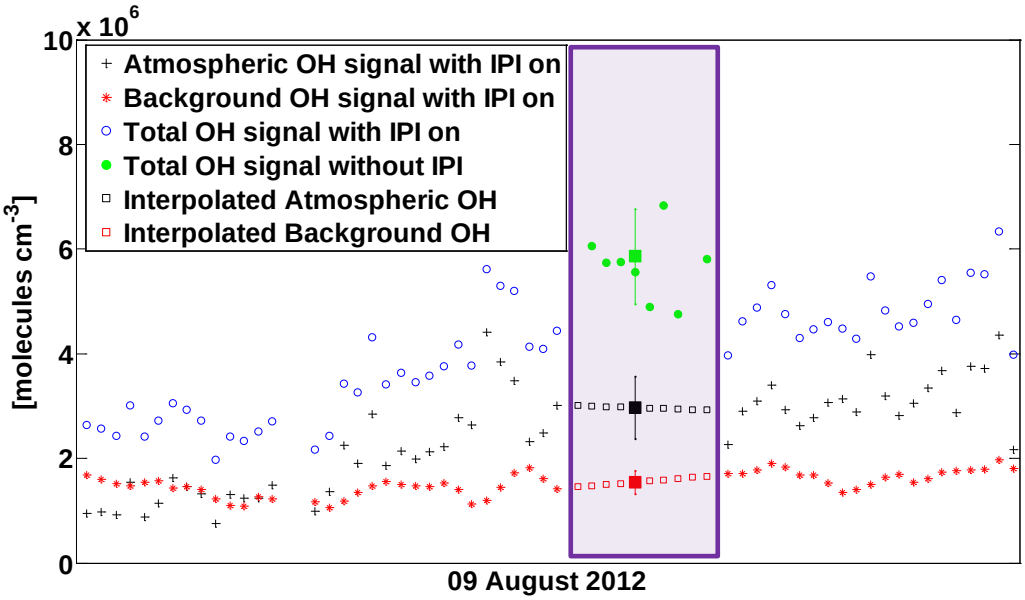

Figure 2.5. Example of an IPI on and off test during the HOPE 2012 campaign. The shaded area represents the test period when IPI was removed from the top of the inlet of the LIF-FAGE instrument. The green circles represent the total OH signal measured without IPI. Black crosses, red stars and blue circles represent, respectively, the atmospheric, the background and the total OH measured with IPI. The filled square markers show the average of the total OH signal measured without IPI (green) and the average of the interpolated signal (open squared markers) before and after the test period for the atmospheric (red) and background (black) OH. The error bars represent the 1σ standard deviation. By using equation 2.5, this test results in an OH loss within IPI of 32%.

The background OH measured with IPI is obtained from the interpolation of the measured background OH signal 12 minutes before and after the removal of IPI and is divided by the loss of the background OH measured during night time tests. The average value obtained for the loss of the atmospheric OH is 34% and the data have been corrected accordingly. The variability observed for the average L_{OH} value, ± 15% (1 σ), was taken into account for the accuracy of the HORUS instrument after the addition of IPI. The accuracy of HORUS was 34% (2 σ) and the accuracy of IPI-HORUS becomes 42% (2 σ). The detection limit of IPI-HORUS is obtained from the statistical significance of the difference between the total OH signal and the background OH signal determined by t-test (1σ) and decreased from 9 x 10^5 molecules cm^{-3} (4 minute data) for the HUMPPA-COPEC 2010 and DOMINO HO_x campaigns to 4 x 10^5 molecules cm^{-3} (4 minute data) for the HOPE 2012 campaign due to higher laser power.

To optimize the OH scavenging efficiency, several titrations of OH were conducted during the campaign with various operational conditions to examine the stability of the instrument

and the reproducibility of the background subtraction. The optimization of the scavenger concentration is also important due to its potential to remove part of the internally produced OH in the low pressure region of the instrument, which would result in the overestimation of the atmospheric OH concentration. The titration experiments were performed by producing a constant above ambient concentration of OH of about ~ 10^9 molecules cm^{-3} in front of IPI using a mercury lamp and ambient air and by varying the concentration of the scavenger to measure the efficiency in the removal of the OH molecules within IPI. By sending a concentration of 2.5 x 10^{15} molecules cm^{-3} of propane, 90% of the initial OH was removed. We calculated the theoretical scavenging efficiency for each OH scavenger deployed during the campaign based on the residence time in IPI after the injection of the scavenger (~ 4 ms) and inside the instrument in the low pressure region (~ 2.5 ms), and on the rate coefficients for the reactions between the respective scavenger and OH at ambient and low pressure (~ 350 Pa) (Sander et al., 2011). Figure 2.6 shows, in blue, the theoretical OH titration efficiency of scavenger depending on the scavenger concentration for the case of propane.

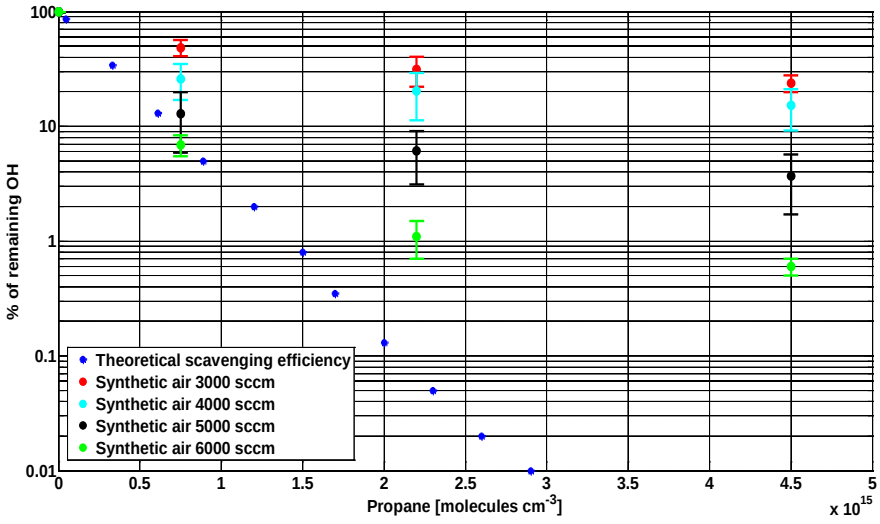

Figure 2.6. Comparison between the calculated theoretical scavenging efficiency of propane and the measured scavenging efficiency at four different synthetic air carrier gas flows for three different concentrations of propane.

Also shown are experimental titrations performed with propane, at different carrier gas flow rates. The carrier gas flow does not have a significant impact on the dilution of the scavenger as it represents a minor percentage of the total flow sampled by IPI. What it does influence is the mixing of the scavenger with the atmospheric air, and thus the scavenging efficiency. The

experimental data show a deviation from the calculated curve. At higher carrier gas flows the experimental data is closer to the model results. The deviation from the modelled data may be related to incomplete mixing between the sampled atmospheric air and the OH scavenger; by increasing the carrier gas flow, and therefore improving the mixing, we would expect to approach the theoretical titration efficiency. The set-up during the HOPE 2012 campaign allowed us to have a stable carrier flow only for flows below 4500 sccm. At higher values, the MFC controlling the carrier flow showed high sensitivity to even small temperature driven changes in the backing pressure of the supply gas. Therefore, the flow was kept stable at 4000 sccm, even though this is suboptimal with respect to mixing, and the amount of OH scavenged was checked regularly by repeated titrations.

The calculated theoretical scavenging efficiency also predicts the amount of OH we would be removing in the low pressure region of the instrument at a certain concentration of scavenger. During the HOPE 2012 campaign the concentration of propane in use was small enough to allow the removal of less than 2% of the OH in the low pressure region. As the calculation assumes perfect mixing, the amount of internal scavenging was tested by changing the propane flow from 5 to 35 sccm whilst keeping a constant and small concentration of atmospheric OH (night time period). Figure 2.7 shows a negligible variation in the background OH signal, well within the precision of the instrument, even when increasing the propane concentration by a factor of 7. Therefore an impact from internal OH scavenging on the determination of the atmospheric OH can be excluded.

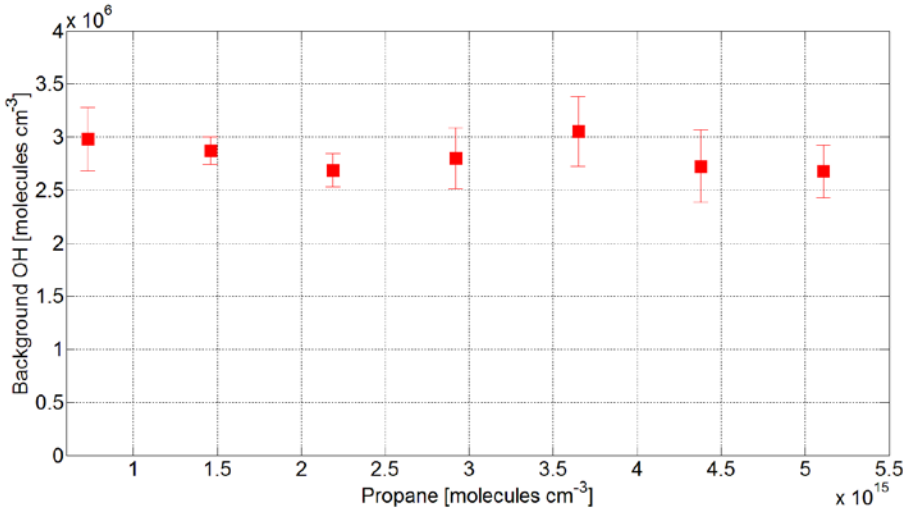

Figure 2.7. Background OH observed at a constant atmospheric OH concentration when injecting different concentrations of propane.

The prototype IPI version was used during the HUMPPA-COPEC 2010 and the DOMINO HO_x campaigns and the instrument was run with the same parameters in both campaigns. Similar tests to the ones previously described were performed during HUMPPA-COPEC 2010 but as shown in figure 2.8, most of the total OH signal measured by the instrument was due to the background OH both during day and night time. In this situation is difficult to account for possible losses of the OH radical because its contribution on the total signal is too small. Total radical loss tests were performed but the results were not as unambiguous as for the HOPE 2012 campaign case; sometimes a small OH loss was observed on IPI but during most of the tests there was no clear indication of OH loss although any OH losses would likely be masked by the high background signal.

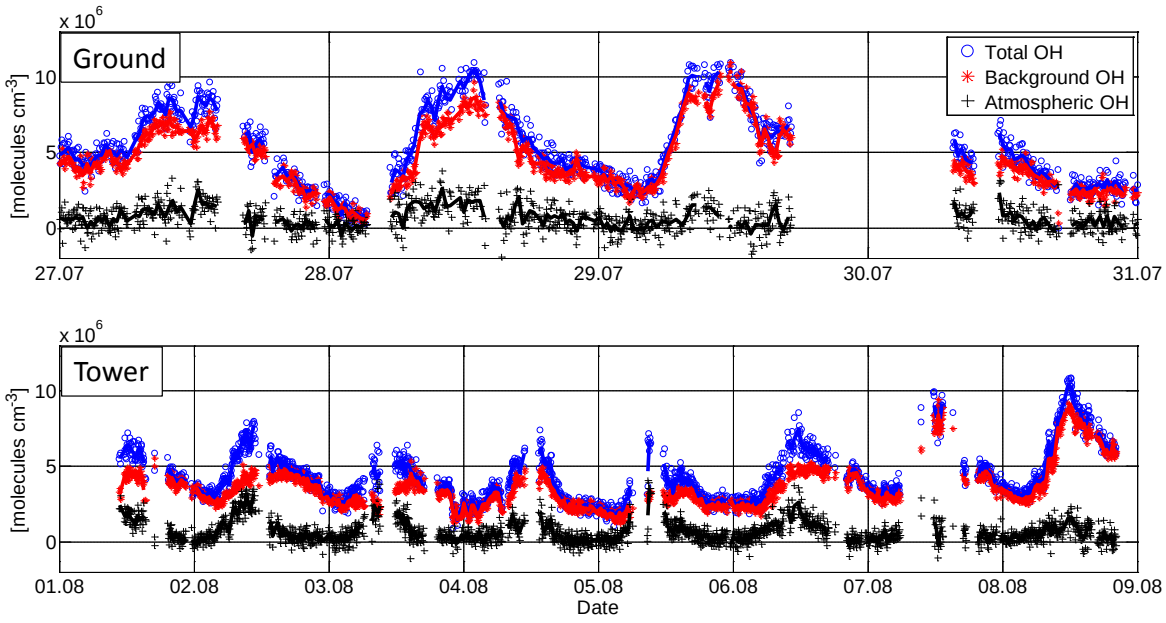

Figure 2.8. OH signals measured by HORUS during HUMPPA-COPEC 2010 campaign. The blue circles represent the total OH signal measured by the instrument in the absence of an OH scavenger. The red stars represent the background OH measured during the injection of an OH scavenger. The black crosses represent the atmospheric OH obtained by difference between total OH and background OH. The solid lines are 30 minutes averages. The top panel shows the data collected on the ground and the bottom panel shows the data collected on the tower. Time is in UTC+2.

Propene was originally selected as scavenger because of its high reaction rate with OH, allowing rapid OH scavenging even at low concentration. However, propene is known to form OH radicals after reaction with ozone with a yield of 0.34 (Atkinson et al., 2006). Hence, by mixing high concentrations of propene with the ambient air we expect formation

of additional OH radicals. During HUMPPA-COPEC 2010 the residence time in IPI after the injection of the scavenger was ~ 2.5 ms such that the concentration of ambient ozone and propene, even if reacting quickly with OH, can be assumed to be constant. The steady state concentration of OH with the concentration of propene within IPI (~ 6 x 10^{14} molecules cm^{-3}) is reached after 0.5 ms, therefore the average steady state OH concentration produced by propene can be calculated by taking into account the average ambient ozone concentration during the campaign, the rate coefficient between ozone and propene, k_1 = 1 x 10^{-17} cm^3 $molecule^{-1}$ s^{-1} at 298K, the OH yield, Y=0.34, and the rate coefficient between propene and OH at 1013 hPa and 298 K, k_2 = 2.9 x 10^{-11} cm^3 $molecule^{-1}$ s^{-1} (Atkinson et al., 2006):

$$[OH] = \frac{[O_3] \times k_1 \times Y}{k_2} \qquad \textit{(Equation 2-6)}$$

This calculation represents an upper limit for the possible production of OH during the injection of propene as scavenger as it does not consider any physical losses for OH or ozone on IPI and also assumes perfect mixing between propene and ambient air. The OH concentration produced during the injection of propene as scavenger depends only on the ozone concentration. The peak mixing ratio of ozone during the HUMPPA-COPEC 2010 campaign was 80 ppbv, which would result in a maximum OH concentration of 2.3 x 10^5 molecules cm^{-3}. For the average ozone value of 44 ppbv the steady state OH concentration would be 1.2 x 10^5 molecules cm^{-3}. This additional OH would cause an underestimation of the atmospheric OH calculated after subtraction of the background OH signal from the total OH measured by the instrument and would increase the uncertainty on our OH measurement. During the HOPE 2012 campaign we performed tests using propene and propane as OH scavengers intermittently at an ambient concentration of ozone of ~ 40 ppbv to estimate the production of OH due to propene ozonolysis. Figure 2.9 shows that there is no significant difference between the atmospheric OH concentration determined with the use of propane and the OH concentration determined using propene as the average value was (0.5 ± 1.5) x 10^5 molecules cm^{-3} (1σ). This value is lower than the theoretical one calculated for the same concentration of ozone indicating additional loss processes. Because the ambient concentrations of ozone and the propene concentration in use during the tests performed in HOPE 2012 and HUMPPA-COPEC 2010 were comparable, assuming similar mixing within the two versions of IPI, we can expect similar OH production of 0.5 x 10^5 molecules cm^{-3}

during the HUMPPA-COPEC 2010 campaign. The value is below the precision of the OH measurement and therefore the data were not corrected for this effect.

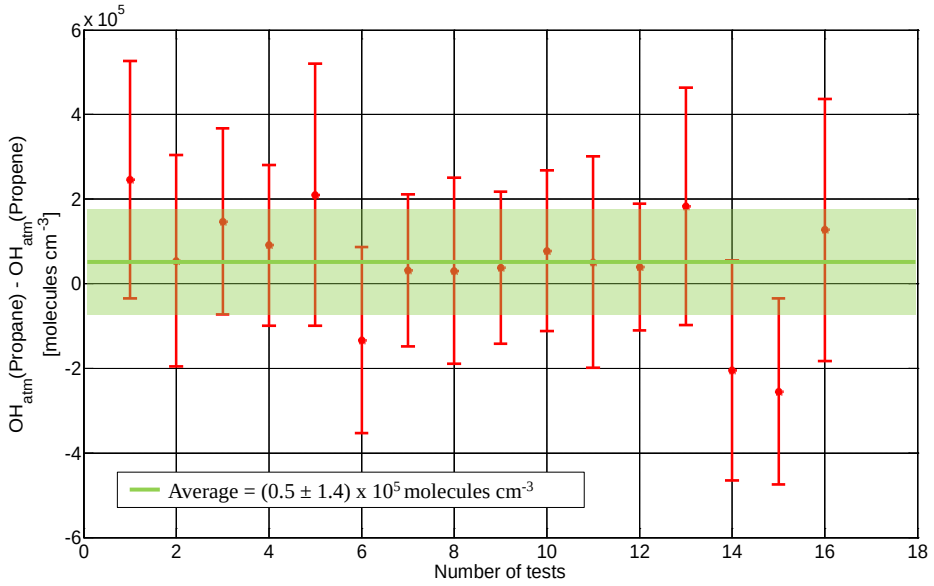

Figure 2.9. Difference between the atmospheric OH concentration determined with the use of propane as scavenger and the atmopspheric OH concentration determined with the use of propene. The points are one hour averages. The green line is the average value of 0.5 x 10^5 molecules cm^{-3} and the shaded area is the 1σ range.

To summarise, IPI prototype was in use during the HUMPPA-COPEC 2010 and DOMINO HOx campaigns. No correction factor, F, from equation 2.3 was applied for radical losses for the atmospheric OH data collected during those campaigns as no clear value for losses of atmospheric OH in IPI was obtained. As propene was used as scavenger aiming at the removal of more than 95% of the atmospheric OH and no additional OH was produced while using it (Figure 2.9) also no correction for the scavenger efficiency was applied. During HOPE 2012 the correction factor includes the 34% average value of losses of atmospheric OH in IPI walls and a point-by-point correction for the scavenger efficiency. The scavenger efficiency is based on the scavenger used and its concentrations and it is obtained from the titration tests performed regularly during the campaign.

2.4 Atmospheric measurements using IPI

Figure 2.8 shows the signals resulting from the first use of HORUS with IPI during the HUMPPA-COPEC 2010 campaign. The top time series highlights the period in which the instrument was on the ground next to a CIMS measuring OH and H_2SO_4 (Petäjä et al., 2009), while the lower series shows the period in which the instrument was operated on a 24 meter tower just above the forest canopy. During the day, within the partially shaded forest canopy, the background OH signal reaches up to 1 x 10^7 molecules cm^{-3} contributing 80% to the total signal. On the tower the maximum value reached by the background OH signal is 7 x 10^6 molecules cm^{-3} contributing up to 60% to the total OH signal measured on the majority of days. During night time the background OH concentration falls below 4 x 10^6 molecules cm^{-3}, but as the atmospheric OH concentration is small the fraction is almost 100%. A side-by-side comparison with the CIMS instrument was performed for the first part of the campaign while both instruments were on the ground. Figure 2.10 shows the relationship between the atmospheric OH measured by the LIF and the OH measured by the CIMS.

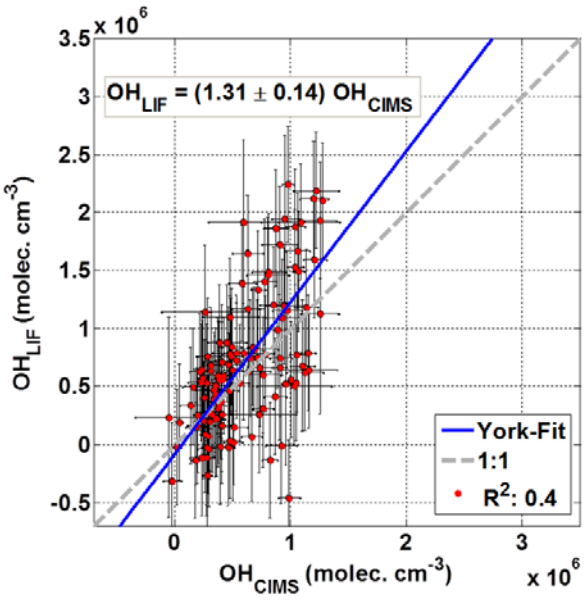

Figure 2.10. Comparison of OH radical measurements by HORUS and CIMS instruments during the HUMPPA-COPEC 2010 campaign based on 30 minute averages. Linear regression following the method of York et al. (2004) yields a slope of 1.31 ± 0.14 and an offset of (-1.2 ± 0.3) x 10^5 molecules cm^{-3}. The precision on the atmospheric OH for both CIMS and LIF-FAGE has been estimated based on the variability of the atmospheric OH signal within two hours and therefore represents an upper limit precision since it is partially influenced by the atmospheric variability of the ambient OH (Hens et al., 2014).

The correlation coefficient, $R^2 = 0.4$, is affected by the large scatter of the LIF OH data due to low laser power, a rapidly ageing detector, and the large contribution that the background signal makes to the total signal. Overall, the LIF measures higher OH values with a comparison slope of 1.30, however the difference is within the accuracy of the instruments (HORUS: 42%, 2σ; CIMS: 64%, 2σ) .

During the DOMINO HO_x campaign in November 2010 (Fig. 2.11), the background OH signal was always below 4 x 10^6 molecules cm^{-3} contributing about 50% to the total OH measured during the day and 100% during the night.

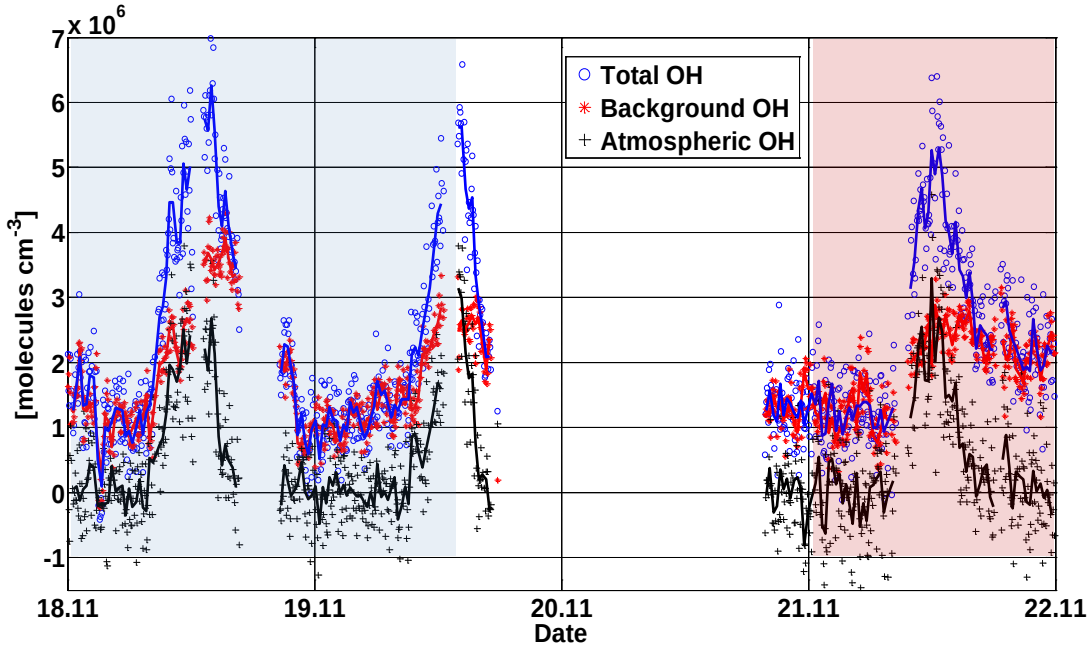

Figure 2.11. OH signals measured by HORUS during the DOMINO HO_x campaign. The blue circles represent the total OH signal measured in the absence of an OH scavenger. The red stars represent the background OH measured during the injection of an OH scavenger. The black crosses represent the atmospheric OH obtained by difference between total OH and background OH. The solid lines are 30 minute averages. The two shaded areas represent the two prevailing wind directions: the blue area during wind from the continental sector and the red area from the Huelva sector. Time is in UTC.

During the three days of measurements, two different wind sectors were sampled; air travelling from the city of Huelva and air travelling over the continent. There appears to be little difference between the contributions of the background signal in either of these wind sectors.

Figure 2.12 shows the OH signals measured by the LIF during the HOPE 2012 campaign for a day at the beginning of the campaign (Fig. 2.12a) and a day at the end of the campaign (Fig.

2.12b). The data shown are representative of the concentrations generally observed during the campaign period.

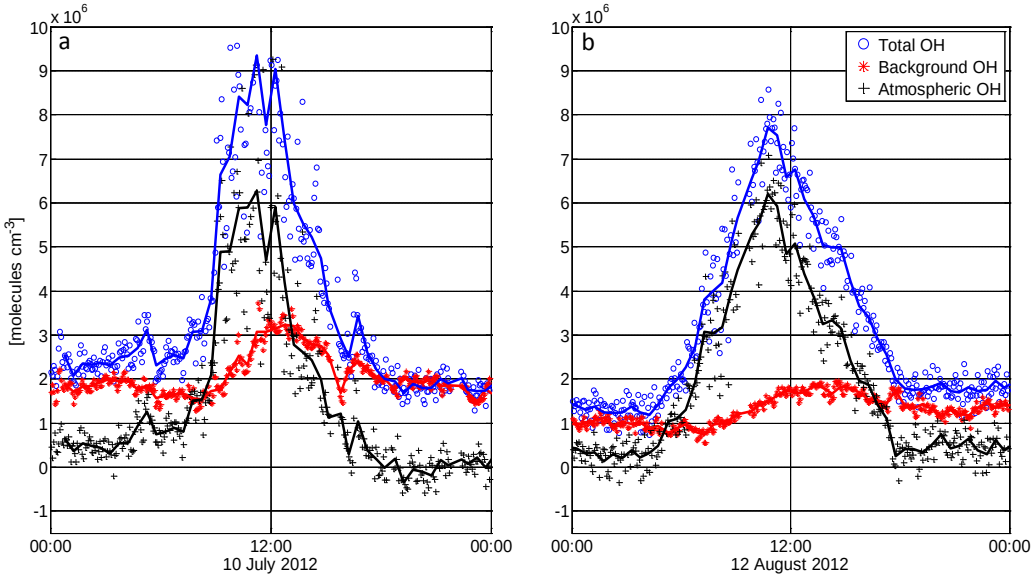

Figure 2.12. OH signals measured by HORUS during the HOPE 2012 campaign for a day at the beginning (a) and at the end (b) of the campaign. The blue circles represent the total OH signal measured in the absence of an OH scavenger. The red stars represent the background OH measured during the injection of an OH scavenger. The black crosses represent the atmospheric OH obtained by difference between total OH and background OH. The solid lines are 30 minute averages. Time is in UTC.

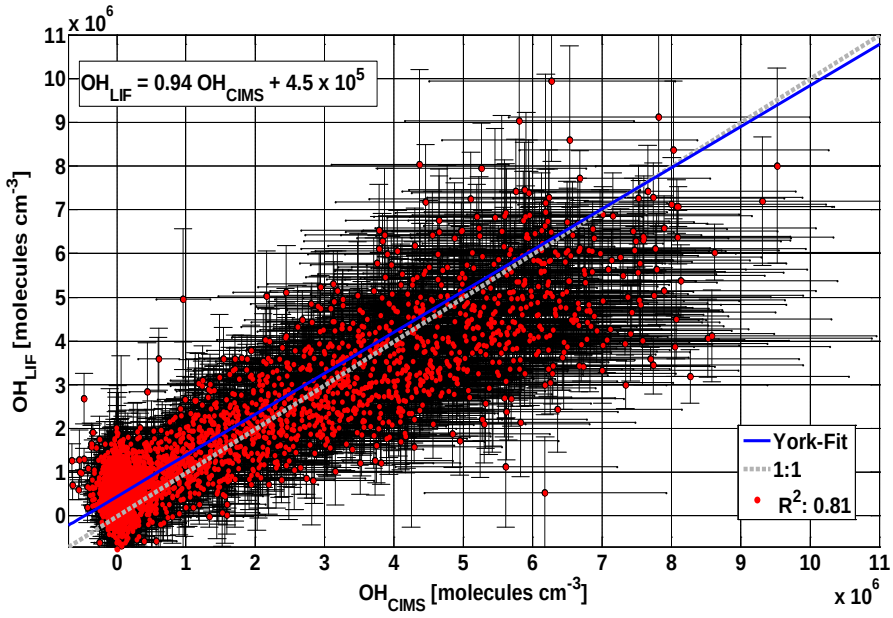

Figure 2.13. Comparison of OH radical measurements by HORUS LIF and DWD-CIMS instruments during the HOPE 2012 campaign based on 4 minute average data. The linear regression follows the

method by York et al. (2004) yields a slope of 0.94 ± 0.01 and an offset of (4.5 ± 0.06) x 10^5 molecules cm^{-3}.

During the whole campaign the HORUS LIF was measuring side-by-side with a CIMS instrument (DWD-CIMS). The agreement between the two measurements of atmospheric OH is good (Fig. 2.13), with a correlation coefficient for the entire data set of $R^2 = 0.81$, a slope of 0.94 and an offset of 4.5 x 10^5 molecules cm^{-3}. The offset is mainly caused by night time atmospheric OH observed during several nights by the HORUS instrument. The night time OH measured by HORUS is not constant: during some nights the two instruments agree, both showing an OH signal scattering around zero. Propane was used as scavenger under the same instrumental conditions during periods when HORUS did and did not measure zero atmospheric OH. No correlation between the atmospheric OH measured during night and the background OH was observed. In addition, preliminary budget calculations suggest that as the OH reactivity measured was very small during night time, the production of OH via recycling of HO_2 through NO and from ozonolysis of VOCs could lead to a concentration of ~ 3 x 10^5 molecules cm^{-3}, similar to what is detected by HORUS. However it is still unclear why the DWD-CIMS has not detected the expected night time OH concentration and further investigations are needed. The background OH signal during the campaign ranged from a minimum of 1x10^6 to a maximum of 7 x 10^6 molecules cm^{-3} on two days during which forest cutting was performed near the site but it was, for the most part, below 4 x 10^6 molecules cm^{-3}. The background signal contributed between 20% and 40% to the total OH signal during daytime and up to 100% of the total OH signal during night time.

The three measurement campaigns show large differences in the background OH signal and its contribution to the total OH signal measured by HORUS. The smallest contribution to the total OH was observed during HOPE 2012, where the total OH measured by HORUS during day time for most of the days would have agreed with the DWD-CIMS instrument within the accuracy of the instruments even without the chemical scavenger method. At the other extreme lies the HUMPPA-COPEC 2010 campaign where the background OH signal within the forest canopy reaches 1 x 10^7 molecules cm^{-3} on top of a smaller atmospheric OH concentration, often below 2 x 10^6 molecules cm^{-3}. The relative contribution of the background signal is lower for the measurement period on the tower where the atmospheric concentration of OH is higher due to larger values of $J_{O(^1D)}$ compared to the location below the canopy. One difference between the conditions in HOPE 2012 and HUMPPA-COPEC

2010 is the measured OH reactivity, which was relatively high during HUMPPA-COPEC 2010, on average 12 s^{-1} with peaks of over 40 s^{-1} (Nölscher et al., 2012) and often below the detection limit during HOPE 2012 (on average 3.5 ± 2 s^{-1}). The average concentration of measured BVOCs (isoprene, (-)/(+) α- pinene, (-)/(+) β-pinene, 3-carene, myrcene, sabinene) is similar for the two campaigns; approximately 300 pptv (Hens et al., 2014) with HUMPPA-COPEC 2010 showing higher concentrations of monoterpenes and large emissions rates of sesquiterpenes (Yassaa et al., 2012) compared to the HOPE 2012 campaign in addition to unexplained OH reactivity (Nölscher et al., 2012) that indicates the presence of unmeasured VOCs (Di Carlo et al., 2004). The interpretation of the DOMINO HO_x data is more complex; this campaign was at the same site of the DOMINO 2008 campaign but only a few trace gases (ozone and NO_x) and some meteorological parameters were measured in 2010. During the DOMINO 2008 campaign HORUS was in use without the injection of a chemical scavenger and due to the observation of an interfering signal during DOMINO HO_x, the OH concentration measured previously should be considered an upper limit. Because DOMINO HO_x was performed during the same month as the DOMINO 2008 campaign and no sign of differences in local pollution (street work, new buildings next to the site, etc.) or unusual weather was observed, we expect a similar amount of background OH, i.e., about 50% of the total OH measured in DOMINO HO_x, for the DOMINO 2008 campaign. During DOMINO 2008 relatively high OH reactivity was measured, with an average of approximately 18 s^{-1} (Sinha et al., 2012), as well as low concentrations of measured BVOCs (mainly isoprene, eucalyptol and (-)/(+) camphor) consistent with low emissions from vegetation during fall, in the range of 50 pptv (Song et al., 2011) with isoprene being the most abundant BVOC measured. The concentration of anthropogenic VOCs (AVOCs) measured was on average 400 pptv consisting mainly of benzene and toluene, although only a fraction of the AVOCs was quantified on this campaign. The highest reactivity was found for air masses arriving from the continental sector due to the likely presence of reactive oxidation products formed from primary anthropogenic emissions, followed by the air coming from the Huelva sector because of the load of AVOCs (Sinha et al., 2012). As shown in figure 2.11, there is no clear difference between the background OH contributions to the total OH signal for the air arriving from those two different wind sectors indicating a similar influence on the background OH signal and a small contribution when compared to the OH background

observed during the HUMPPA-COPEC 2010 where the measured BVOC concentrations were higher.

In summary, when the instrument was located within the canopy of a monoterpene dominated forest environment with high BVOC concentrations and high OH reactivity, the OH measurements with HORUS was strongly affected by an interference resulting in a high background OH signal. Aged air masses containing oxidation products from anthropogenic emissions and primary AVOCs such as benzene and toluene measured in high concentrations during DOMINO 2008 seem to give rise to a smaller background OH signal. The HUMPPA-COPEC 2010 campaign was an extreme case where most of the total OH measured by the instrument was due to the background OH signal, in part because of the large background, but also because the atmospheric OH concentration was low. In contrast, during DOMINO HO_x the total OH signal was not completely dominated by the contribution from the background signal even though the atmospheric OH concentration is comparable to that observed during HUMPPA-COPEC 2010. During HOPE 2012, a higher OH concentration in combination with a relatively low background OH signal, comparable to that in DOMINO $HO_{x,}$ makes the contribution of the background OH to the total OH small during daytime. It is also evident that for all three measurement campaigns performed with IPI nearly the entire nocturnal OH signal detected is due to the background OH in the instrument and not due to atmospheric OH.

2.5 Hypothesis about the origin of the background OH

2.5.1 Instrumental tests

The background OH measured with the HORUS instrument changes during the day and varies with different environments. As mentioned in the introduction, LIF-FAGE instruments are known to be affected by interferences (Holland and Hessling, 1995; Martinez et al., 2004); most of the known interferences are caused by laser photolysis or by fluorescence of other molecules in the vicinity of 308 nm wavelength. An interference caused by laser photolysis can be detected by observing a square dependency of the signal with laser power while a spectral interference can be eliminated by tuning the excitation laser on and off

resonance with the OH transition line at 308 nm. Interferences caused by laser photolysis occur when an atmospheric trace gas is photolysed by one photon of the laser beam and produces OH directly that can then be excited by a second photon of the same laser. This could happen, for example, with HONO, HNO_3 and ROOH. Other species such as ozone and acetone can also be photolysed by the laser beam but, as the photolysis does not produce OH directly, the laser pulse of HORUS is too short (15 ns) to allow the excitation of the resultant OH to happen within the same pulse. If the transport of these OH molecules out of the detection volume is sufficiently fast, the subsequent laser pulse will not be able to excite them. If the transport time is not sufficient, the subsequent pulse will excite the formed OH. Both laser generated interferences will show a square dependency with the laser power. Although interferences tests were performed on GTHOS (Ren et al., 2004), the HORUS instrument based on GTHOS also makes use of a White cell to increase the sensitivity of the HO_x measurements. Test results for the species listed above (Ren et al., 2004) showed that the ambient concentration needed for these species to produce a detectable OH interference in the instrument has to be well above "usual" ambient conditions and higher than the values observed during the field campaigns described in this paper. Nevertheless, to test whether the origin of the background OH signal is photolytic, during the HUMPPA-COPEC 2010 and HOPE 2012 campaigns the laser power was varied by a factor of four. The background OH signal did not show any dependency when plotted against the laser power at the OH cell (Fig. 2.14).

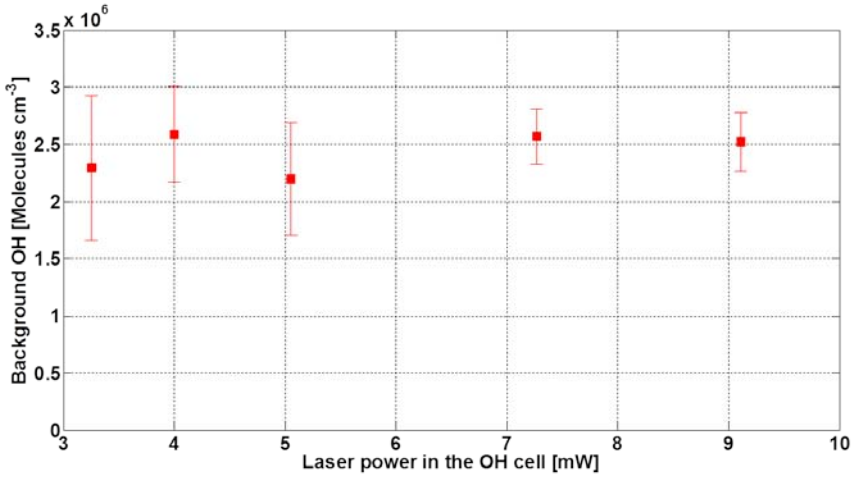

Figure 2.14. Background OH measured during the night (low variability) at 5 different values of laser power at the OH detection cell.

Therefore, we can exclude that the background OH signal is generated by the laser within the main air flow.

Since the residence time of an air parcel in the detection area of the White cell of HORUS instrument is more than two times shorter than the time period between two consecutive laser pulses at a laser repetition rate of 3000 Hz, interferences due to double pulsing are unlikely to happen. Still, if air is collected in pockets in the White cell arms (Fig. 2.15) for an extended period of time there could be production of OH.

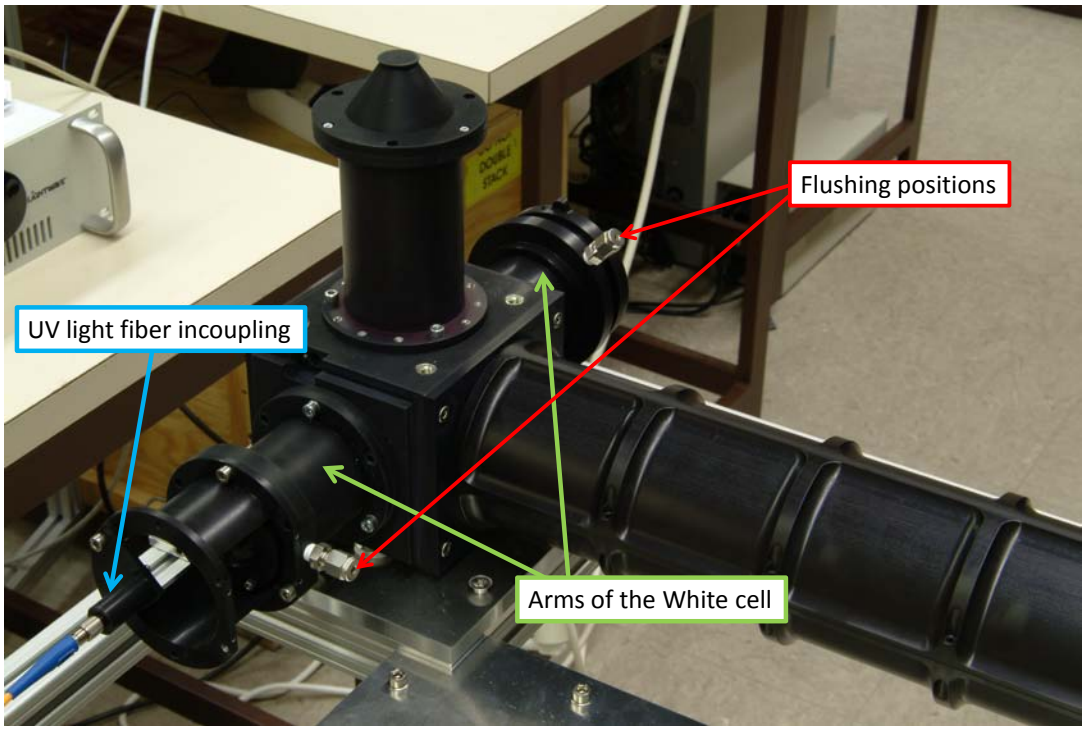

Figure 2.15. Picture of the White cell in use in the HORUS instrument highlighting arms and flushing positions of the White cell and position of the UV fiber incoupling.

To inhibit this, the arms of the White cell are constantly flushed with synthetic air that avoids deposition of particles on the mirrors and prevents the air from becoming stagnate. In addition, baffles are mounted between the arms of the White cell and the detection cell helping to reduce the scatter light of the laser and reduce the opening between the White cell arms to the detection cell letting less air to pass. To confirm that we are not affected by formation of OH in pockets in the White cell arms, the flushing flow inside the White cell was increased by a factor of two. Figure 2.16 shows a test completed during HOPE 2012 in the evening, when the background OH was measured for different flushing flows in the cell. There is a general decreasing trend in the background OH due to ambient variability of the

signal but no difference is observable when changing the flushing in the cell for two consecutive periods.

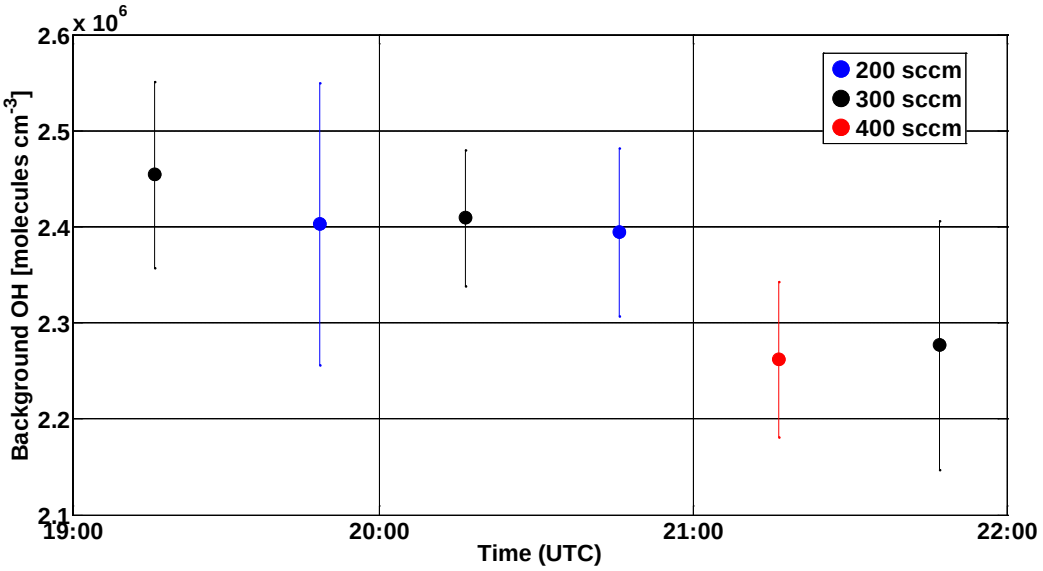

Figure 2.16. Background OH measured while changing the flushing inside the White cell. The circles represent the averages over 30 minutes.

No difference in the background OH was also observed when comparing the signal detected during night time with and without baffles and while flushing the White cell pockets with C_3F_6, an OH scavenger, instead of with synthetic air. This confirms that the background OH signal in the detection volume is not formed in air pockets inside the White cell.

The background OH is also not formed by a leakage/back flushing of NO into the OH cell during the injection in the HO_2 cell as no difference in the signal was observed during two consecutive periods with and without NO injection.

Finally, the possibility of formation of OH from reactions happening on walls was investigated by changing the material of the instrument inlet and by coating the inside walls with heavy water and detecting OD, but again no significant difference in the signal was observed nor was OD detected.

The results of the previously described tests show that it is unlikely that the background OH is an instrumental artefact and it is likely that the signal measured during field campaigns is caused by one or more atmospheric trace gases sampled by the instrument.

3.3.2 Criegee intermediates hypothesis

The pressure inside the instrument (~ 3.5 hPa) is such that bimolecular reactions with the concentrations of trace gases in the atmosphere are negligible in the transient time in the instrument. As laser photolysis and spectral interference can also be excluded from generating an OH signal within the HORUS instrument, one possible explanation for the background OH observed could be the unimolecular decomposition of an atmospheric trace gas species inside the instrument with formation of OH. Possible candidates are Criegee intermediates formed during the ozonolysis of unsaturated compounds. Criegee intermediates are known to promptly decompose and produce OH at low pressure (Criegee, 1975; Neeb and Moortgat, 1999; Donahue et al., 2011; Vereecken and Francisco, 2012). To test for this within the HORUS instrument, an ozonolysis experiment with propene was performed at ambient pressure (930 hPa) and temperature (293 K) in a flow tube connected to the inlet of HORUS. Initially, ozone (1.3 x 10^{13} molecules cm^{-3}), produced by passing pure oxygen in front of a mercury lamp, was injected into the flow tube (Fig 2.17, green shaded area) at ambient pressure. Subsequently, a high concentration of OH was produced from photolysis of water by a mercury lamp, and introduced into the flowtube (Fig 2.17, yellow shaded area). Propane was then injected into the flow tube at a concentration, 2.5 x 10^{16} molecules cm^{-3}, enough to remove 99% of the observed OH (Fig 2.17, blue shaded area). The mercury lamp was then removed and the propane injection was stopped. Only ozone and propene were injected into the flow tube (Fig 2.17, orange shaded area). It is possible to observe a high OH signal generated from the ozonolysis of propene. To assess if the OH is only formed in the flow tube at ambient pressure or partly in the low pressure segment of the instrument, the same concentration of propane used to remove 99% of the OH produced from the photolysis of water was injected. It is possible to observe that, despite sending the same amount of propane, there is only a small reduction in the OH signal. As the concentration of propane injected was sufficient to remove the OH generated in the flow tube at ambient pressure, the remaining OH still observed by HORUS has to be generated inside the low pressure segment of the instrument.

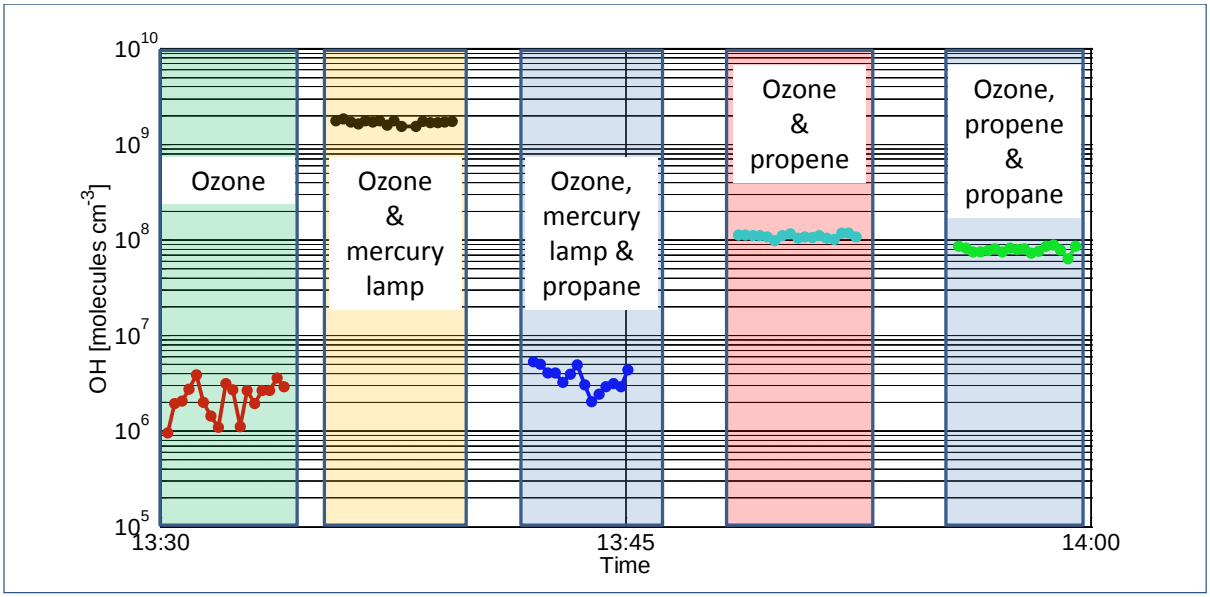

Figure 2.17. Ozonolysis test of propene in the presence of propane as an OH scavenger. The green shaded area represents the signal observed by HORUS when only ozone was injected in the flow tube. The yellow area shows the OH signal generated by photolysis of water. The first blue shaded area shows the reduction of the OH signal generated by photolysis of water after the addition of propane to the flow tube. The pink shaded area shows the signal measured while injecting ozone and propene into the flow tube. The second blue shaded area shows the small reduction observed in the signal when injecting propane into the flow tube to scavenge the OH produced.

This test indicates how the HORUS instrument is sensitive to OH formed within the instrument during ozonolysis of propene. A more detailed description of the experimental setup together with modelling and a thorough description of the chemistry of Criegee intermediates and investigation of their impact on the IPI-LIF-FAGE can be found in Novelli et al. (2014b). To understand if the signal observed by HORUS during the ozonolysis of propene in presence of an OH scavenger originated from walls or pockets of air in the White cell, the experiment was repeated using a single pass setup. The dependency of the signal on the laser beam position within the detection cell was tested by moving the laser beam from the centre of the cell towards the sides. Figure 2.18 shows no clear dependency of the signal detected during ozonolysis of propene in the presence of an OH scavenger on the position of the laser beam. As for the background OH observed during field measurement, this confirms that the signal is not due to the White cell structure.

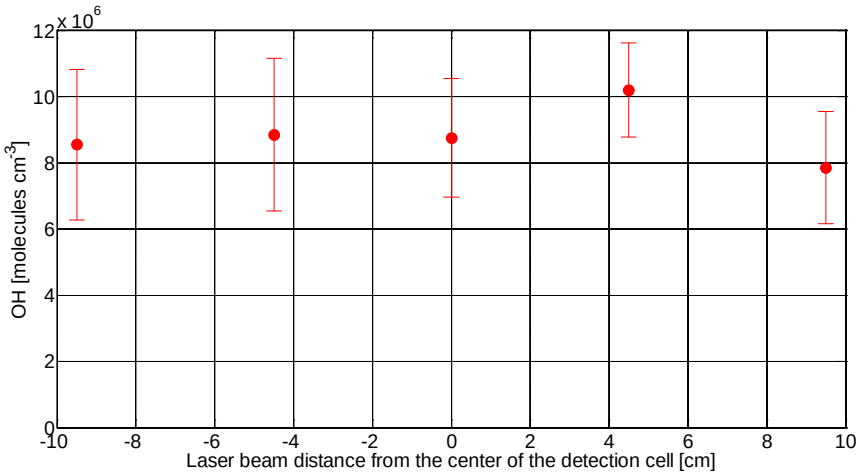

Figure 2.18. OH signal detected during the ozonolysis of propene in the presence of an OH scavenger for different positions of the laser beam inside the detection cell.

The previous test indicates that the HORUS instrument is sensitive to OH formed within the instrument during ozonolysis of propene but more laboratory and field tests are necessary to completely ascertain whether the background OH observed during field campaigns entirely originates from the same chemical processes.

2.6 Possible influence on earlier measurements

The background OH signal depends on the type of environment and appears to be strongly related to the VOC concentration and type of VOC prevalent. It is possible that previous campaigns performed with LIF instruments without applying a chemical scavenger method have been affected by an interfering species in a similar manner as described in this manuscript. However, as underscored previously by Mao et al. (2012), the design of each particular LIF-FAGE system is likely to determine whether, and to what extent, the instrument suffers from this interference and so we will confine this discussion to the HORUS instrument.

The environment of previous campaigns may give an indication as to whether the measured OH was affected by significant inferences. The first campaign with HORUS consisted of a formal blind comparison, HOxCOMP, between several LIFs, a CIMS and a DOAS instrument both in a chamber and in ambient air. The results of the campaign are

comprehensively described in Schlosser et al. (2009). During daytime, the agreement between all the instruments in the chamber was good with a regression slope between the MPI LIF and the FZJ-DOAS of one, but in ambient air the MPI LIF instrument measured higher concentrations of OH than the CIMS (Schlosser et al., 2009). As we noticed an unattributed change in the calibration factor of the instrument of 30%, we cannot exclude a change in the same order of magnitude in the calibration source between the period in the chamber and in ambient that might explain the difference between the OH concentration measured by the MPI LIF and the one measured by the CIMS in ambient air. Night time data from HORUS are not shown either from the chamber period nor in ambient air because of large unexplained measured OH signals up to 4×10^6 molecules cm^{-3} (Kubistin, 2009). Based on what we have learned since the use of IPI, it is likely that the high night time signal was due to a chemical interference in the HORUS instrument, however during day time its concentration appeared to be low enough in that specific environment, as to not produce a significant OH interference (i.e., within the accuracy of the instrument). Two subsequent campaigns, using HORUS, were performed without IPI. GABRIEL, an aircraft based campaign, took place in October 2005 over the tropical rain forest in equatorial South America (Kubistin, 2009). Measured OH was much higher than predicted by a traditional chemical mechanism. Further analysis indicated that OH might be recycled within the isoprene degradation scheme. (Lelieveld et al., 2008; Kubistin et al., 2010; Taraborrelli et al., 2012). Although without IPI we cannot completely rule out a possible interference for our measurements, laboratory tests and quantum mechanical calculation as follow up studies to GABRIEL provided evidence for the proposed OH recycling, which was previously not accounted for (Dillon and Crowley, 2008; da Silva, 2010a; Peeters and Müller, 2010; Crounse et al., 2011). Even though laboratory (Crounse et al., 2011) and chamber studies (Fuchs et al., 2013) predict a smaller concentration of OH from the recycling of isoprene then reported in Lelieveld et al. (2008), measurements with a different LIF-FAGE instrument in the Borneo rainforest during the OP3 campaign (Whalley et al., 2011) also showed a large discrepancies between measured and modelled OH using the traditional chemical mechanism. The elevated concentration of OH measured during OP3 was supported from co-measurements of formaldehyde and glyoxal made with a DOAS (Whalley et al., 2011). In addition, a side-by-side airborne comparison between the aircraft configuration of the GTHOS LIF instrument (ATHOS - Airborne Tropospheric Hydrogen Oxides Sensor)

employed without a chemical scavenger method and a CIMS (Ren et al., 2012), showed good agreement even at higher levels of isoprene. The aircraft campaign HOOVER, performed without IPI in the upper troposphere across Europe in September 2007 (Regelin et al., 2013) showed good agreement between the measured OH and a simple box model. This, together with the observations during other HORUS field campaigns and preliminary laboratory tests, suggests that the background OH observed by HORUS might be related to shorter-lived species, which likely do not have a significant impact on the upper troposphere due to the relatively large distance between the emission source and the measurement point.

2.7 Conclusions

An improved methodology to measure the OH radical with a LIF-FAGE instrument has been developed and deployed in three different environments. Results show that the use of the IPI-LIF-FAGE technique for HORUS results in good agreement with OH data measured with two different CIMS instruments during two campaigns. A thorough and careful characterisation of the operational parameters was necessary to find the optimum conditions to avoid inefficient mixing of the scavenger and the sampled air, excessive titration of OH in the low pressure side of the instrument and large losses of OH on the walls of IPI. The best results were achieved when using propane as OH scavenger in a concentration of 2.5×10^{15} molecules cm^{-3} with a carrier gas flow of at least 6000 sccm and a residence time after the injection of the scavenger of ~ 4 ms. The use of a chemical scavenger method revealed the presence of a background OH signal that, using the same calibration factor as for atmospheric OH, spanned a concentration of 5×10^5 to 1×10^7 molecules cm^{-3} in the environments described. Without the chemical scavenger method the atmospheric OH measured during the HUMPPA-COPEC 2010, DOMINO HO_x and HOPE 2012 campaigns, during day and night time, would have been overestimated. Further investigations into the origin and cause of such a background OH signal will be the subject of ongoing work though it is already clear that the background OH has a strong connection with the type of environment in which the instrument is deployed. Although it is very likely that the presence and extent of a chemical interference in different LIF-FAGE systems for the measurement of OH are dependent on the

particular instrument design, our experience shows that the determination of the background OH should be a prerequisite for these systems and the ambient measurement of OH.

3 Direct observation of OH formation from stabilised Criegee intermediates

A. Novelli[1], L. Vereecken[1], J. Lelieveld[1] and H. Harder[1]

[1] {Atmospheric Chemistry Dept., Max Planck Institute for Chemistry, 55128 Mainz, Germany}

Manuscript published in Physical Chemistry Chemical Physics

Abstract. The *syn*-CH_3CHOO Criegee intermediate formed from the ozonolysis of propene and (E)-2-butene was detected via unimolecular decomposition and subsequent detection of OH radicals by a LIF-FAGE instrument. An observed time dependent OH concentration profile was analysed using a detailed model focusing on the speciated chemistry of Criegee intermediates based on the recent literature. The absolute OH concentration was found to depend on the steady state concentration of *syn*-CH_3CHOO at the injection point while the time dependence of the OH concentration profile was influenced by the sum of the rates of unimolecular decomposition of *syn*-CH_3CHOO and wall loss. By varying the most relevant parameters influencing the SCI chemistry in the model and based on the temporal OH concentration profile, the unimolecular decomposition rate k(293 K) of *syn*-CH_3CHOO was shown to lie within the range 3-30 s^{-1}, where a value of 20 ± 10 s^{-1} yields the best agreement with the CI chemistry literature.

3.1 Introduction

Criegee intermediates (CI, carbonyl oxides) are key intermediates in the atmospheric

ozonolysis of unsaturated compounds. This class of reactions has been studied for many years (Atkinson and Arey, 2003) because of its importance in the oxidation of volatile organic compounds (VOC) in the boundary layer, and plays a key role in the formation of free radicals and secondary organic aerosol (Johnson and Marston, 2008). Ozonolysis of alkenes in the gas phase proceeds via the Criegee mechanism (Criegee, 1975; Donahue et al., 2011) depicted in Figure 3.1.

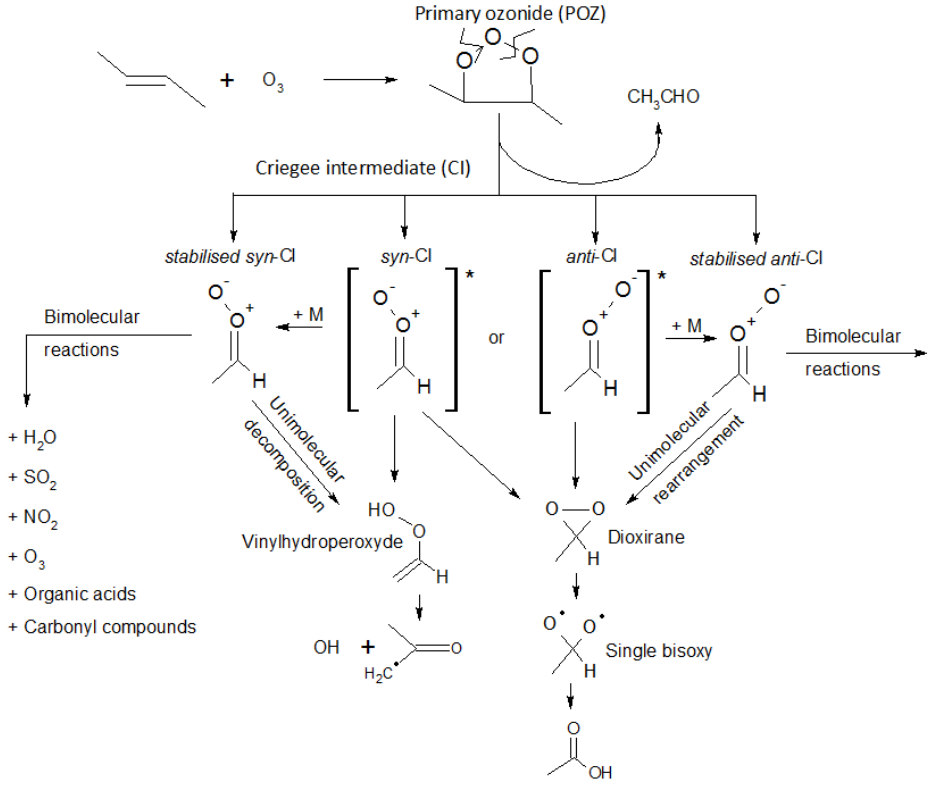

Figure 3.1. Cycloaddition of ozone across an unsaturated compound and potential fates of the Criegee intermediate formed.

The addition of ozone across the double bond forms a primary ozonide (POZ) which quickly decomposes forming a Criegee intermediate (CI) and a carbonyl compound. The fate of the Criegee intermediate depends on its nascent energy content, which we broadly divide in two populations (Kroll et al., 2001; Donahue et al., 2011; Drozd and Donahue, 2011): thermally stabilized and chemically activated. The chemically activated Criegee intermediate has a high energy content and therefore a comparatively short lifetime. Typically, it will decompose through the vinyl hydroperoxide (VHP) or ester channels discussed below, though depending on the reaction rates at the given energy and the rate of energy loss in collisions with the bath

gas, it can form a stabilised Criegee intermediate (SCI). For example, chemically activated CH_2OO will mostly decompose, as the internal energy is distributed across only a few degrees of freedom, leading to very fast unimolecular reactions, while larger CI such as those obtained from terpenoid ozonolysis will mostly stabilise at 1 atm. The SCI has a longer lifetime owing to its lower thermal energy content: in the atmosphere its fate depends on the competition between unimolecular decomposition and reaction with atmospheric trace gases. The two main unimolecular decomposition channels accessible to both chemically activated and stabilised CI are the ester and the VHP channel, whose contributions depends on the substituents on the carbonyl carbon atom and their orientation relative to the outer CI oxygen atom (Vereecken and Francisco, 2012) (Fig.3.1). CI can isomerise by ring closure, forming a dioxirane that in turn re-isomerizes to an ester or an acid; for small alkenes these latter compounds will receive enough internal energy to immediately decompose forming CO_2, OH, CO, HO_2, H_2O and alkyl fragments. If the outer oxygen is pointing towards a suitable H-atom such as in an alkyl group (*syn*-CI) a faster 1,4-H-shift is accessible, yielding a vinyl hydroperoxide which promptly decomposes forming OH and a vinoxy radical (Paulson et al., 1999; Johnson and Marston, 2008; Drozd and Donahue, 2011; Lu et al., 2014). This path is a major non-photolytic source of OH radicals in the atmosphere (Gutbrod et al., 1997; Anglada et al., 2002; Kuwata et al., 2005) and appears to be especially important during winter, at night and indoors (Taatjes et al., 2014). CI with more complex substituents are subject to additional unimolecular rearrangements (Vereecken and Francisco, 2012). For the CI discussed in this paper, *syn*-CI yield OH radicals through the VHP channel, while *anti*-CI and CH_2OO rearrange through the ester channel.

Historically (Johnson and Marston, 2008) it was assumed that the fate of SCI formed in the atmosphere would mainly be reaction with water or unimolecular decomposition (Johnson et al., 2001). Several laboratory studies during the last two years (Taatjes et al., 2012; Welz et al., 2012; Ouyang et al., 2013; Taatjes et al., 2013; Buras et al., 2014; Liu et al., 2014b; Stone et al., 2014; Welz et al., 2014) report measured rate coefficients for the reaction between SCI and several atmospheric trace gases such as SO_2, NO, NO_2, H_2O, acetone, acetaldehyde and organic acids. For some coreactants, these studies have reported larger rate coefficients than expected (Hatakeyama et al., 1986). Likewise, CI photolysis reactions were shown to occur (Beames et al., 2013; Liu et al., 2014a) on a time scale similar to measured CI decomposition (Horie et al., 1997; Berndt et al., 2012). Theoretical work (Mansergas and Anglada, 2006;

Vereecken and Francisco, 2012; Kjaergaard et al., 2013; Su et al., 2014; Vereecken et al., 2014a) suggested the possible importance of reactions between SCI and ozone, RO_2, alcohols, OH, HO_2, and self reaction. The use of these updated rate coefficients in simple model analysis (Vereecken et al., 2012; Boy et al., 2013; Ouyang et al., 2013; Percival et al., 2013; Pierce et al., 2013; Sarwar et al., 2013; Sarwar et al., 2014; Taatjes et al., 2014) reveals how, depending on the environment, the loss of some of the SCIs analysed is not only caused by reaction with water, but includes a number of other trace gases, indicating that SCIs might impact oxidation processes in the atmosphere. As highlighted by Taatjes et al. (2014) SCI have not yet been directly observed in the atmosphere. Still, SCI have been invoked to explain additional oxidation of SO_2 in the boreal forest (Mauldin III et al., 2012), and as the cause of internally generated OH within a LIF (laser induced fluorescence) FAGE (fluorescence assay by gas expansion) instrument (Mao et al., 2012) measuring in a forest. During ambient measurements using a LIF-FAGE system we also detected a sizable background signal in a number of environments(Novelli et al., 2014a), which may owe its presence to the detection of ozonolysis products.

In this paper, we demonstrate the direct formation of OH radicals from SCI decomposition within a LIF-FAGE instrument, presenting results from the reaction of ozone with propene, (E)-2-butene and ethene as SCI sources. The time-dependent OH profiles are analyzed using a detailed chemical model including updated chemistry of CI, yielding an upper and lower limit for the syn-SCI decomposition rate. The relevance for atmospheric chemistry and for OH-measurements based on LIF-FAGE instruments is discussed.

3.2 Methodology

3.2.1 Laboratory instrumentation

The ozonolysis experiments (Fig. 3.2) were carried out in a quartz flow tube (inner diameter 4.5 cm; length 50 cm) at ambient pressure (980 hPa) and temperature (293 K) using nitrogen (Westfalen, 99.999%) with 5 % of oxygen (Westfalen, 99.999%) as a bath gas.

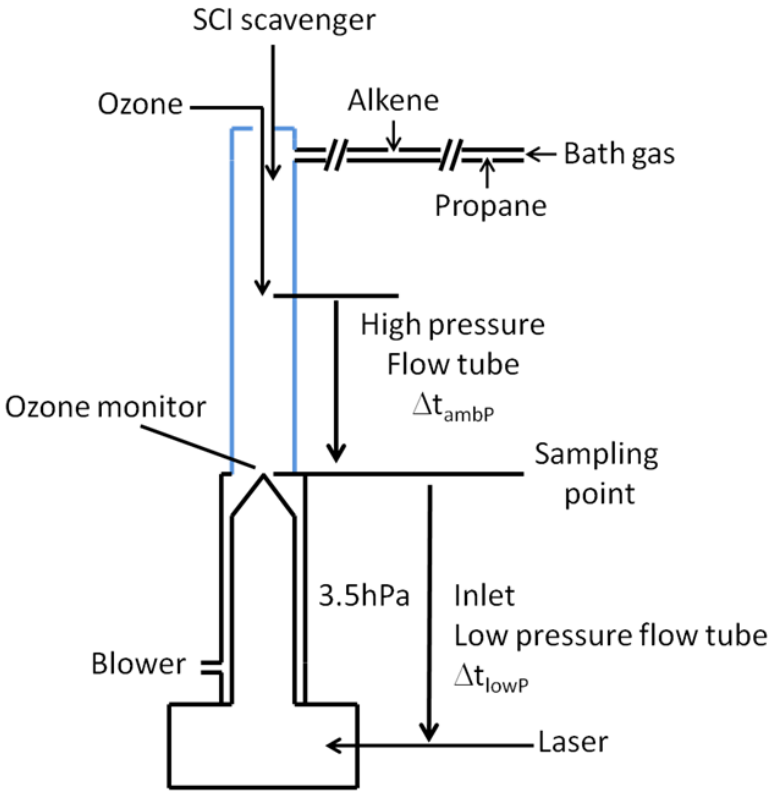

Figure 3.2. Schematic of the key features of the experimental setup.

The flow tube is directly connected to the inlet of the LIF-FAGE instrument used to measure the concentration of OH during the experiments. A blower was connected to the base of the flow tube after the sampling position of the LIF-FAGE instrument in order to assure sampling from the center and reduce wall effects. The resulting gas flow of nitrogen in the flow tube was 15000 sccm. By titrating OH with methane at the flow conditions described above, the residence time in the flow tube at ambient pressure (Δt_{ambP}) was measured to be 2.5 s. Ozone was produced outside the tube by passing pure oxygen in front of a mercury UV lamp (Hg(Ar) Pen Ray lamp) and was injected together with nitrogen to improve the mixing in the center of the flow tube. The initial ozone concentration in the flow tube was monitored using an ultraviolet photometric ozone analyser (Thermo Environmental Instruments: 49C) by measuring the attenuation of light in the absorption cell at a wavelength of 254 nm.

The alkenes tested were ethene (Air Liquide, 99.99 +%), propene (pure, Aldrich 295663, 99+% and Air Liquide 10% in nitrogen) and (E)-2-butene (Sigma-Aldrich, 295086, 99+%). The alkenes were added via a MFC and injected in a stream flow of nitrogen to enhance the mixing and then injected at the top of the tube. Additionally, propane (Westfalen 3.5, 99.95% purity) was used to scavenge the OH radicals formed at ambient pressure in the flow tube and

was added directly in the stream flow of nitrogen. A mixture of SO_2 in synthetic air (Air Liquide, 2%) was used as a SCI scavenger during some experiments as well as acetic acid (AppliChem, 96%) and water vapor. The flow of SO_2 was controlled with an MFC and injected at the top of the flow tube, while acetic acid vapour was added to the flow tube by passing a small flow of nitrogen through a bubbler filled with bulk acetic acid. Water vapor was produced by passing nitrogen through a bubbler filled with deionized water and the concentration of water vapor in the flow tube was measure with a high-precision chilled mirror dewpoint hygrometer (Michell Instruments, model S4000).

The OH concentration was measured with HORUS (Hydroxyl Radical Measurement Unit based on fluorescence Spectroscopy), the LIF-FAGE instrument in use at the Max Planck Institute for Chemistry in Mainz described in detail elsewhere.(Martinez et al., 2010; Novelli et al., 2014a) Only a brief description highlighting the features particularly relevant for the current experiments is given. The inlet sampled the reaction mixture with a 1 mm nozzle pinhole from the centre of the flow tube. The OH radical was detected in the low-pressure segment of the instrument (~ 3.50 hPa) by measuring the fluorescence signal after excitation with a UV pulsed light at around 308 nm. The temperature in the low-pressure segment of the instrument was measured with a thermistor positioned in the center of the air flow and, at a distance of 13 cm from the pinhole and beyond, is equal to ambient temperature, ~ 293 K. Shorter distances could not be examined due to practical limitations. The pressure in the detection axis was sufficiently low to prevent most of the bimolecular reactions (see below). In order to avoid formation of OH radical in the detection cell of the instrument via reactions initiated by the laser beam, such as photolysis of ozone, and formation of OH radicals after reaction of $O(^1D)$ with water molecules, the repetition rate of the Nd:YAG laser was 1500 Hz. With this repetition rate, the residence time of the air sample in the detection cell was five times shorter than the time period between two laser pulses.

By using different inlet lengths it was possible to measure the concentration of OH after different “residence” times inside the low pressure segment of the instrument (Δt_{lowP}), between the sampling point and the laser beam. To characterize the residence time, a Nd:YAG laser (Quantel Brilliant) at 266 nm and with a 6 ns laser pulse was used to produce OH directly in front of the inlet nozzle by photolysis of ozone and the subsequent reaction of $O(^1D)$ with water. The residence time of the OH produced was measured using a Turbo-MCS (multichannel scaler, EG&G ORTEC's) and by starting the scan at the pulse of the Brilliant

laser. An OH concentration profile in time was obtained and the maximum occurrence of OH concentration was adopted as the residence time. The test was repeated for all inlet lengths used during the experiments and results are shown in figure 6.1.

3.2.2 Characterization of wall losses

In order to improve the understanding about the origin of the OH signal in the LIF-FAGE instrument and to better characterize the evolution of the hydroxyl radicals (HO_x) radicals in the low-pressure region of the instrument, tests to determine the losses of OH and hydroperoxyl radical (HO_2) inside the instrument have been performed. The HO_x radicals have been produced before the inlet by passing humidified air in front of a mercury lamp with a known actinic flux and in the setup used to calibrate the instrument for field measurement, as described elsewhere.(Martinez et al., 2010) OH was detected as described in the previous section while HO_2 was detected as OH after reaction with nitric oxide (NO) injected immediately before the detection cell. Wall losses of radicals as a function of residence time were determined by varying the injection position at a constant radical concentration and the results are shown in figure 6.2 and 6.3 for OH and HO_2 respectively. By using a chi-square fit an effective "unimolecular" loss rate on walls of 55 s^{-1} for OH and 26 s^{-1} for HO_2 was extrapolated.

3.2.3 Box model

The results obtained from the different experiments were compared against the results of a box model based on the Master Chemical Mechanism (MCM) version 3.2 (Jenkin et al., 1997; Saunders et al., 2003), available at http://mcm.leeds.ac.uk/MCM, and the simulations were integrated using FACSIMILE (Curtis and Sweetenham, 1987). To simulate our experiments, ethene, propene and (E)-2-butene MCM schemes were modified and extended to fully describe production and destruction of speciated stabilized and excited CI formed in the ozonolysis. The full mechanism for the alkenes studied is presented in the supplementary information. The main extensions concerning the CI formation are the inclusion of direct formation of thermal SCI, and explicit speciation of different CI conformers (*syn* and *anti*) which effectively act as different species owing to the high barrier (over 20 kcal mol^{-1}) for

syn-anti isomerisation (Vereecken and Francisco, 2012; Nakajima and Endo, 2014). The yields of formation of OH and SCIs were guided by the values used in the MCM scheme (Table 3.1). As there is quite a large uncertainty between different studies on the SCI yields we allowed the value to change between 0.35 (Niki et al., 1981) and 0.5 (Horie and Moortgat, 1991) for ethene, 0.16 (Rickard et al., 1999) and 0.35 (Horie and Moortgat, 1991) for propene and 0.15 (Rickard et al., 1999) and 0.4 (Berndt et al., 2012) for (E)-2-butene in the sensitivity studies on model parameters (Table 3.1).

Table 3.1. Yields of SCI, of CH_2OO (a), *syn*- CH_3CHOO (b) and *anti*-CH_3CHOO (c).

Alkenes	**SCI[a]**	**SCI yield range[b]**	**Ratio range a:b:c[b,c] (C. D. Rathman et al., 1999; Fenske et al., 2000b; Kroll et al., 2002)**
Ethene	0.4	0.35 – 0.5	1 : 0 : 0 - 1 : 0 : 0
Propene	0.24	0.16 – 0.35	0.5 : 0.5 : 0.0 - 0.5 : 0.1 : 0.4
(E)-2-butene	0.18	0.15 – 0.4	0 : 0.8 : 0.2 - 0 : 0.2 : 0.8

a. As used in the MCM mechanism.
b. Range of values examined for the SCI yield, and for the ratios of the different SCI during the sensitivity study of the model (see main text).
c. The yields are showed as a fraction of the total SCI yield.

Yields of formation of *syn* relative to *anti* SCI were based on theoretical (C. D. Rathman et al., 1999; Fenske et al., 2000b) and experimental (Kroll et al., 2002) studies when available (Table 3.1). Given the high uncertainty we varied these yields in the sensitivity study by a factor of 4 to estimate their impact on the model results. Another important difference with the MCM is the inclusion of a larger number of bimolecular reactions involving SCI based on recent experiments (Berndt et al., 2012; Taatjes et al., 2012; Taatjes et al., 2013; Buras et al., 2014; Stone et al., 2014) and theoretical studies (Mansergas and Anglada, 2006; Vereecken et al., 2012, 2014a) (Table 3.2). In table 3.2 the values of the CI-specific rate coefficients with H_2O and $(H_2O)_2$, the relative rate predictions by Anglada et al. (2011) and Ryzhkov and Ariya (2004) were scaled to match the absolute value for *anti*-$CH_3CHOO + H_2O$ as measured by Taatjes et al. (2013).

Table 3.2. Rate coefficients for reactions of Criegee intermediates in laboratory and atmospheric reaction conditions

Coreactants	CI	k (298K)	References
H_2O	H_2COO	$2x10^{-16}$ cm^3 s^{-1}	41
	syn-CH_3CHOO	2×10^{-19} cm^3 s^{-1}	(Anglada et al., 2011)
	anti-CH_3CHOO	1×10^{-14} cm^3 s^{-1}	(Taatjes et al., 2013)
$(H_2O)_2$	H_2COO	7×10^{-11} cm^3 s^{-1}	(Ryzhkov and Ariya, 2004; Ryzhkov and Ariya, 2006; Vereecken et al., 2012)
	syn-CH_3CHOO	3×10^{-14} cm^3 s^{-1}	(Ryzhkov and Ariya, 2004; Ryzhkov and Ariya, 2006; Vereecken et al., 2012)
	anti-CH_3CHOO	5×10^{-11} cm^3 s^{-1}	(Ryzhkov and Ariya, 2004; Ryzhkov and Ariya, 2006; Vereecken et al., 2012)
Ketones	all	2×10^{-13} cm^3 s^{-1}	(Taatjes et al., 2012)
Aldehydes	all	1×10^{-12} cm^3 s^{-1}	(Stone et al., 2014)
Hydroxyl compounds	all	5×10^{-12} cm^3 s^{-1}	(Vereecken et al., 2012)

Carboxylic acids	all	2.5×10^{-10} cm^3 s^{-1}	(Welz et al., 2014)
Ethene	H_2COO	6×10^{-16} cm^3 s^{-1}	(Buras et al., 2014)
Propene	H_2COO	2×10^{-15} cm^3 s^{-1}	(Buras et al., 2014)
	syn-CH_3CHOO	2×10^{-18} cm^3 s^{-1}	(Vereecken et al., 2014a)
	anti-CH_3CHOO	9×10^{-15} cm^3 s^{-1}	(Vereecken et al., 2014a)
(E)-2-butene	*syn*-CH_3CHOO	1.7×10^{-19} cm^3 s^{-1}	(Vereecken et al., 2014a)
	anti-CH_3CHOO	1.4×10^{-15} cm^3 s^{-1}	(Vereecken et al., 2014a)
NO_2	all	2×10^{-12} cm^3 s^{-1}	(Taatjes et al., 2013; Stone et al., 2014)
SO_2	H_2COO	4×10^{-11} cm^3 s^{-1}	(Welz et al., 2012)
	syn-CH_3CHOO	2×10^{-11} cm^3 s^{-1}	(Taatjes et al., 2013)
	anti-CH_3CHOO	7×10^{-11} cm^3 s^{-1}	(Taatjes et al., 2013)
O_3	all	4×10^{-13} cm^3 s^{-1}	(Vereecken et al., 2014b)

CO	all	4×10^{-14} cm^3 s^{-1}	(Vereecken et al., 2012)
OH	all	5×10^{-12} cm^3 s^{-1}	(Vereecken et al., 2012)
HO_2	all	5×10^{-12} cm^3 s^{-1}	(Vereecken et al., 2012)
RO_2	all	5×10^{-12} cm^3 s^{-1}	(Vereecken et al., 2012)
Organic peroxides	all	$3x10^{-12}$ cm^3 s^{-1}	(Vereecken et al., 2014b)
decomposition	all *syn*-CI	$3 - 76^a$ s^{-1}	(Horie and Moortgat, 1991; Fenske et al., 2000a)
H_2COO	H_2COO	4×10^{-10} cm^3 s^{-1}	(Su et al., 2014)
CI + CI	all	3×10^{-11} cm^3 s^{-1}	(Buras et al., 2014)

a. Range of values from experimental studies.

The unimolecular decomposition rate coefficient of SCI is highly uncertain, with literature data (Horie and Moortgat, 1991; Fenske et al., 2000a; Berndt et al., 2012; Taatjes et al., 2013) spanning well over an order of magnitude; we estimate this rate parameter from the comparison of model and experiment together with wall losses of SCI, which could not be experimentally determined; these two parameters are strongly coupled in our analysis (see below). Wall-losses of OH (55 s^{-1}) and HO_2 (26 s^{-1}) in the low-pressure segment of the instrument as determined earlier were also included in the model. The concentrations of alcohols, aldehydes, ketones, organic acids and peroxides formed during the ozonolysis were summed to allow for their reactions with SCI. The initial conditions for each of the experiments, as shown in Table 3.3, were used for the initialization of the corresponding box models.

Table 3.3. Initial concentrations for the ozonolysis experiments in the flow tube.

Species	Alkenes [molecules cm^{-3}]	SCI scavenger [a]
Ethene	1.1×10^{16}	Water vapor
Propene	3.5×10^{15}	Water vapor, SO_2
	1.8×10^{15}	
(E)-2-butene	1.4×10^{15}	SO_2, acetic acid

Propane and ozone concentrations were 2.5×10^{16} and 1.3×10^{13} molecules cm^{-3}, respectively, for all experiments unless indicated.

a. Added during some experiments.

The box model runs are not used to obtain optimal fits of kinetic parameters to the observations; rather, we adhere as much as possible to the available literature data, and analyze the experimental data against this model, within the respective margins of the uncertainty, to elucidate the underlying chemistry and to obtain uncertainty intervals for the rate of unimolecular decomposition.

3.3 Results

3.3.1 Comparison of model and experiment

The qualitative comparison of the kinetic box model results against the experimental data is based on the absolute OH concentration and its time dependence. As shown below for each of the reaction systems, the OH concentration time profile in the low pressure flow tube is determined primarily by (pseudo) first order reaction kinetics, i.e., wall losses and unimolecular decay of SCI and OH radicals. Hence, the absolute height of the OH profile predicted by the model is determined mainly by the SCI steady state concentration $[SCI]_{SS}$ at the sample point. Many kinetic parameters in the model that determine this steady state concentration carry a comparatively large uncertainty: rate coefficients for SCI unimolecular and bimolecular reactions, the yield of SCI and its speciation into *syn*- and *anti*-SCI in the

ozonolysis reaction, etc. The uncertainties of each of these parameters only affect the model to experiment intercomparison to the extent to which they affect $[SCI]_{SS}$, and hence can be lumped into an uncertainty factor governing this $[SCI]_{SS}$. In this work, we allow for the steady state concentration to be adjusted by a small factor to fit the absolute profile heights.

The time profile of the OH signal shows a steep rise of the OH concentration by SCI decomposition until steady state is reached with OH loss processes, followed by a slower decay of the steady-state OH signal by depletion of the SCI. This time dependence is determined mostly by the ratio of total SCI loss to OH loss rates, where the OH wall loss has been measured directly, and the bimolecular reactions of OH operate under pseudo first order conditions and have well known rate coefficients. This indicates that the uncertainty of the time dependence in our model is sensitive mostly to the sum $k_{uni}(SCI \rightarrow OH) + k_{wall}(SCI)$ of unimolecular SCI decomposition to OH and wall losses, respectively. The contribution of each parameter in this sum affects the absolute OH signal, but this cannot be distinguished from uncertainties of $[SCI]_{SS}$ at the sample point; this makes it infeasible to derive an accurate unimolecular rate coefficient for OH formation from syn-SCI from our present set of data.

A quantitative uncertainty analysis is given below.

3.3.2 Propene

Figure 3.3 shows a typical evolution of the OH radical concentration measured with our LIF-FAGE instrument averaged over several experiments of propene ozonolysis (red bullets), and compared to a model simulation (black line).

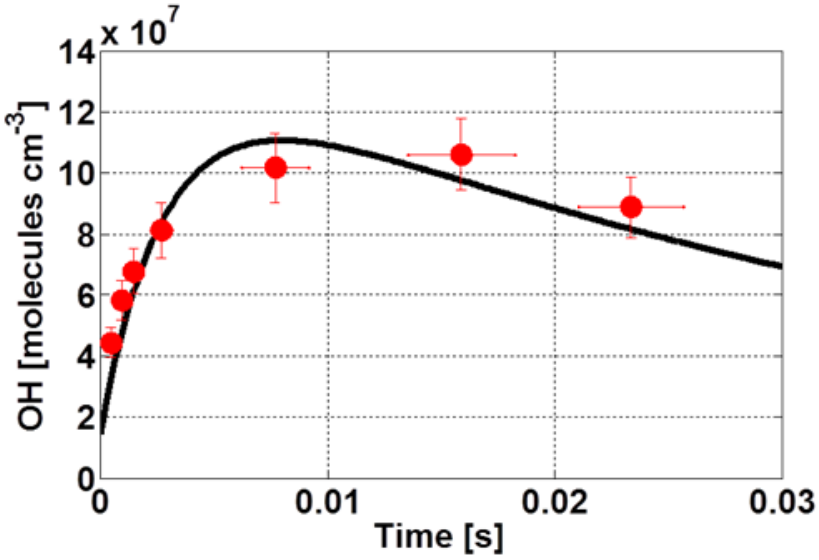

Figure 3.3. Temporal profile of the OH signal (red bullets) inside the detection cell of the LIF-FAGE instrument for the ozonolysis reaction of propene, and the model simulation (black line).

The model reproduces the experimental data within their uncertainty ranges, as discussed in more detail below. The model adequately simulates the observed data with injection of different propane concentrations in the flow tube (Fig. 6.4). The modelling study shows that at ambient pressure the OH radical (Fig. 6.5a) is formed mainly by unimolecular decomposition of chemically activated *syn*-CH_3CHOO, and removed quickly by propene and propane scavengers, leading to a negligible OH concentration. Stabilized *syn*-CH_3CHOO (Fig. 6.6a) formed in the ozonolysis of propene attains a slowly decreasing steady state concentration, where the relative contributions of the individual loss reactions change with time owing to the change in concentration of the bimolecular coreactants. The main loss paths are unimolecular decomposition and reaction with ozone, whereas reaction with organic peroxy radicals (RO_2), alcohols, aldehydes and organic peroxides become more important at later reaction times. As the rate coefficients for these reactions are uncertain, a number of different scenarios will be discussed in detail later. In the low pressure region inside the inlet (Fig. 6.6b) the ozonolysis reaction is effectively stopped, such that there is no additional formation of SCIs. Their losses are governed by the unimolecular decomposition and wall losses. Unimolecular decomposition of *syn*-CH_3CHOO is the dominant source, > 95%, of the OH radicals observed, while OH loss is determined by residual scavenging by propene and propane, and by wall loss (Fig. 6.5b). The degree of OH scavenging was varied in a series of experiments with lower propene concentrations and with different addition of propane (Fig

6.7). By using lower concentrations of propene, the OH concentration profile shows a less steep decrease slope as implied by the reduced removal of OH. The box model again reproduces these data, indicating that OH loss is simulated realistically. Table 6.1 lists the predicted concentrations of SCIs at the sampling point together with the peak concentration of OH observed for the different experiments.

3.3.3 (E)-2-butene

Figure 3.4 shows the evolution of the average OH radical concentration measured with our LIF-FAGE instrument during several experiments of ozonolysis of (E)-2-butene (red bullet) compared with a model simulation (black line). Likewise, the factors influencing the steady state concentration of the SCI in the ambient pressure region are similar (Fig 6.10) with unimolecular decomposition and reaction with O_3 and RO_2 being the main loss processes for *syn*-CH_3CHOO at the beginning of the flow tube, and with the relative importance of reactions with aldehydes, alcohols and peroxides increasing when approaching the sample point. Similar to the propene experiment the relative importance and contribution of the coreactants towards the total losses of *syn*-CH_3CHOO depends on its unimolecular decomposition rate, and different scenarios will be discussed later. Table 6.2 lists the predicted concentrations of SCIs at the sampling point together with the peak concentration of OH observed for the different experiments.

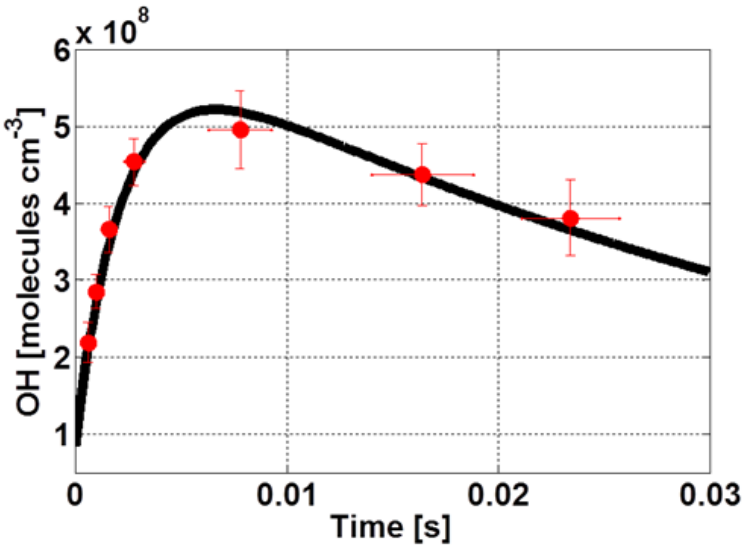

Figure 3.4. Temporal profile of the OH signal (red bullets) inside the detection cell of the LIF-FAGE instrument for the ozonolysis reaction of (E)-2-butene, and model simulation (black line).

3.3.4 Ethene

The ozonolysis reaction of ethene does not form SCI that are expected to decompose thermally to OH, and hence this reaction serves as a blank experiment quantifying the formation of OH from the basic alkene ozonolysis reaction intermediates and from the CH_2OO SCI also formed in propene ozonolysis. Figure 6.11 shows that the OH concentration quickly grows to 6.5 x 10^6 molecules cm^{-3}, observed after ~ 1 ms, and then decreases quickly. These concentrations are a factor of 20-100 below those observed for propene and (E)-2-butene, indicating that this OH contribution is negligible in the latter experiments. By increasing the amount of propane injected in the flow tube (Fig. 6.12) we observe a decrease in the measured OH concentration, showing clearly that some residual OH scavenging occurs in the low pressure region of the LIF-FAGE, affecting the OH time profile.

3.3.5 Experiments with SCI scavengers

In some experiments water vapor, SO_2 and acetic acid were used to scavenge the SCIs: water vapor reacts with different Criegee intermediate conformers at different rates spanning from 1 x 10^{-14} cm^{-3} $molecule^{-1}$ s^{-1} for the reaction with *anti*-CH_3CHOO (Taatjes et al., 2013) to less than 4 x 10^{-15} cm^{-3} $molecule^{-1}$ s^{-1} and 9 x 10^{-17} cm^{-3} $molecule^{-1}$ s^{-1} for reaction with *syn*-CH_3CHOO (Taatjes et al., 2013) and CH_2OO (Stone et al., 2014), respectively. SO_2 and acetic acid both react very fast with SCI (Taatjes et al., 2013; Welz et al., 2014), ~ 4 x 10^{-12} cm^{-3} $molecule^{-1}$ s^{-1} and ~ 2.5 x 10^{-10} cm^{-3} $molecule^{-1}$ s^{-1}, respectively, and do not show a large difference in rate between different SCI conformers. These experiments were completed with the inlet length normally used during measurements of OH radicals in the atmosphere (14 cm inlet, 2.4 ms residence time). Figure 6.13 shows the decay of the OH signal observed during ozonolysis of propene with addition of water vapor between 0 and 2.3 x 10^{17} molecules cm^3. With the addition of similar concentrations of water vapor no change in the OH signal was detected during the ozonolysis of ethene. Figure 6.14 shows the disappearance of the OH peaks over the background spectrum with the addition of SO_2 during ozonolysis of propene. Precise determination of the OH concentration was not possible due to the spectral interference of SO_2 at the wavelength of detection of OH (308 nm). Figure 6.15 shows the decay of OH radical during ozonolysis of (E)-2-butene during the addition of acetic acid.

3.4 Discussion

Figures 3.3 and 3.4 show the OH signal during ozonolysis of different alkenes, and how the OH concentration depends strongly on the residence time within the LIF-FAGE instrument: in all experiments OH increase steeply to a maximum value followed by a more gradual decrease. This OH formation process has recently been suggested (Mao et al., 2012; Novelli et al., 2014a) as a source of interference in the measurement of ambient OH concentrations using LIF-FAGE instruments. The signal was proposed to originate from SCI decomposition, which would imply that Criegee intermediates are present in the troposphere in sufficiently high concentrations to affect the chemistry. Here, we present the first experimental evidence showing that the source of the OH is indeed unimolecular decomposition of syn-CH_3CHOO, followed by our analysis of the reaction kinetics involving SCI chemistry.

3.4.1 SCI as the OH source

Firstly, we can rule out that the observed OH is sampled from the high pressure flow tube, as OH is scavenged by the alkene and the added propane OH scavenger; residual OH would also not increase initially, but start at a maximum value and decrease monotonically. Secondly, the source of OH cannot be a bimolecular reaction. The pressure in the low pressure section of the instrument during the experiment was ~ 3.5 hPa, diluting the concentrations of all species by a factor of 300, therefore most bimolecular reactions would decline or be fully prohibited. Especially for the ozonolysis of the alkenes studied, a well-known source of OH, the reaction is too slow to be relevant at such pressure producing less than 5% of the total OH observed inside the instrument. For the reactants with highest concentrations, i.e., alkenes and propane, we observe some residual scavenging in the low pressure region, which is due to their high rate of reaction with OH. Any other molecule, apart from the initial reagents, can only be present in a concentration that is several orders of magnitude lower and therefore cannot be significant in the low pressure segment of the instrument. The OH within the instrument thus originates from the unimolecular decomposition of a transient species formed in the ozonolysis of the alkene. Theoretical (Gutbrod et al., 1997; Vereecken and Francisco, 2012) and experimental (Paulson et al., 1999; Kroll et al., 2001; Donahue et al., 2011) studies

strongly suggest that *syn*-CH_3CHOO is the source of OH by 1,4-H-migration, forming vinyl hydroperoxide that quickly decomposes to vinoxy radicals + OH. However, we cannot *a priori* preclude the possibility of other compounds decomposing to OH. These pathways include hot acid decomposition from dioxirane formed in the ester channel of all CIs, and thermal decomposition of stabilized ROOH hydroperoxide (including VHP). In order to confirm the role of *syn*-CH_3CHOO in the formation of OH in the instrument, we performed several experiments with SO_2, water vapor, and acetic acid, known SCI scavengers. SO_2 was shown experimentally to react very fast with all CI (Taatjes et al., 2013), but unfortunately it causes a high spectral interference in the OH measurements. By recording fluorescence spectra during the ozonolysis of propene before and after the addition of different concentrations of SO_2 (Fig. 6.14) it is possible to observe how even a small concentration of SO_2 strongly influences the OH spectrum and removes the OH peaks superimposed on the background, for all concentrations of SO2 used. The concentration of SO_2 added in the flow tube was small enough to avoid OH scavenging by SO_2, i.e., the OH radical lifetime was a factor of 50 smaller towards reaction with SO_2 compared to propene, indicating that the disappearance of the OH signal is not due to removal of OH radical by SO_2. While these experiments strongly point towards SCI scavenging, the spectral interference makes the results harder to interpret quantitatively, e.g., it is not possible to reliably derive a relative rate coefficient for SCI+SO_2 (see supporting information). SO_2 is not expected to react at an appreciable rate with ROOH molecules or any traditional intermediates formed in the ozonolysis of alkenes, leaving SCI, or products derived directly from SCI chemistry as OH sources. Similar experiments with added acetic (Fig. 6.15) acid also show a fast decrease in generated OH, but difficulties in quantifying the added concentrations of acetic acid prohibits the rate analysis of SCI scavenging. As with SO_2, we propose that acetic acid does not readily react with any intermediates other than SCI, again pointing to SCI as the likely source of OH.
The decay of the OH concentration with the addition of water vapor during the ozonolysis of propene (Fig. 6.13) likewise is consistent with SCI scavenging with a rate coefficient of SCI loss towards H_2O of ~ 3 x 10^{-17} cm^3 $molecule^{-1}$ s^{-1}, in agreement with the upper limit of 4 x 10^{-15} cm^3 $molecule^{-1}$ s^{-1} measured by Taatjes et al. (2013) and in fair agreement with the (scaled) theoretical predictions listed in table 3.2. A more detailed discussion is available in the supporting information. The rate coefficient between H_2O and *anti*-CH_3CHOO has been measured (Taatjes et al., 2013) at 1 x 10^{-14} cm^3 $molecule^{-1}$ s^{-1}, which is too fast to explain the

water-dependent signal decrease observed during our experiment. Hence, the OH we observe does not originate from *anti*-CH_3CHOO, and hence also not from dioxiranes or hot acid decomposition formed in the SCI ester channel. This is also in agreement with the very small yields of OH formation observed in ozonolysis reaction of ethene, a source of CH_2OO. Most of the literature data (Vereecken and Francisco, 2012) point to VHP as a very short-lived species that promptly decomposes to vinoxy radical + OH upon formation from the higher energy *syn*-SCI prior to collisional thermalization. Drozd et al. (Drozd et al., 2011) observed secondary OH formation in chamber experiments on a time scale of 0.5 s, which was attributed to some VHP stabilization aided by the existence of a (small) energy barrier in the VHP decomposition channel. However, given our residence time of the order of milliseconds, we would not be sensitive to OH formation on this timescale. We thus conclude that the LIF-FAGE instrument is sensitive only to *syn*-CH_3CHOO, and generally SCI that decompose thermally to OH via the VHP channel.

3.4.2 Box model results

The time dependence of the OH concentration in the low pressure section of the instrument is largely determined by the ratio of total SCI loss to OH loss rates; the OH loss rates are known given that the OH wall loss was measured directly, and the bimolecular reactions of OH occur under pseudo first order conditions and have well known rate coefficients. As shown in figures 3.5 and 3.6, by changing the total loss of *syn*-CH_3CHOO in the model simulation a change in the shape of the time dependence OH concentration was obtained. Within the error bounds of our experimental results we obtain a total SCI loss rate of $23 \pm 7\ s^{-1}$. Using literature data for the bimolecular reaction rates in the high pressure section, the model also reproduces the absolute OH concentrations within a factor 1.8 (propene) and 1.7 ((E)-2-butene), indicating that the model is remarkably accurate relative to the *a priori* uncertainties on the steady state SCI concentration at the sample point. Given that the total loss is the sum of the unimolecular decomposition rate and wall losses, the highest total SCI loss of $30\ s^{-1}$ thus translates into an upper limit for the unimolecular decomposition rate of *syn*-CH_3CHOO of $30\ s^{-1}$; faster unimolecular rates would lead to disagreement of the time-dependent OH concentration profile between experimental data and model (Fig. 3.5 and 3.6). The available

experimental data on the unimolecular decomposition rate of CH_3CHOO are few and span a large range: the values reported from experimental studies are 2.5 s^{-1} (Horie et al., 1999), 2.9 s^{-1} (Horie et al., 1997), 76 s^{-1} (Fenske et al., 2000a), and < 250 s^{-1} (Taatjes et al., 2013). A direct comparison of these rates against our results is difficult as most of the experimental data lump *syn*- and *anti*-CH_3CHOO, regardless of their strongly differing chemistry. The results by Fenske et al. (2000) of 76 s^{-1}, the only experimental value unambiguously higher than our rate, results in clear disagreement with our observed time-dependence (Fig 3.5 and 3.6). It is important to note that the reported uncertainty of the latter decomposition rate is a factor of 3 and therefore the upper limit determined in this study lies within the uncertainty range. Our upper limit result is also in agreement with theoretical calculations from Kuwata et al. (2010) who estimate a unimolecular decomposition rate for *syn*-CH_3CHOO and *anti*-CH_3CHOO of 24 s^{-1} and 64 s^{-1}, respectively, though with a high degree of uncertainty.

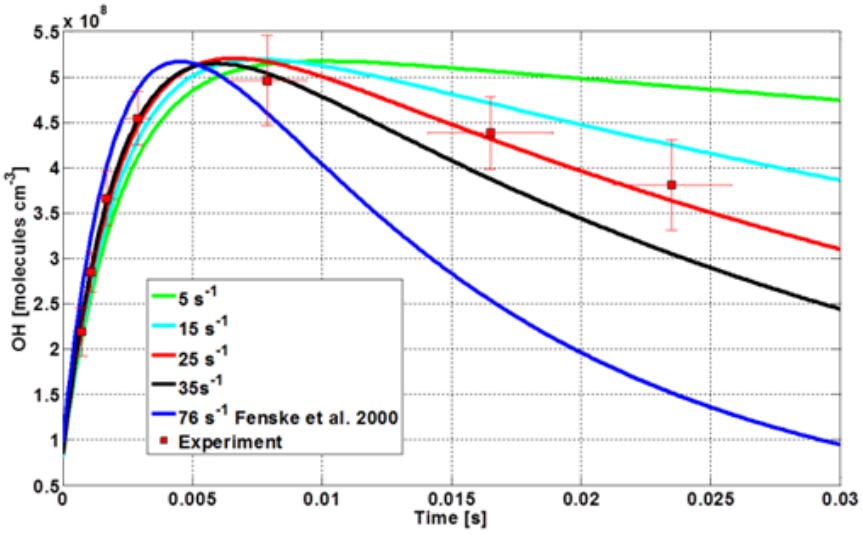

Figure 3.5. Comparison between OH concentrations observed during the ozonolysis of (E)-2-butene (red squares) and different model simulation (lines) with a total loss of *syn*-CH_3CHOO ranging from 5 to 76 s^{-1}. The model results are scaled to match the measured peak [OH], emphasizing the difference in time-dependence.

The unimolecular decomposition rate is expected to be strongly dependent on temperature (Berndt et al., 2014b). The strong pressure drop while sampling the air into the instrument leads to expansion cooling of the gas. The air quickly returns to ambient temperatures; we have established that at most at 13 cm (~ 1 millisecond) behind the pinhole the ambient temperature is regained. The expansion cooling therefore affects at most the first two points measured closest to the pinhole. These points have a negligible impact on our analysis of the

time profile (Fig 3.5 and 3.6), well below the uncertainties induced by other aspects of this work, and thus do not affect the conclusions applicable to 293 K.

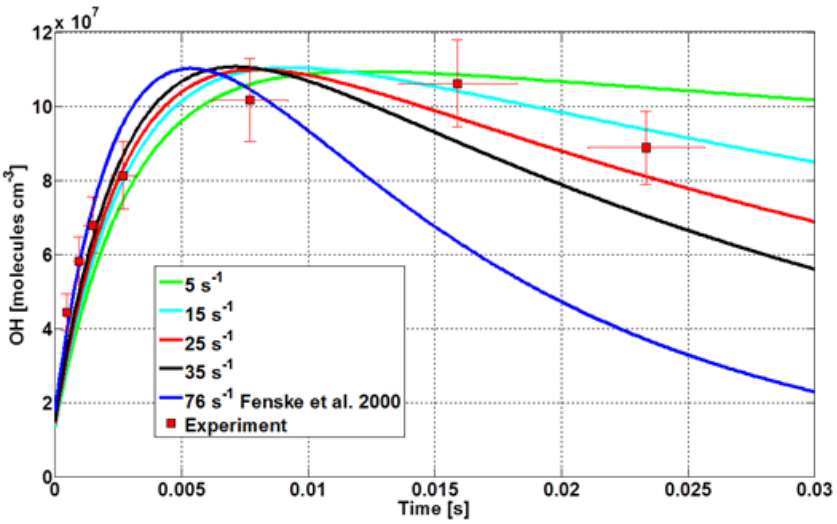

Figure 3.6. Comparison between OH concentrations observed during the ozonolysis of propene (red squares) and different model simulation (lines) with a total loss of *syn*-CH_3CHOO ranging from 5 to 76 s^{-1}. The model results are scaled to match the measured peak [OH], emphasizing the difference in time-dependence.

Determining a lower limit on the unimolecular rate, while maintaining a total loss rate of 30 s^{-1}, is less straightforward. The model contains a set of bimolecular reactions involving SCIs, where the coreactants are the initial reactants or are formed in the ozonolysis reaction, and thus have concentrations changing in time. Unfortunately there are only few accurate measurements of rate coefficients for different CI isomers. Some experimental data is available for CH_2OO chemistry, and with the help of theoretical studies it is possible to extrapolate these rate coefficients to several other reactants and SCI although with high uncertainty. In addition, the yields of SCI are uncertain and the relative yields of *syn* and *anti* have not yet been measured. We estimate a lower limit for the unimolecular decomposition rate of *syn*-CH_3CHOO by maximally decreasing the SCI losses by removing all bimolecular reactions, while increasing the yield to a reasonable maximum, i.e., the SCI is formed as 100% syn-CH_3CHOO, while the SCI yield is increased to the high end of the IUPAC recommendation uncertainty interval (Table 3.1). Using this scenario, it was no longer possible to match the OH time profile with unimolecular decomposition rates below 3 s^{-1}. This is a very conservative lower limit as many of the bimolecular reaction rates of SCI were

measured, and often appear to be faster than theoretical predictions. We therefore performed a sensitivity analysis with the model using more realistic uncertainty intervals on the kinetic parameters, i.e., varying the bimolecular reactions rates by a factor of 3 and the SCI yields and the *syn*-SCI yield within the total SCI yields in the range listed in table 3.1. We find that the combined uncertainty of the SCI concentration at the sample point under this error model is only a factor 1.5 to 3, depending on the unimolecular decomposition rate adopted.

The best agreement between the absolute OH concentrations measured and model predicted is well within this factor of 3, for unimolecular decomposition rates closer to our upper limit, 30 s^{-1}. To reproduce the absolute OH concentrations using our lower limit of 3 s^{-1}, one would need significant downscaling of the bimolecular rate coefficients, with significant deviations from the literature data by up to orders of magnitude. We therefore propose a less stringent lower limit of 10 s^{-1} for the syn-CH_3CHOO unimolecular decomposition rate coefficient, which is the lowest value that still allows us to model the absolute OH concentrations with a deviation equal to the more realistic error simulation obtained above. It should be emphasized that this limit is not based on direct experimental observations but rather on achieving reasonable agreement between our experiment and the available literature data.

3.4.3 Contributions under atmospheric conditions

The inferred unimolecular decomposition rate coefficient for *syn*-CH_3CHOO of 20 ± 10 s^{-1} together with the most recent rate coefficients for reactions between SCI and atmospheric trace gas species (Table 3.2) allow us to improve our earlier assessment (Vereecken et al., 2012, 2014a) of the relative contribution of many coreactants in the atmosphere to the atmospheric fate of a set of SCI. The major differences are a higher unimolecular decomposition rate for the different SCI and a significantly faster reaction rate with organic acids as recently measured by Welz et al. (2014) As no direct measurements are available for the unimolecular rate decomposition of CH_2OO, *anti*-CH_3CHOO and $(CH_3)_2COO$ we used the value of 20 s^{-1} measured for *syn*-CH_3CHOO for CH_2OO and $(CH_3)_2COO$. In the case of CH_2OO this rate is likely an overestimate as most of theoretical calculations (Vereecken and Francisco, 2012) predict a higher energy barrier for CH_2OO decomposition compared to *syn*-CH_3CHOO. For $(CH_3)_2COO$ the barrier heights derived theoretically (Vereecken and Francisco, 2012) are a bit lower than those for *syn*-CH_3CHOO possibly indicating the

unimolecular decomposition rate of 20 s^{-1} might be an underestimation. For *anti*-CH_3CHOO the value of 60 s^{-1} was used as calculated by Kuwata et al. (2010); the value predicted in their study for *syn*-CH_3CHOO, 24 s^{-1}, is in fair agreement with the value measured in this study.

Table 3.4. Loss path contributions (fraction) as a function of CI substituents and environment.

	Boreal forest		**Tropical forest**	**Mega city**	**Rural Europe**	
H_2COO	**Day**	**Night**	**Day**	**Day**	**Day**	**Night**
H_2O	0.01	0.01		0.01	0.01	0.01
$(H_2O)_2$	0.99	0.99	1	0.98	0.99	0.99
Ester channel				0.01		
***anti*-CH_3CHOO**						
H_2O	0.25	0.39	0.18	0.35	0.26	0.46
$(H_2O)_2$	0.75	0.6	0.82	0.63	0.73	0.52
Ester channel		0.01		0.01	0.01	0.02
Carboxylic acids				0.01		
***syn*-CH_3CHOO**						
H_2O	0.01					
$(H_2O)_2$	0.11	0.08	0.3	0.03	0.14	0.03
VHP	0.42	0.77	0.45	0.27	0.57	0.85
NO_2			0.02	0.02		
SO_2	0.01	0.01		0.03	0.01	
O_3	0.01	0.01		0.01	0.01	0.02
Carbonyl compounds				0.01		0.01
Carboxylic acids	0.42	0.12	0.22	0.57	0.27	0.09

Hydroxyl compounds	0.02	0.01	0.01	0.06		
$(CH_3)_2COO$						
H_2O	0.02	0.03	0.04	0.01	0.02	0.01
$(H_2O)_2$			0.01		0.01	
VHP	0.47	0.82	0.62	0.28	0.64	0.87
NO_2				0.02		
SO_2	0.01	0.01		0.03	0.01	
O_3	0.01	0.01		0.01	0.02	0.02
Carbonyl compounds				0.01		0.01
Carboxylic acids	0.47	0.12	0.32	0.58	0.30	0.09
Hydroxyl compounds	0.02	0.01	0.01	0.06		

Table 3.4 lists the predicted contributions of the various loss processes in different environments as defined earlier (Birmili et al., 2003; Handisides et al., 2003; Shirley et al., 2006; Case Hanks, 2008; Lelieveld et al., 2008; Fortner et al., 2009; Junninen et al., 2009; Petäjä et al., 2009; Wood et al., 2009; Vereecken et al., 2012, 2014a) updated by using carboxylic acid concentrations from Limón-Sánchez et al. (2002) for urban conditions and Grossmann et al. (2003) for the rural Europe environment, respectively. Compared to these earlier estimates, even with a faster unimolecular rate for both CH_2OO and *anti*-CH_3CHOO and a very fast reaction rate with organic acids, these two SCIs are still found to be lost mainly via reaction with water dimers both during day and nighttime. Recent studies (Berndt et al., 2014c) show that this reaction is indeed very fast at least for CH_2OO, with $k(SCI + (H_2O)_2)/k(SCI + SO_2) = 0.29$. Therefore, model studies on the impact of CI on the chemistry of the atmosphere should incorporate water dimer reactions. As the unimolecular decomposition rate and the reaction rate with organic acids are very fast for both *syn*-CH_3CHOO and $(CH_3)_2COO$, these become the main loss path in all environmental conditions analysed contributing for up to 80% of the total loss of the two conformers. Reaction with SO_2 still occurs even though it only represents a very minor SCI loss. During nighttime, as

the concentrations of most coreactants are lower than during daytime, the main loss for both *syn*-CH_3CHOO and $(CH_3)_2COO$ is represented by unimolecular decomposition via the VHP channel, representing a potentially important source of ambient OH radical.

3.5 Conclusions

A LIF-FAGE instrument, normally operated for in-situ atmospheric OH measurements, was used to observe directly, for the first time, the OH formation from unimolecular decay of *syn*-CH_3CHOO Criegee intermediates generated in the ozonolysis reaction of a set of alkenes. Using scavenging experiments and extensive comparison with the available literature data on CI chemistry we could exclude other reactions and compounds as the potential OH source. In particular, CH_2OO and *anti*-CH_3CHOO are not the source of the OH, in agreement with mechanistic understanding of carbonyl oxide chemistry.

A clear time dependence of the OH signal was observed, showing a fast rise to the steady state concentration, followed by a more gradual decay following depletion of the SCI reactants. Based on the shape of this temporal OH profile, we determined the *syn*-SCI decomposition rate coefficient k(293 K) to be within the range of 3 to 30 s^{-1}. The lower limit of this interval is increased to 10 s^{-1} based on the level of agreement between measured and modelled absolute OH concentrations, where the higher values yield the best correspondence with the literature data on SCI formation and bimolecular reactions.

The formation of OH from *syn*-SCI decomposition within the FAGE instrument corroborates earlier reports on interferences of the OH measurements (Mao et al., 2012; Novelli et al., 2014a). It was recently proposed to estimate and correct for this by pulsed scavenging of the OH to distinguish the background, SCI-generated OH from the atmospheric OH. The observed time dependence of the OH signal in the current work also suggests that very short inlets would be less affected by the interference, though the interfering signal is strictly speaking only eliminated at zero length. For all other inlet lengths the amount of SCI-generated OH depends on the concentration of *syn*-SCI within the reactant mixture and the rate coefficients for decomposition for each of the SCI in the sampled air. As this reaction system is currently insufficiently characterized, it is recommended that FAGE measurements incorporate blank measurements by OH scavenging techniques to improve the reliability of

the ambient OH detection. Our current experiments do not fully exclude other interferences in FAGE OH measurements that cannot be eliminated with the proposed technique.

4 Identification of Criegee intermediates as potential oxidants in the troposphere

A. Novelli[1], K. Hens[1], C. Tatum Ernest[1], M. Martinez[1], A. C. Nölscher[1], V. Sinha[2], W. Song[1], P. Paasonen[3], T. Petäjä[3], M. Sipilä[3], P. Keronen[3], T. Elste[4], C. Plass-Dülmer[4], G. J. Phillips[1,5], J. Williams[1], H. Fischer[1], L. Vereecken[1], J. Lelieveld[1] and H. Harder[1]

[1]{Atmospheric Chemistry Dept., Max Planck Institute for Chemistry, 55128 Mainz, Germany}

[2]{Department of Earth and Environmental Sciences, Indian Institute of Science Education and Research Mohali, Sector 81 S.A.S. Nagar, Manauli PO, Mohali 140 306, Punjab, India}

[3]{Dept. Phys., P.O. Box 64. 00014 University of Helsinki, Finland}

[4]{German Weather Service, Meteorological Observatory Hohenpeissenberg (MOHp), Albin-Schwaiger-Weg 10, 83282 Hohenpeissenberg, Germany}

[5]{Department of Natural Sciences, University of Chester, Thornton Science Park, Chester, CH2 4NU, UK}

Manuscript in preparation

Abstract. In this paper we examine an extensive dataset from the HUMPPA-COPEC 2010 and the HOPE 2012 field campaigns, together with available literature data, which suggests the presence of stabilized Criegee intermediates (SCI) in the troposphere. For the campaigns

described, the background OH signal observed in the IPI-LIF-FAGE instrument in use at the Max Planck Institute for Chemistry is proposed to be caused by stabilised Criegee intermediates. This proposal is based on the observed correlations with temperature, concentrations of unsaturated volatile organic compounds and concentrations of ozone. The background OH concentration also correlates with the unknown production rate of sulfuric acid. A range for the stabilised Criegee concentration of 10^4 to 10^6 molecules cm^{-3} is calculated for two environments, Boreal forest and rural Germany. There are, however, large uncertainties in these calculations owing to the many unknowns associated with the chemistry of Criegee intermediates.

4.1 Introduction

Criegee intermediates (CI), or carbonyl oxides, are formed during the ozonolysis of unsaturated organic compounds (Criegee, 1975; Johnson and Marston, 2008; Donahue et al., 2011): ozone attaches to the double bond forming a primary ozonide (POZ) that, in the gas phase, quickly decomposes forming a Criegee intermediate and a carbonyl compound. The CI exists as thermally stabilized CI (SCI) and chemically activated CI (Kroll et al., 2001; Drozd et al., 2011). The chemically activated Criegee intermediates have a high energy content and in the atmosphere will either undergo unimolecular decomposition or will be stabilized by collisional energy loss, forming SCI.

For many decades the chemistry of Criegee intermediates was investigated both with theoretical (Vereecken and Francisco, 2012) and with indirect experimental studies (Johnson and Marston, 2008; Taatjes et al., 2014). During the last few years, numerous experimental studies specifically on stabilized Criegee intermediates have been performed subsequent to their first detection by Welz et al. (2012). Many laboratories have now detected SCI with various techniques (Berndt et al., 2012; Ouyang et al., 2013; Taatjes et al., 2013; Ahrens et al., 2014; Buras et al., 2014; Liu et al., 2014a; Novelli et al., 2014b; Sheps et al., 2014; Stone et al., 2014) and have confirmed that they are very reactive towards many atmospheric trace gases. Currently, the most studied Criegee intermediates are formaldehyde oxide, CH_2OO, acetaldehyde oxide, CH_3CHOO (*syn* and *anti*, *i.e.* with the outer oxygen pointing towards or away from an alkyl group, respectively) and acetone oxides, $(CH_3)_2COO$.

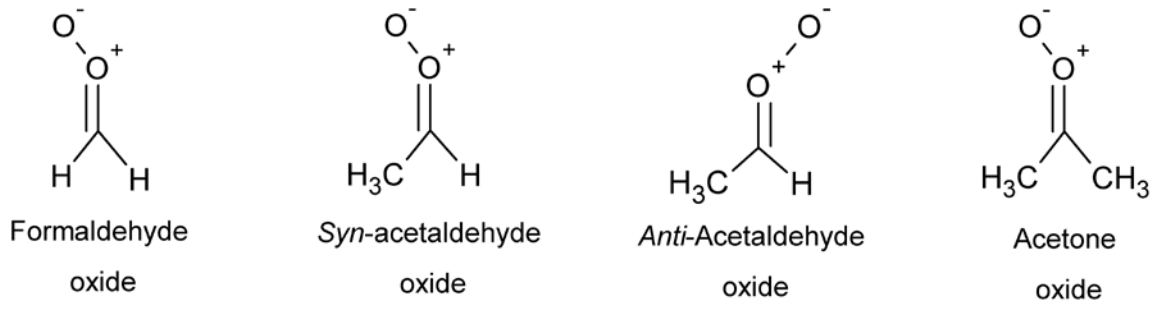

The importance of Criegee intermediates as oxidants in the atmosphere depends on their rate coefficient with water vapour as water is ubiquitously present in high concentrations in the boundary layer. The rate of this reaction strongly depends on the CI conformation (Aplincourt and Ruiz-López, 2000; Tobias and Ziemann, 2001; Ryzhkov and Ariya, 2003; Kuwata et al., 2010; Anglada et al., 2011) and until now the rate coefficient has been measured only for *anti*-CH_3CHOO (Taatjes et al., 2013; Sheps et al., 2014) while a lower limit is available for CH_2OO (Stone et al., 2014) and *syn*-CH_3CHOO (Taatjes et al., 2013; Sheps et al., 2014). The large uncertainties in these rate coefficients make it difficult to estimate the importance of Criegee intermediates and the impact they may or may not have as oxidants in the atmosphere. Additionally, a recent study from Berndt et al. (2014c) suggested that the reaction between CH_2OO and water dimers is faster than the reaction with water vapor, in agreement with the theoretical study by Ryzhkov and Ariya (2004) which indicates the reaction with water dimers to be between 400 and 35000 times faster than the reaction with water vapor depending on the conformers. Another important reaction of CI that depends on the CI conformation is their unimolecular decomposition. The unimolecular decomposition rate depends on the CI conformer for not only the rate of the reaction, but also for the products formed. *Anti*-SCI are likely to decompose via the ester channel forming an ester or an acid as final product while *syn*-SCI will form a vinyl hydroperoxide (VHP) which promptly decomposes forming hydroxyl radicals (OH) and a vinoxy radical (Paulson et al., 1999; Johnson and Marston, 2008; Drozd and Donahue, 2011; Vereecken and Francisco, 2012). Larger and more complex conformers such as hetero-substituted or cyclic structures are subject to additional unimolecular rearrangements (Vereecken and Francisco, 2012). On the unimolecular decomposition rates and products few experimental data are available (Horie et al., 1997; Horie et al., 1999; Fenske et al., 2000a; Novelli et al., 2014b). More is available from theoretical studies explicitly focusing on the path followed by different

conformers (Anglada et al., 1996; Aplincourt and Ruiz-López, 2000; Kroll et al., 2001; Zhang and Zhang, 2002; Nguyen et al., 2009b; Kuwata et al., 2010).

Most of the experimental and theoretical information available and described above refers only to the smaller conformers. These compounds are likely to be formed in a relatively high proportion in the atmosphere as they can originate from any unsaturated compound with a terminal double bond, but they are far from describing the entire Criegee intermediate population.

As SCI were found to react quickly with many trace gases, different model studies were done on the impact SCI might have as oxidant in the atmosphere (Vereecken et al., 2012; Boy et al., 2013; Percival et al., 2013; Pierce et al., 2013; Sarwar et al., 2013; Novelli et al., 2014b; Sarwar et al., 2014; Vereecken et al., 2014a). Some of these studies focused in particular on the possible impact that SCI might have on the formation of sulfuric acid (H_2SO_4) in the gas phase after Mauldin III et al. (2012) suggested that Criegee intermediates are the missing SO_2 oxidant needed to close the sulfuric acid budget in a boreal forest. This is supported by theoretical and laboratory studies with a rate coefficient between SCI and sulphur dioxide (SO_2) in the order of ~ 10^{-11} cm^3 $molecules^{-1}$ s^{-1} (Aplincourt and Ruiz-López, 2000; Jiang et al., 2010; Kurtén et al., 2011; Vereecken et al., 2012; Welz et al., 2012; Taatjes et al., 2013; Liu et al., 2014b; Sheps et al., 2014; Stone et al., 2014). The model studies showed that, depending on the environment, SCI can potentially have an important impact on the H_2SO_4 formation. All these studies are affected by the large uncertainties and the many simplifications used to cope with the lack of data on the reactions of many SCI with various trace gas species, the speciation of SCI, and finally the steady state concentration of SCI in the troposphere. Until now, no direct or reproducibly indirect method has been shown to detect the steady state concentration of SCI in the troposphere.

In this paper, we first aim to estimate the concentration of SCI in the troposphere, based on the data collected during the HUMPPA-COPEC 2010 campaign (Williams et al., 2011) in a boreal forest and the HOPE 2012 campaign in rural Germany. The budget analysis of SCI is approached from four different directions: from an unknown H_2SO_4 production rate (Mauldin III et al., 2012), from the measured unsaturated volatile organic compounds (VOC), from the OH reactivity (Nölscher et al., 2012) and from an unidentified production rate of OH (Hens et al., 2014). Secondly, we present measurements obtained using our inlet pre-injector laser-induced fluorescence assay by gas expansion technique (IPI-LIF-FAGE) (Novelli et al.,

2014a) during the HUMPPA-COPEC 2010 and the HOPE 2012 campaigns. A recent laboratory study performed with the same instrumental setup showed that the IPI-LIF-FAGE system is sensitive to the detection of the OH formed from unimolecular decomposition of SCI (Novelli et al., 2014b). Building on this study, the background OH (OH_{bg}) (Novelli et al., 2014a) measured during the two field campaigns is investigated in comparison with many other trace gases in order to understand if the observations in controlled conditions are transferable to the ambient measurements.

4.2 Instrumentations and field sites

4.2.1 IPI-LIF-FAGE description

A comprehensive description of the IPI-LIF-FAGE ground based instrument, HORUS (Hydroxyl Radical Measurement Unit based on fluorescence Spectroscopy), is given by Novelli et al. (2014a) and only some important features of the instrument will be highlighted here. The IPI-LIF-FAGE instrument is made of five parts: the inlet pre injector (IPI), the inlet and detection system, the laser system, the vacuum system and the instrument control and data acquisition unit. The air is pulled through a critical orifice into a low pressure region (~300-500 Pa) where the OH molecules are selectively excited by pulsed UV light around 308 nm. The light is generated by a Nd:YAG pumped, pulsed, tunable dye laser system operated at a pulse repetition frequency of 3 kHz aligned through a white cell with 32 reflections (White, 1942). The air sample intersects the laser beam and the fluorescence signal from the excited OH molecules is detected using a gated micro-channel plate (MCP) detector. IPI is used to measure a chemical zero to correct for possible internal OH signal generation. In the IPI, an OH scavenger is added to the sample air, 5 cm in front of the inlet pinhole in such a concentration to allow a known, high proportion of atmospheric OH to be scavenged (~ 90%). The OH scavenger is added every other two minutes allowing the instrument to measure a total OH signal (OH_{tot}) when there is no injection of OH scavenger, and a background OH signal (OH_{bg}) when the OH scavenger is injected. The difference between these two signals gives the atmospheric OH concentration (OH_{atm}). The efficiency of this technique for measuring OH with this particular LIF-FAGE instrument is described together with the IPI characterisation in Novelli et al. (2014a). The background OH signal

does not originate from the instrument but is created from one or more atmospheric trace gases that decompose forming OH inside the low pressure region of the IPI-LIF-FAGE.
The HORUS instrument is calibrated for OH by the production of a known amount of OH and hydroperoxyl radicals (HO_2) from the photolysis of water at 185 nm using a mercury lamp. A more detailed description of the instrument calibration is reported by Martinez et al. (2010) and Hens et al. (2014). A calibration factor for the background OH signal observed by the HORUS instrument is currently not available. Therefore this signal will be discussed and plotted in counts per seconds (cps) of the fluorescence of the OH measured by the MCP, normalized by the laser power and corrected for quenching and sensitivity changes towards the detection of OH. The sensitivity of the instrument towards the OH radical is affected by the alignment of the white cell, the optical transmission of the components used, the sensitivity of the MCP, the water vapor concentration causing quenching of the excited OH, the internal pressure affecting number density of the available OH and collisional quenching of the excited OH and the internal temperature. These factors affect the sensitivity of HORUS towards the species causing the background OH in a similar manner as they mainly impact how sensitive the instrument is to the detection of OH. This allows for a qualitative investigation of the signal compared with the many trace gas species measured during both campaigns, and is able to give a good indication of the possible origin of the species decomposing into OH inside the low pressure segment of the HORUS instrument.

4.2.2 Measurement site and ancillary instrumentation

We present measurements from two sites, a boreal forest site in Finland and a rural site in Southern Germany. The HUMPPA-COPEC 2010 (Hyytiälä United Measurements of Photochemistry and Particles in Air – Comprehensive Organic Precursor Emission and Concentration study) campaign took place during the summer of 2010 at the SMEAR II station in Hyytiälä, Finland (61° 51’ N, 24°17’ E, 181 m a.s.l.) in a boreal forest dominated by Scot Pines (*Pinus Silvestris L.*). The site has continuous measurements of several trace gases and meteorological parameters as well as particles size, distribution and composition (Junninen et al., 2009). Further details and a more complete description of the site, the instrumentation and the meteorological conditions during the campaign can be found in Williams et al. (2011) and Hens et al. (2014). During the campaign the IPI-LIF-FAGE

instrument was run on the ground side-by-side with the CIMS instrument measuring OH and H_2SO_4 for the first period of the campaign, between the 27th and the 31st of July. In August the instrument was moved to the top of the HUMPPA tower above the canopy and measured there for the remaining part of the campaign. The data are therefore separated into ground and tower periods. A brief description of the instruments used in this study is given here. Ozone and NO_x were measured using a 3-channel chemiluminescence detector (CLD, ECO-Physics CLD 790 SR) described in Hosaynali Beygi et al. (2011). A gas chromatograph (GC, Agilent Technologies 6890A) coupled to a mass-selective detector (MS, Agilent Technologies MSD 5973 *inert*) was used for the measurements of BVOC (Yassaa et al., 2012). The total OH reactivity was measured by the comparative reactivity method (CRM) (Sinha et al., 2008) for two different heights one within and one above the canopy (18 and 24 m, respectively) (Nölscher et al., 2012). Sulfur dioxide (SO_2) was measured with a fluorescence analyzer (Model 43S, Thermo 20 Environmental Instruments Inc.). Aerosol size distributions between 3 nm to 950 nm were measured with a Differential Mobility Particle Sizer (DMPS) (Aalto et al., 2001). The size distributions were used to calculate loss rates of gas-phase sulfuric acid via the condensation sink (CS) method presented by Kulmala et al. (2011). Sulfuric acid (H_2SO_4) and OH radicals were measured on the ground by a chemical ionization mass spectrometer (CIMS) (Petäjä et al., 2009).

The HOPE 2012 (Hohenpeißenberg Photochemistry Experiment) campaign was conducted during the summer 2012 at the Meteorological Observatory in Hohenpeissenberg, Bavaria (47° 48’ N, 11° 2’ E). The observatory is operated by German Weather Service (DWD) and is located at an altitude of 985 m a.s.l. and about 300 m above the surrounding terrain, which consists mainly of meadows and coniferous forests. More information about the site can be found in Handisides et al. (2003). As for the previous campaign, a brief description of the measurements performed during the campaign and relevant for this study is given below. Ozone was measured by UV absorption with TEI 49C (Thermo Electron Corporation, Environmental Instruments) (Gilge et al., 2010). Nonmethane hydrocarbons (NMHC) were measured with a GC-flame ionization detection (FID) system (series 3600CX, Varian, Walnut Creek, CA, USA) (Plass-Dülmer et al., 2002). BVOC were detected using a GC (Agilent 6890) with a FID running in parallel with a MS (Agilent Technologies MSD 5975 *inertXL*) described by Hoerger et al. (2014). Photolysis frequencies ($J(NO_2)$ and $J(O^1D)$) were measured next to the IPI-LIF-FAGE with the same a set of filter radiometer (Junkermann et

al., 1989) as the one used during the HUMPPA-COPEC 2010 campaign. The OH reactivity was measured with two instruments for a short period of time between the 10th till the 18th of July. One method is the CRM and the same instrument of the HUMPPA-COPEC 2010 campaign was used. The second method used a CIMS instrument. The CIMS (Berresheim et al., 2000) was used during the campaign to measure H_2SO_4 and OH radicals and it was also implemented to measure OH reactivity. As the data will be used only in a qualitative way for the current study, a very short description of this novel technique suffices here; a detailed description of the instrument will be given in a future publication. The CIMS instrument enables the measurement of OH radical by converting them into H_2SO_4 after reaction in a chemical reactor with SO_2. A second SO_2 injection was performed 15 cm after the first injection closer to the MS. These two injections are cycled every five minutes allowing the measurements of the OH decay. The total OH reactivity is then calculated correcting for the formation of ambient OH between the two injections and wall losses. The uncertainty is estimated at ± 2 s^{-1} and the limit of detection is 2 s^{-1}. SO_2 was measured with a fluorescence analyzer and aerosol size distributions were measured and used to calculate loss rates of gas-phase sulfuric acid utilizing condensation sink (CS) presented by Kulmala et al. (2011).

4.3 Estimates of ambient SCI concentration during the HUMPPA-COPEC 2010 and HOPE 2012 campaigns

Figure 4.1 summarises the steady state concentration of SCI calculated starting from the H_2SO_4 budget, the measured unsaturated VOC and OH reactivity (R), and the OH budget for the HUMPPA-COPEC 2010 and HOPE 2012 campaigns. As detailed below, the steady state concentration of SCI is estimated to lie between 5 x 10^3 and 2 x 10^6 molecules cm^{-3} for the boreal forest environment during the HUMPPA-COPEC 2010 campaign and between 1 x 10^4 and 1 x 10^6 molecules cm^{-3} for rural Germany during the HOPE 2012 campaign (Fig. 4.1). Despite the many uncertainties related to the chemistry of SCI both in production and loss processes, we believe that the concentration of SCI, although spanning over two orders of magnitude, represents the best estimate that can be made for the environments studied here.

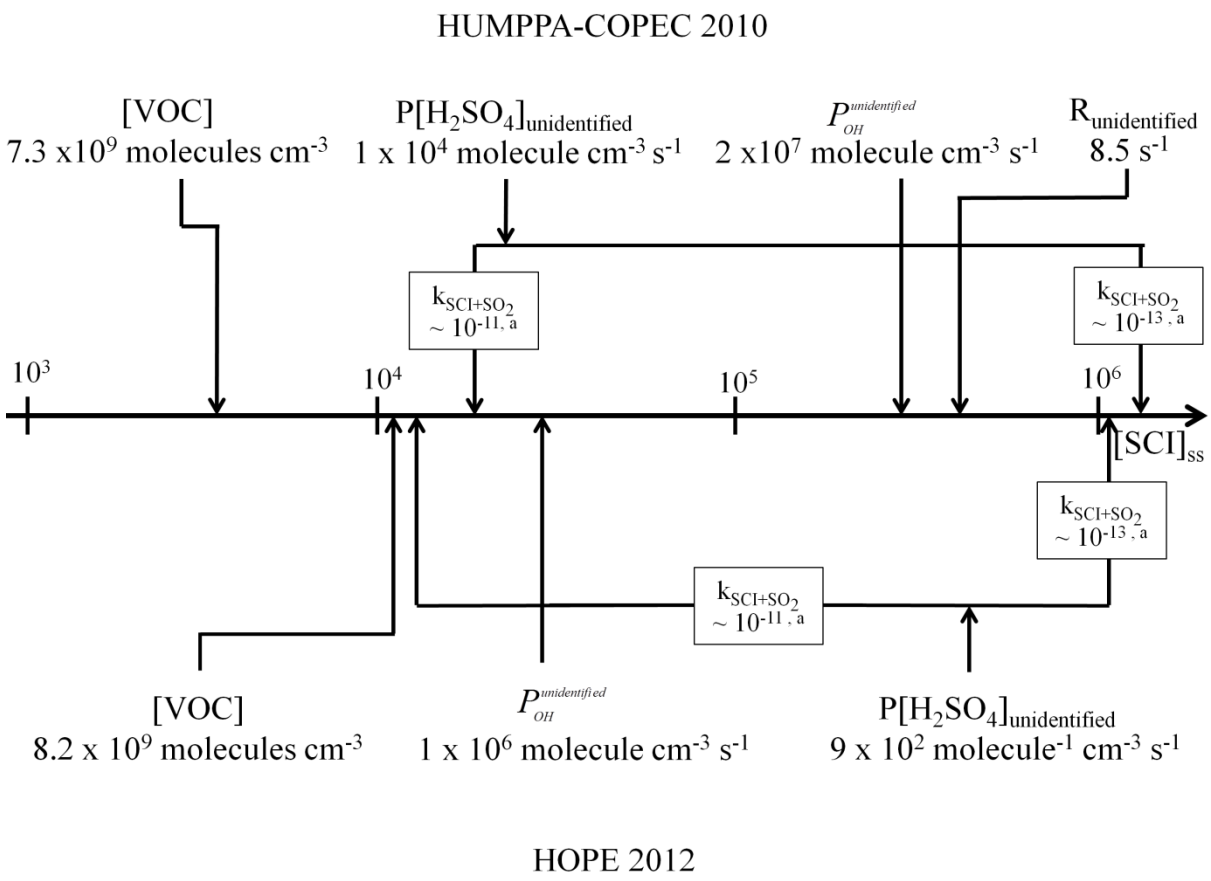

Figure 4.1. Schematic of the estimated steady state concentration of SCI ($[SCI]_{ss}$, molecules cm^{-3}) observed during the HUMPPA-COPEC 2010 and HOPE 2012 campaign starting from different sources and loss processes. [a], cm^3 $molecule^{-1}$ s^{-1}.

4.3.1 Missing H_2SO_4 oxidant

The study of Mauldin III et al. (2012) in a boreal forest during the HUMPPA-COPEC 2010 campaign showed a consistent disagreement between the measured H_2SO_4 in the gas phase and the calculated H_2SO_4 concentration when considering oxidation of SO_2 from OH radical as the only production path and the condensation sink (CS) onto pre-existing aerosol particles as the sole loss process (Eq. 4.1).

$$[H_2SO_4] = \frac{k_{OH+SO_2} \times [OH] \times [SO_2]}{CS} \qquad \textit{(Equation 4-1)}$$

The sulfuric acid in the gas phase calculated with eq. 4.1 was only half of the total H_2SO_4 observed in the field, outside the uncertainties associated with the calculation of the

formation channel and the condensation sink. All the calculated values that follow are listed with their 1σ variability when available. During the HUMPPA-COPEC 2010 campaign the unexplained H_2SO_4 production rate was on average in the order of 1 ± 1 (1σ) x 10^4 molecules cm^{-3} s^{-1}, for an average concentration of SO_2 during the campaign of 1 ± 1 (1σ) x 10^{10} molecules cm^{-3}, an average H_2SO_4 concentration of 2 ± 2 (1σ) x 10^6 molecules cm^{-3}, a condensation sink of 10 ± 4 (1σ) x 10^{-3} s^{-1} and a OH concentration of 7 ± 8 (1σ) x 10^5 molecules cm^{-3} (Boy et al., 2013). Although no unambiguous evidence links SCI to the missing oxidant, laboratory tests performed with a similar instrument (Berndt et al., 2012; Berndt et al., 2014a) confirm the role SCI can have in the oxidation of SO_2 and formation of H_2SO_4. Assuming that SCI are the only other species in addition to OH oxidizing SO_2, and knowing the rate coefficient of SCI and OH with SO_2, it is possible to calculate the steady state concentration of SCI in that environment:

$$[H_2SO_4] = \frac{(k_{OH+SO_2} \times [OH] + k_{SCI+SO_2} \times [SCI]) \times [SO_2]}{CS} \qquad \textit{(Equation 4-2)}$$

The rate coefficient between OH and SO_2 at standard pressure and temperature is 1.3 x 10^{-12} cm^3 $molecule^{-1}$ s^{-1} (Atkinson et al., 2004). The rate coefficient of SCI with SO_2 has been determined by several groups, and the values cluster around two numbers. The first value of ~ 5 x 10^{-13} cm^3 $molecule^{-1}$ s^{-1} has been obtained by Mauldin III et al. (2012) and Berndt et al. (2014a) while a second value of ~ 3.3 ± 2 (1σ) x 10^{-11} cm^3 $molecule^{-1}$ s^{-1} has been obtained by a number of other groups (Welz et al., 2012; Taatjes et al., 2013; Liu et al., 2014b; Sheps et al., 2014; Stone et al., 2014). The disagreement could be explained by the fact that Mauldin III et al. (2012) and Berndt et al. (2014a) rather than measuring the direct reaction rate of SCI with SO_2 measure the total rate of formation of H_2SO_4. If, as suggested by Vereecken et al. (2012), the secondary ozonide (SOZ) formed from the reaction between SCI and SO_2 can stabilise for larger SCI and undergo bimolecular reaction without formation of SO_3, the difference in rate coefficient observed for the different experiments could be partly explained. Conversely, experiments by Carlsson et al. (2012) and Ahrens et al. (2014) observed high yields of SO_3 close to unity suggesting that the SOZ is not lost in the conditions used, i.e. in chambers with no presence of water and at high concentrations of reactants. At the same time, these reaction conditions differ from the other studies which were performed either in ambient or with lower concentrations of reagents and in presence of water. Hence, as there is

still a large uncertainty on the rate coefficient, both values were used in this budget analysis. The steady state concentration of SCI was calculated using the measured data and eq. 4.2 yielding an average [SCI] = 3 ± 2 (1σ) x 10^4 molecules cm^{-3} for a rate coefficient of 3.3 x 10^{-11} cm^3 $molecule^{-1}$ s^{-1}, as opposed to the value of 2 ± 2 (1σ) x 10^6 molecules cm^{-3} obtained with the lower rate coefficient (5 x 10^{-13} cm^3 $molecules^{-1}$ s^{-1}). Note, however, that both values for the steady state concentration of SCI remain in agreement with what was obtained in two different scenarios, polluted and pristine environments, by Welz et al. (2012) starting from the concentrations of measured VOC and O_3.

A similar estimate for the SCI steady state concentration was done for the HOPE 2012 campaign. During this campaign, the H_2SO_4 concentration can be mainly explained by the reaction between OH and SO_2. Figure 4.2 shows the correlation between the total production rate of H_2SO_4 ($P[H_2SO_4]_{tot}$) calculated from the product of measured H_2SO_4 and condensation sink (CS), as well as the production rate of H_2SO_4 from the reaction of OH and SO_2. The linear regression following the York method (York et al., 2004) yields a slope of 0.90 ± 0.02 with a negligible intercept.

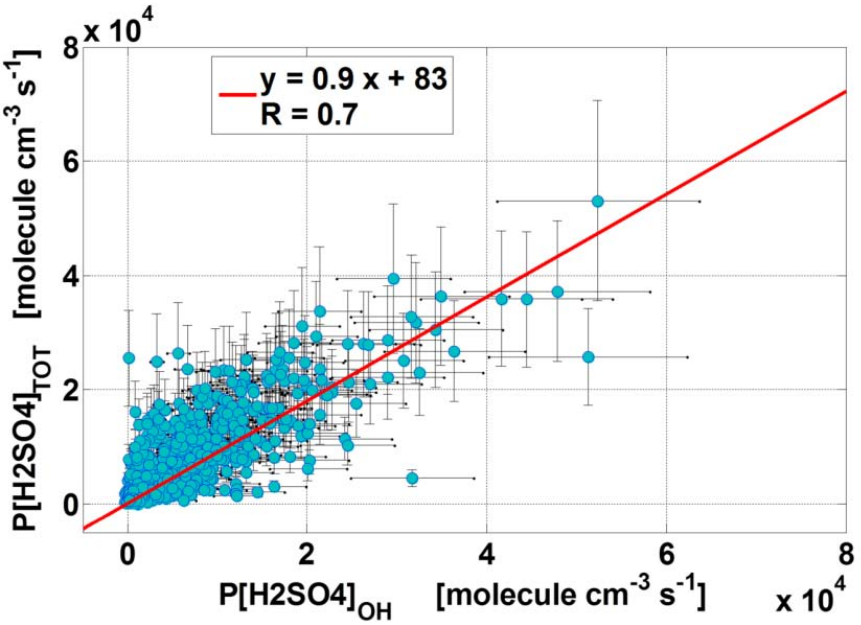

Figure 4.2. Comparison between the total production rate of H_2SO_4 ($P[H_2SO_4]$tot) and the production rate of H_2SO_4 from the reaction between OH and SO_2. The linear regression following the method of York (York et al., 2004) yields a slope of 0.9 ± 0.02 and a negligible intercept of 0.08x10^4 molecule cm-3 s-1.

The remaining observed unexplained production rate of H_2SO_4 was 9.2 ± 5 (1σ) x 10^3 molecules cm^{-3} on average during this campaign. The average H_2SO_4 concentration in this environment, 8.5 ± 8.5 (1σ) x 10^5 molecules cm^{-3} was smaller than that observed for the HUMPPA-COPEC 2010 campaign (2 ± 2 (1σ) x 10^6 molecules cm^{-3}), while the average OH concentration was higher, 1.6 ± 1.6 (1σ) x 10^6 molecules cm^{-3} compared to 7 ± 8 (1σ) x 10^5 molecules cm^{-3} observed during the HUMPPA-COPEC 2010 campaign. Average condensation sink (CS) was 7 ± 3 (1σ) x 10^{-3} s^{-1} and average SO_2 concentration was 2.5 ± 2 (1σ) x 10^9 molecules cm^{-3}. The steady state concentration of SCI was calculated using the measured data and eq. 4.2 yielding to an average [SCI] of 1 ± 2 (1σ) x 10^4 molecules cm^{-3} when using the fast rate coefficient between SCI and SO_2 (3.3 x 10^{-11} cm^3 $molecule^{-1}$ s^{-1}) and 1 ± 2 (1σ) x 10^6 molecules cm^{-3} for the lower rate coefficient (5 x 10^{-13} cm^3 $molecule^{-1}$ s^{-1}). Compared to the HUMPPA-COPEC 2010 campaign, as both the total H_2SO_4 concentration and the unexplained H_2SO_4 production rate were smaller, the steady state concentration of SCI obtained is of a factor of 2 smaller.

4.3.2 Measured unsaturated VOC and OH reactivity

Another way to estimate SCI concentration comes from analyzing their production and loss processes. In a forest, SCI are formed from the ozonolysis of unsaturated BVOCs. During the HUMPPA-COPEC 2010 campaign unusually high temperatures for a Boreal forest were measured during the entire campaign (Nölscher et al., 2012; Hens et al., 2014). It is possible to calculate an average steady state concentration for SCI using the following equation

$$[SCI] = \frac{k_{VOC+O_3} \times [VOC] \times [O_3] \times Y_{SCI}}{L_{SCI\,syn}} \qquad \textit{(Equation 4-3)}$$

Where k_{VOC+O_3} is the average rate coefficient for the average mixture and concentration of VOC, [VOC], Y_{SCI} is the yield of SCI in the ozonolysis reaction, and L_{SCIsyn} is the total loss of syn-SCI. L_{SCIsyn} of 40 s^{-1} was used as obtained from the model described by Novelli et al. (2014b), which accounts for many possible losses of SCI including the reaction with water dimers and unimolecular decomposition. The latter study also suggests that anti-acetaldehyde

oxide and formaldehyde oxide react quickly with water and water dimers and that their contribution can be neglected. We thus obtain that [SCI] ≈ [SCI_{syn}] The average concentration of ozone, [O_3], during the campaign was 1.1 ± 0.2 (1σ) x 10^{12} molecules cm^{-3} and the sum of the measured unsaturated VOC (isoprene, (−)/(+) α -pinene, (−)/(+) β-pinene, 3-carene, and myrcene) concentration was 7.3 ± 7 (1σ) x 10^9 molecules cm^{-3}. The average rate coefficient across these compounds, weighted by the abundance of the different unsaturated species measured, is 7 x 10^{-17} cm^3 $molecule^{-1}$ s^{-1} (Atkinson et al., 2006). A yield of SCI formation (Y_{SCI}) of 0.4 was estimated based on the data by Hasson et al. (2001). The steady state concentration of SCI was calculated using the measured data for [O_3] and [VOC] and an average value of 40 s^{-1} for L_{SCIsyn} as this value was found to be rather constant and mainly dependent on the unimolecular decomposition rate of the SCI. Using eq. 4.3 an average [SCI] of ~ 5 ± 4 (1σ) x 10^3 molecules cm^{-3} was found.

This estimate can be further refined by correcting for VOC that were not directly quantified. An average of OH reactivity, R = 12 ± 10 (1σ) s^{-1}, was measured during the campaign (Nölscher et al., 2012). During HUMPPA-COPEC 2010, on average, 70 % of the OH reactivity was not explainable (R_{unex} = 8.5 s^{-1}) by the measured trace gases (organic and inorganic) during the campaign (Nölscher et al., 2012), suggesting that this unidentified OH reactivity might give a more representative indication of the VOC concentrations during the campaign as OH reacts very quickly with BVOCs. Assuming a lumped rate coefficient k_{VOC+OH} between OH and the fraction of unspeciated VOC of 1 x 10^{-11} cm^3 $molecule^{-1}$ s^{-1}, typical for an OH addition to a C=C double bond, one can calculate the concentration [$VOC_{unknown}$] of VOC that would be necessary to close the OH reactivity budget (Eq. 4.4)

$$R_{unex} = k_{VOC+OH} \times [VOC_{unknown}] \qquad \textit{(Equation 4-4)}$$

Using eq. 4.4 with measured data, an average [$VOC_{unknown}$] of 8.6 ± 8.2 (1σ) x 10^{11} molecules cm^{-3} was found. This value was inserted into eq.4.3 and a concentration of SCI of ~ 6 ± 6 x 10^5 molecules cm^{-3} is obtained. To this, we add the SCI concentration calculated from the measured unsaturated VOC, 5 ± 4 (1σ) x 10^3 molecules cm^{-3} to obtain the SCI from all VOC.

During the HOPE 2012 campaign a larger number of unsaturated trace gases, both anthropogenic and biogenic, was measured. The average concentration of O_3 was 1 ± 0.2 x 10^{12} molecules cm^{-3}. The sum of the measured unsaturated VOC concentration (isoprene, (−)/(+) α-pinene, (−)/(+) β-pinene, 3-carene, myrcene, limonene, 2-methylpropene, butene,

cis-ocimene, camphene, sabinene, γ-terpinene, terpinolene, propene) was 8.2 ± 7 (1σ) x 10^9 molecules cm^{-3} and the average rate coefficient across these compounds, k_{VOC+OH}, weighted by the abundance of the different unsaturated species measured was 1 x 10^{-16} cm^3 $molecule^{-1}$ s^{-1}. For the Y_{SCI} the same value of 0.4 was used while for the L_{SCIsyn} the value of 32 s^{-1} obtained from the model described by Novelli et al. (2014b) for the rural European environment was used. Using these values in eq. 4.3 results in a steady state concentration of [SCI] = 1 ± 0.7 (1σ) x 10^4 molecules cm^{-3}.

During the HOPE 2012 campaign the total OH reactivity (R) was on average equal to 3.9 ± 3 (1σ) s^{-1}. By using the measured trace gas species it is possible to calculate the expected OH reactivity. During the HOPE 2012 campaign the total OH reactivity (R) was on average equal to 3.9 ± 3 (1σ) s^{-1}. By using the measured trace gas species it is possible to calculate the expected OH reactivity. An average value of 3.2 s^{-1} was calculated. This, together with the uncertainty of the measurement (± 2 s^{-1}), indicates that during the HOPE 2012 campaign the measured OH reactivity can be explained by the measured trace gases.

4.3.3 Unidentified OH production rate

During the HUMPPA-COPEC 2010 campaign, the numerous measurements performed (Williams et al., 2011) allowed the calculation of a detailed OH budget (Hens et al., 2014). Most of the OH production during daytime is due to photolysis of O_3 and recycling of HO_2 back to OH via reaction with NO and O_3. This result holds for both high (R > 15 s^{-1}) and low OH (R≤ 15 s^{-1}) reactivity episodes in that campaign. While the OH budget can be closed during day time ($J_{O(1D)}$ > 3 x 10^{-6} s^{-1}) for low OH reactivity periods, during periods with high OH reactivity there was a large unidentified production rate of OH, $P_{OH}^{unidentified}$ = 2 ± 0.7 (1σ) x 10^7 molecule cm^{-3} s^{-1}. In addition, for both periods, during night time ($J_{O(1D)} \leq 3 \times 10^{-6}$ s^{-1}), the IPI-LIF-FAGE and the CIMS instruments measure a non-negligible OH concentrations (Hens et al., 2014) where most of the OH production is from unknown sources ($P_{OH}^{unidentified}$ = 1 ± 0.9 (1σ) x 10^6 molecule cm^{-3} s^{-1} and $P_{OH}^{unidentified}$ = 1.7 ± 0.7 (1σ) x 10^7 molecule cm^{-3} s^{-1} for low and high reactivity, respectively). Our hypothesis is that ozonolysis of VOC could represent the missing source. Indeed, formation of OH from oxidation of unsaturated VOC

has been shown to be an important source of OH in winter, indoors and possibly during night time (Harrison et al., 2006; Johnson and Marston, 2008; Shallcross et al., 2014). As OH formation from ozonolysis proceeds through Criegee intermediates (Fig. 4.3), we can estimate an SCI concentration from the OH budget.

Assuming all of the unidentified OH production, $P_{OH}^{unidentified}$, comes from VOC ozonolysis with a certain OH yield Y_{OH}, we can write:

$$P_{OH}^{unidentified} = k_{voc+O_3} \times [VOC_{unknown}] \times [O_3] \times Y_{OH} \qquad \textit{(Equation 4-5)}$$

where the rate coefficient k_{VOC+O_3}, the concentration [VOC], and the OH yield Y_{OH} are suitably averaged over the VOC mixture, and where we consider only the VOC that were not already included in the OH budget, i.e. the VOC causing the unknown OH reactivity discussed above. The average total OH yield from ozonolysis, Y_{OH}, is roughly estimated at 0.6 based on observed OH yields across the available literature data (Atkinson et al., 2006). OH formation in ozonolysis occurs through two channels (Fig. 4.3): immediate formation by prompt decomposition of chemically activated CI^*, and delayed OH by formation of SCI followed by their thermal decomposition; there are also product channels not yielding OH. The prompt yield of OH, $Y_{OH}^{CI^*}$ can be roughly estimated at ~ 0.4 from SCI scavenging experiments (Atkinson et al., 2004); the remaining yield Y_{OH}^{SCI} is then formed from SCI, where $Y_{OH} = Y_{OH}^{CI^*} + Y_{OH}^{SCI}$ and hence $Y_{OH}^{SCI} \approx 0.2$.

We adopt a value for Y_{SCI} of 0.4, as used above in section 4.3.2. The SCI formed do not all decompose to OH, e.g. *anti*-CI tend to form esters instead. We label all SCI able to yield OH as SCI_{syn}, without mandating a speciation but following the observation that *syn*-CI usually yield OH through the vinylhydroperoxide channel. The total SCI yield is then divided into a fraction, Y_{syn}, forming SCI_{syn}, and the remainder, Y_{anti}, forming non-OH-generating SCI. Little information is available on the Y_{syn}:Y_{anti} ratio; only a few theoretical calculations on smaller alkenes and few monoterpenes are available (C. D. Rathman et al., 1999; Fenske et al., 2000b; Kroll et al., 2002; Nguyen et al., 2009a; Nguyen et al., 2009b) Across most of these compounds the ratio of syn- to anti-SCI are always within a factor of 5. Based on this, we roughly estimate the ratio of Y_{syn} to Y_{anti} as 1:1, *i.e.* $Y_{syn} = Y_{anti} = 0.2$.

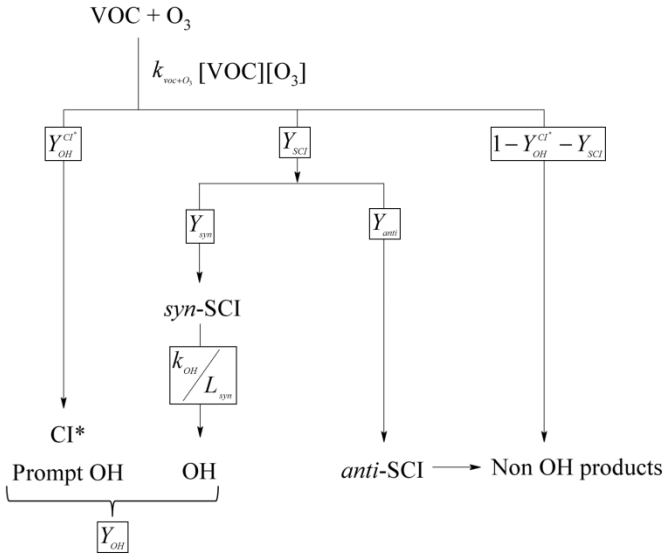

Figure 4.3. Schematic representation of the formation of OH from ozonolysis of unsaturated VOC.

The production of OH from SCI_{syn} formed from VOC not included in the OH budget is then $k_{OH} \times [SCI_{syn}]_{ss}$, where we estimate $k_{OH} \approx 20\ s^{-1}$ as measured by Novelli et al. (2014b) for *syn*-CH_3CHOO, and where the steady state concentration of the SCI_{syn} , $[SCI_{syn}]_{ss}$, is determined by the ratio of the formation processes and the sum L_{SCIsyn} of the loss processes already defined above:

$$\left[SCI_{syn}\right]_{ss} = \frac{k_{voc+O_3} \times \left[VOC_{unknown}\right] \times \left[O_3\right] \times Y_{SCI} \times Y_{syn}}{L_{SCI_{syn}}} \qquad \textit{(Equation 4-6)}$$

Merging the above equations, expressing the measured OH production from unknown sources as the sum of direct OH production from CI^* and indirect from SCI_{syn}, we obtain:

$$P_{OH}^{unidentified} = k_{voc+O_3} \times \left[VOC_{unknown}\right] \times \left[O_3\right] \times \left(Y_{OH}^{CI^*} + Y_{SCI} \times Y_{syn} \times \frac{k_{OH}}{L_{SCI_{syn}}} \right) \qquad (7)$$

The measured $P_{OH}^{unknown}$ and $[O_3]$, and the estimates of the other parameters allows us to calculate the factor $k_{voc+O_3} \times [VOC_{unknown}]$. Substituting this factor into eq. 4.6 yields an

estimate of the steady state concentration of SCI_{syn}. With a value of $P_{OH}^{unidentified}$ of 1 x 10^6 molecules cm^{-3} s^{-1} as observed for low reactivity episodes and at night during HUMPPA, a steady state concentration of SCI_{syn} of 2 x 10^4 molecules cm^{-3} is calculated. For high reactivity episodes during HUMPPA, the missing $P_{OH}^{unidentified}$ of 2 x 10^7 molecules cm^{-3} s^{-1} results in a SCI concentration of 5 x 10^5 molecules cm^{-3}. To obtain the total SCI concentration, we then need to add the non-OH-producing SCI. Here, we assume that these are mostly *anti*-SCI or H_2COO, both of which react rather quickly with H_2O or $(H_2O)_2$, (Novelli et al., 2014b) and that their contribution can be neglected. We thus obtain that [SCI] ≈ [SCI_{syn}]. To this, we add the SCI concentration calculated from the measured unsaturated VOC (section 4.3.2), 5 ± 4 (1σ) x 10^3 molecules cm^{-3}, to obtain the SCI from all VOC.

During HOPE 2012 a preliminary OH budget analysis suggests an unknown OH production source of $P_{OH}^{unknown}$ ~ 1 ± 2 x 10^6 molecules cm^{-3} s^{-1} over the entire campaign. By using this value in eq. 4.7 together with the L_{SCI} = 34 s^{-1} for this environment, a steady state concentration of SCI_{syn} of 3 x 10^4 molecules cm^{-3} can be estimated. To this, we add the SCI concentration calculated from the measured unsaturated VOC (section 4.3.2), 1 ± 0.7 (1σ) x 10^4 molecules cm^{-3}, to obtain the SCI from all VOC.

Using eq. 4.7, for a given set of yields, unimolecular decomposition rates and SCI losses, the relative contribution of SCI and CI^* to the total production rate of OH can be estimated. With the yields considered in this study and for a unimolecular rate decomposition of SCI into OH of 20 s^{-1}, the SCI would contribute up to 12 % to the total formation of OH from ozonolysis of VOC in both environments. This indicates that the SCI do not have a large impact in the production of OH radicals and at the same time emphasizes how important a correct estimate of VOC concentration is for modeling the OH radical.

4.4 Results and discussion

Novelli et al. (2014a) showed that the OH_{bg} does not originate from within the instrument. Tests performed by changing the laser power whilst measuring during night time, when the contribution of the OH_{bg} to the OH_{tot} measured by the instrument is highest, showed no quadratic dependency of the signal on the laser power. Additionally, during the HUMPPA-

COPEC 2010 and HOPE 2012 campaigns, the correlation factor of the OH_{bg} with the laser power was R = 0.002 and R = 0.2, respectively. This strongly indicates that the OH_{bg} does not arise from laser generated interference. The hypothesis we formulate about the origin of the OH_{bg} is based on the laboratory studies (Novelli et al., 2014b), in which we found that the OH is generated internally from unimolecular decomposition of SCI. The following analysis describes the observed behaviour of the signal during the campaign and its relationship to other observed chemical tracers and discusses if this is compatible with our hypothesis.

4.4.1 Correlation of OH_{bg} with temperature

The time series of the background OH signal measured during the HUMPPA-COPEC 2010 and HOPE 2012 campaigns are shown together with temperature and $J(O^1D)$ values in figure. 4.4. Increases and decreases of the OH_{bg} signal follows the temperature changes. On the tower during the HUMPPA-COPEC 2010 and during the HOPE 2012 campaigns the OH_{bg} does not change drastically between minimum and maximum values and never reaches zero. During the HUMPPA-COPEC 2010 campaign the OH_{bg} shows a strong correlation with temperature (Fig. 4.5) with a correlation coefficient, R = 0.8 for the exponential fit. The presence of an exponential dependency with temperature is in agreement with data shown by Di Carlo et al. (2004) for the unexplained OH reactivity and indicates how the species responsible for the OH_{bg} strongly correlates with biogenic VOC (BVOC) such as monoterpenes and sesquiterpenes whose emissions are shown to correlate with temperature (Hakola et al., 2003; Duhl et al., 2008). During the HOPE 2012 campaign, a strong correlation with temperature was not observed (R = 0.5, Fig. 6.16 (SI)). However, during the HOPE 2012 campaign the IPI-LIF-FAGE instrument was located at a larger distance from the forest compared to the HUMPPA-COPEC 2010 campaign and was much more influenced by anthropogenic emissions. The difference between the two campaigns in the correlation of the background OH and the temperature could then be explained by the VOC sources, i.e. mainly biogenic in the boreal forest versus anthropogenically influenced in southern Germany. This also remains consistent with the large unknown OH reactivity during HUMPPA-COPEC 2010which was not observed during the HOPE 2012 campaign where the OH reactivity budget can be closed with the measured trace gases.

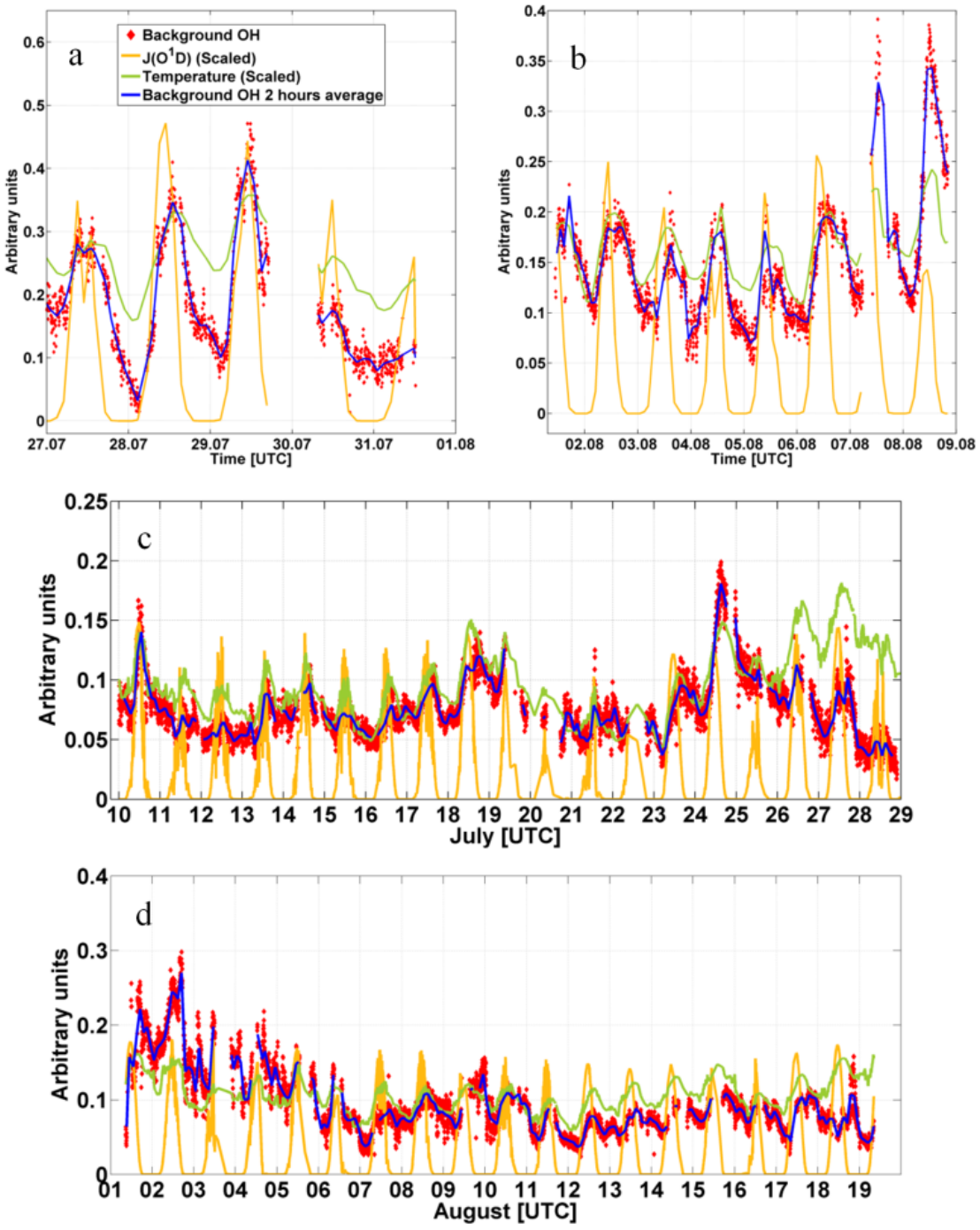

Figure 4.4. Background OH (red diamonds) measured during the HUMPPA-COPEC 2010 (a, ground and b, tower) and the HOPE 2012 (c, July and d, August) campaigns together with scaled $J(O^1D)$ and scaled temperature values.

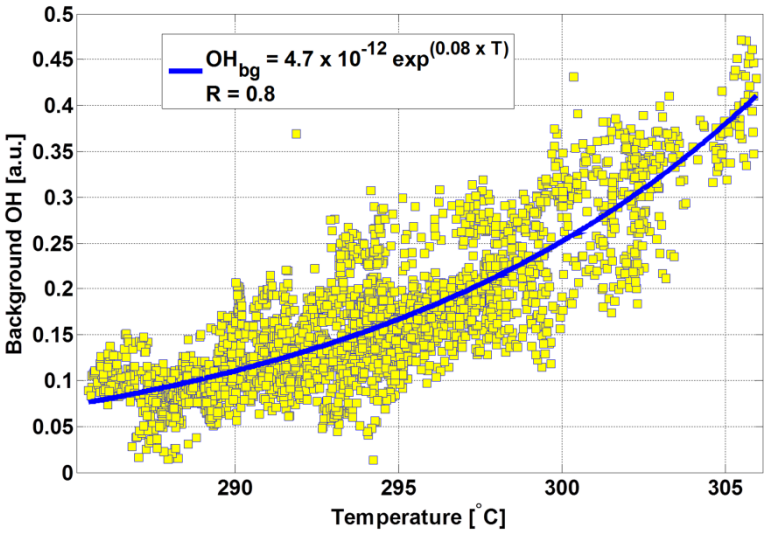

Figure 4.5. Comparison between the background OH and the temperature during the HUMPPA-COPEC 2010 campaign.

During both campaigns little correlation, R = 0.2, was observed between the background OH and J(O^1D). This suggests that the OH_{bg} does not primarily originate from photolytic species.

4.4.2 Correlation of OH_{bg} with OH reactivity

As described in section 4.3, during the HUMPPA-COPEC 2010 campaign high average OH reactivity was observed (~ 12 s^{-1}) and of this, between 60 % and 90 % is not explainable by the loss processes calculated from the measured species (Nölscher et al., 2012). A large unknown fraction in the reactivity has often been observed, especially in forested environments (Di Carlo et al., 2004; Sinha et al., 2008; Edwards et al., 2013) indicating a large fraction of unknown BVOC or their secondary products. The OH_{bg} shows some correlation with the measured OH reactivity at 18 m, for the period on the ground (R = 0.4), and the measured OH reactivity at 24 m, for the period on the tower (R = 0.4) (Fig. 4.6). The correlation improves considerably when restricting the analysis to only night time data (between 20 and 8 local time) with a correlation factor R = 0.6 for both ground and tower periods. The improvement in the correlation when considering only night time data strongly suggests that the background OH is related to night time oxidation processes such as ozonolysis of BVOC. This would also be in agreement with the large unknown OH production (section 4.3.3) observed, especially during nigh time, which could be explained by

formation of OH from ozonolysis of BVOC. A correlation between the OH_{bg} and the OH reactivity was also observed in a study by Mao et al. (2012) in a Ponderosa pine plantation (California, Sierra Nevada Mountains) dominated by isoprene where likewise high values of OH reactivity were observed (~ 20 s^{-1}).

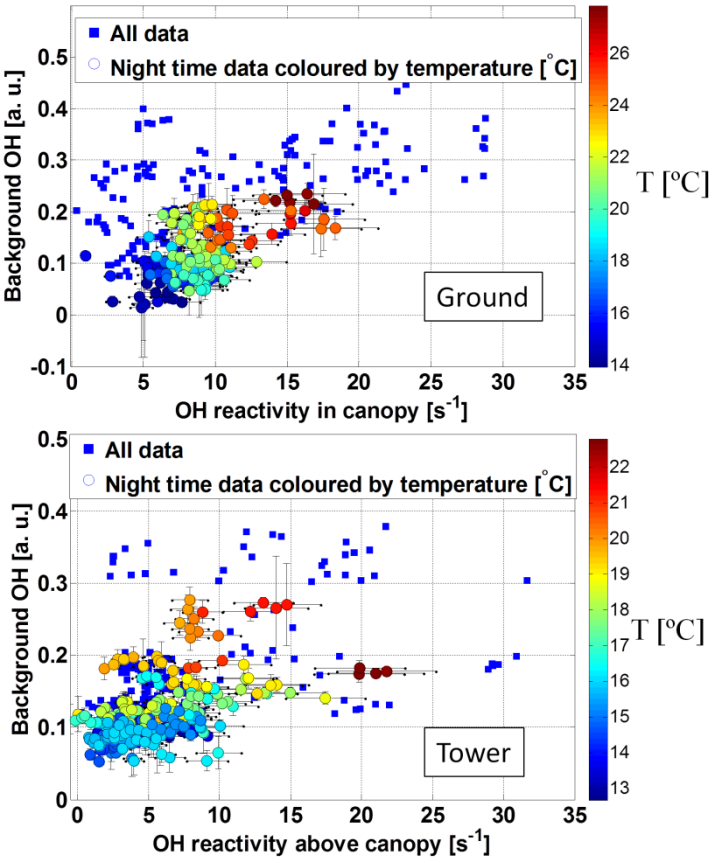

Figure 4.6 Comparison between OH_{bg} and OH reactivity for ground and tower periods during the HUMPPA-COPEC 2010 campaign. Square markers represent the daytime data, round markers represent night time data and are coloured by temperature (right legend).

During the HOPE 2012 campaign such a correlation with the OH reactivity was not observed. The OH reactivity was, on average, 3 times smaller than during the campaign in Finland and 75% of it can be explained by reaction of OH with methane, formaldehyde, acetaldehyde, inorganic compounds (NOx, SO_2, CO) and anthropogenic VOC. Only a very small fraction of the OH reactivity is caused by reaction of OH with BVOC in this environment. These observations are consistent with OH_{bg} originating from BVOC-related species.

4.4.3 Correlation of OH_{bg} with ozonolysis chemistry

During the HUMMPA-COPEC 2010 campaign a good correlation with O_3, R = 0.7 (Fig. 6.17 (SI)), indicates that the background OH likely originates from ozonolysis processes. A comparison of the background OH with the product of ozone and measured unsaturated VOC does not show the same relationship. During the period of measurements made on the ground, no co-located BVOC measurements were available and therefore no comparison with the OH_{bg} data is shown here. For the tower period, no correlation (R = -0.02) between OH_{bg} and the product of O_3 and the BVOC concentration can be seen when using the measured data with the GC-MS. As most of the OH reactivity remains unexplained, the lack of correlation is not that surprising as the species of VOC responsible for the formation of SCI detected by the HORUS instrument likely lies within the large fraction of unmeasured species. Conversely, during the HOPE 2012 campaign a weak correlation is observed between background OH and ozone (R = 0.5, Fig. 6.18 (SI)), but when comparing it with the product of measured unsaturated VOC (see list in section 4.3.2) and ozone, the correlation improves remarkably (R = 0.8, Fig. 4.7). These are good indications that the species causing the background OH originates from ozonolysis of unsaturated compounds.

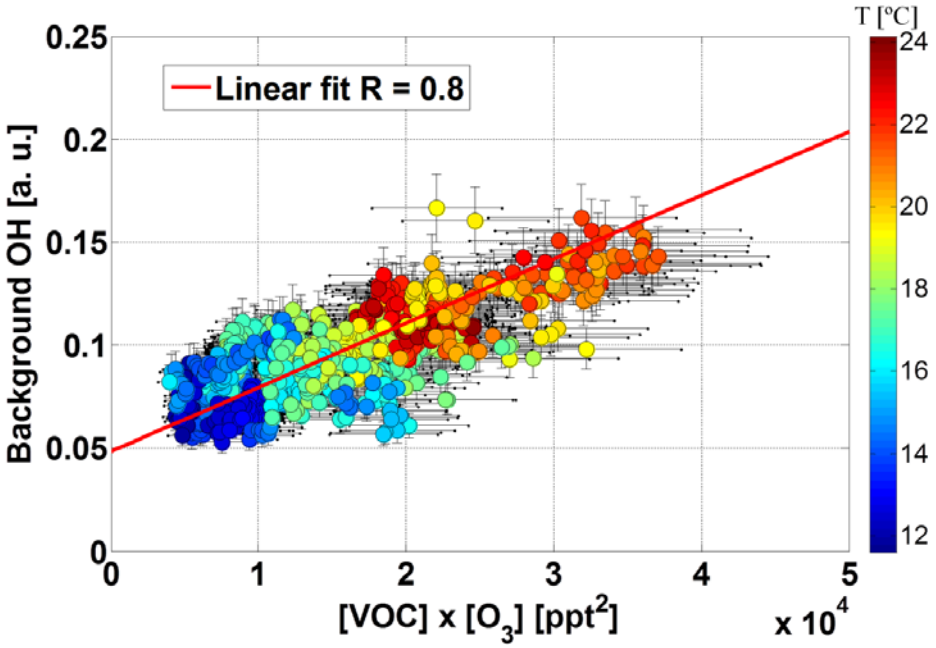

Figure 4.7. Comparison between the OH_{bg} and the product of measured unsaturated VOC and O_3 during the HOPE 2012 campaign. The data is coloured by temperature (right legend)

4.4.4 Correlation of OH_{bg} with $P[H_2SO_4]_{unex}$

During both campaigns, measurements of H_2SO_4, SO_2, OH and CS (condensation sink) were performed allowing the calculation of the sulfuric acid budget in the gas phase. As shown by Mauldin III et al. (2012), during the HUMPPA-COPEC 2010 campaign the well established SO_2 oxidation process driven by OH (Wayne, 2000), eq. 4.1, was not sufficient to explain the measured concentration of H_2SO_4. As shown in section 4.3.1, half of the production rate of H_2SO_4, ~ 1 x 10^4 molecules cm^{-3} s^{-1}, was not explained by the OH radicals only (Fig.4.8).

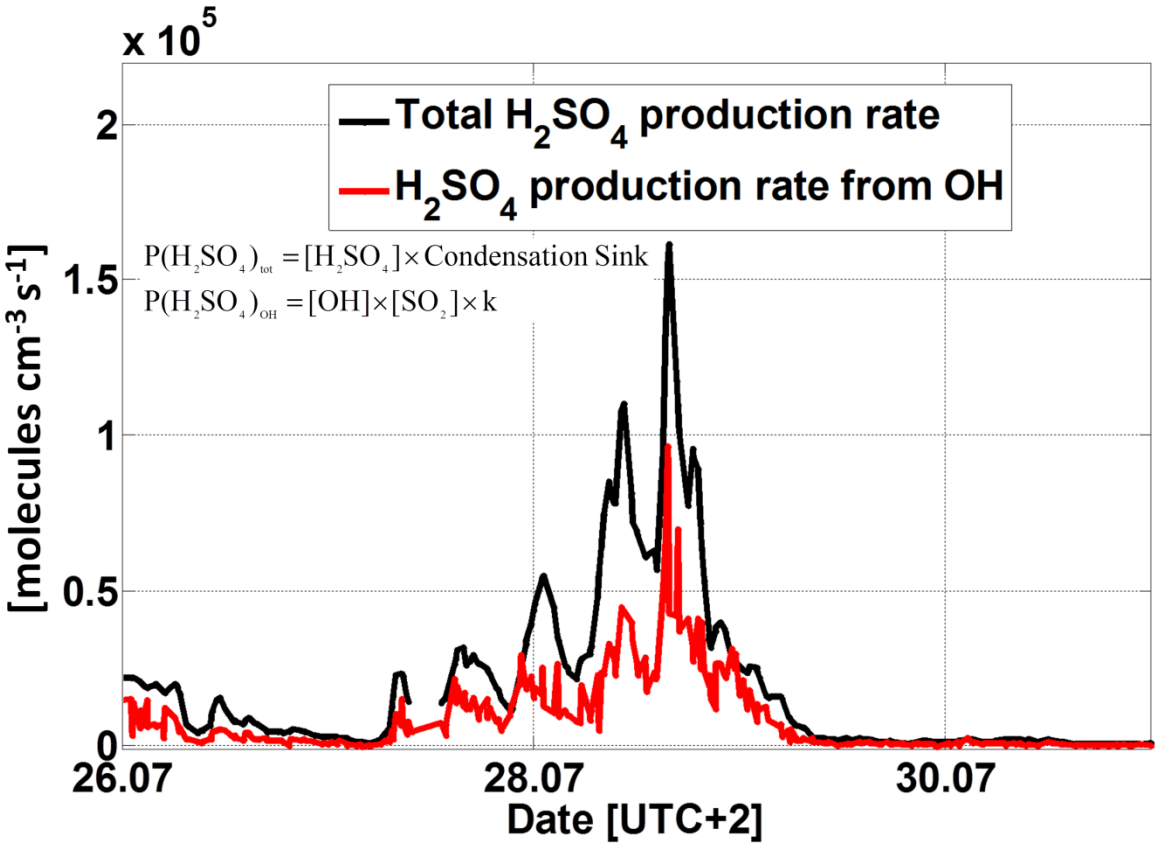

Figure 4.8. Comparison between the total H_2SO_4 production rate calculated from the measured H_2SO_4 and the production rate of H_2SO_4 involving only the OH radical in the oxidation process of SO_2 for the ground period during the HUMPPA-COPEC 2010 campaign.

The missing oxidant is assumed to be SCI, as discussed in section 4.3.1, because of their fast rate coefficient with SO_2. As our hypothesis about the origin of the OH_{bg} points also towards the same species, we compared the $[H_2SO_4]_{unex}$ observed during the HUMPPA-COPEC 2010 campaign with the OH_{bg} multiplied by SO_2 for the ground period when both instrument (HORUS and CIMS) measured side-by-side (Fig. 4.9). The two datasets have a correlation

coefficient, R = 0.6 indicating that, whichever species is responsible of the oxidation of SO_2, is related reasonably strongly with the formation of OH within the HORUS instrument.
During the HOPE 2012 campaign, the same budget calculation shows only a small fraction (10%) of missing H_2SO_4 production rate.

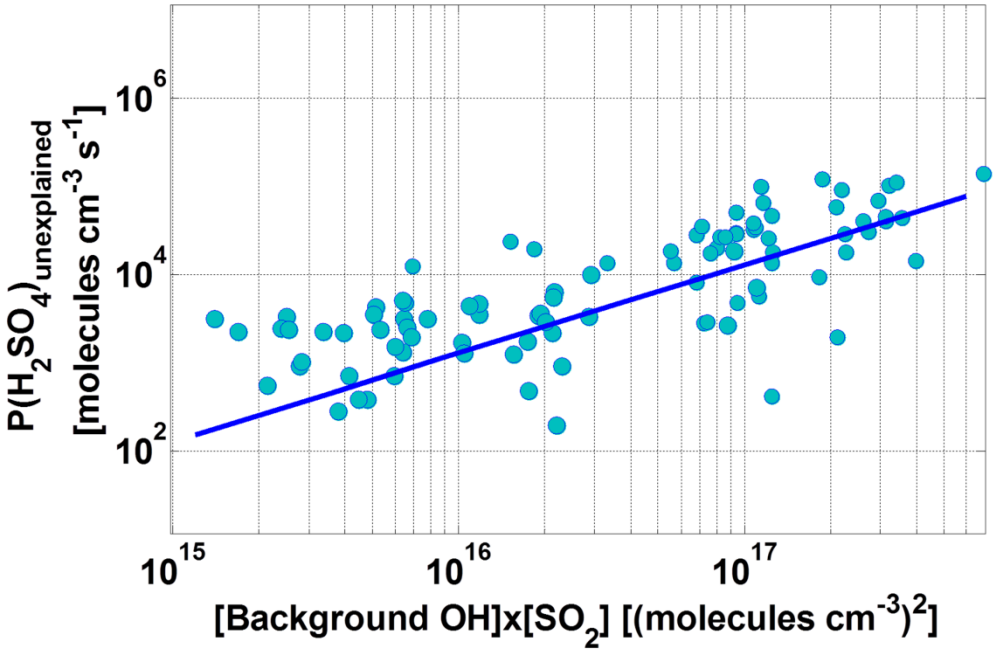

Figure 4.9. Comparison between the production rate of H_2SO_4 not explainable by the oxidation of SO_2 performed by the OH radical and the OH_{bg} multiplied by SO_2 during the ground period of the HUMPPA-COPEC 2010 campaign.

Assuming SCI to be the unknown SO_2 oxidant, the results observed in both campaigns are in agreement with the modeling study by Boy et al. (2013). In their study, they analysed the same sites described in this study. Similar to our result, they found a larger contribution of the SCI in the formation of H_2SO_4 for the boreal forest compared to the rural Germany. As the OH concentration differs by, on average, less than 50% between the two environments, a similar concentration of SCI in HOPE to that calculated for HUMPPA-COPEC 2010 would contribute up to 30 % in the formation of H_2SO_4. The H_2SO_4 budget during this campaign can be almost closed by using only the measured OH concentrations, suggesting that the concentration of SCI in this environment is smaller than the one during the HUMPPA-COPEC 2010 campaign. This is consistent with the calculation from section 4.3 based on the smaller reactivity and hence smaller VOC load measured for this environment

4.4.5 Scavenging experiments

A series of scavenging tests of the OH_{bg} were performed during the HOPE 2012 campaign to attempt to ascertain the identity of the interfering species. SO_2 was chosen as scavenger for the species causing the OH_{bg} as it has been shown in several laboratory studies to react quickly with SCI ($k \sim 3.3 \times 10^{-11}$ cm^3 $molecules^{-1}$ s^{-1}) mostly independently of their structure (Welz et al., 2012; Taatjes et al., 2013). The injection of SO_2 was performed through the IPI system together with an OH scavenger. First the OH scavenger was injected within IPI in order to remove the atmospheric OH; then, the SO_2 was injected in addition to the OH scavenger in order to remove the remaining OH_{bg} (Fig. 4.10).

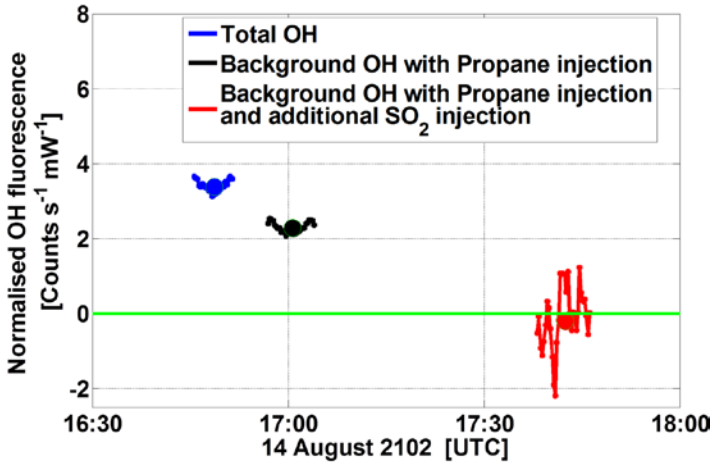

Figure 4.10. SO_2 injection test within IPI during the HOPE 2010 campaign. The blue signal represents the total OH measured by the instrument when no injection is performed. The black signal is the background OH signal when propane (2.5×10^{15} molecules cm^{-3}) is added within IPI, scavenging over 90 % of ambient OH. The red signal is the background OH signal observed when in addition to propane SO_2 (1×10^{13} molecules cm^{-3}) is injected within IPI.

With the addition of SO_2 (1×10^{13} molecules cm^{-3} in the sampled air) it is possible to remove the OH_{bg} signal from the instrument and the instrument does not detect any OH signal, although noise on the zero is large. The increase in noise on the zero is caused by a spectral interference arising from the addition of SO_2. However it is clear from the fluorescence spectra recorded while injecting SO_2 (Fig. 4.11) that there are no characteristic OH lines and therefore no OH radicals. The concentration of SO_2 is small enough as to not scavenge SCI

inside the low pressure section of the instrument and it is not additionally removing atmospheric OH within IPI as the lifetime of OH towards SO_2 is 200 times longer than towards propane.

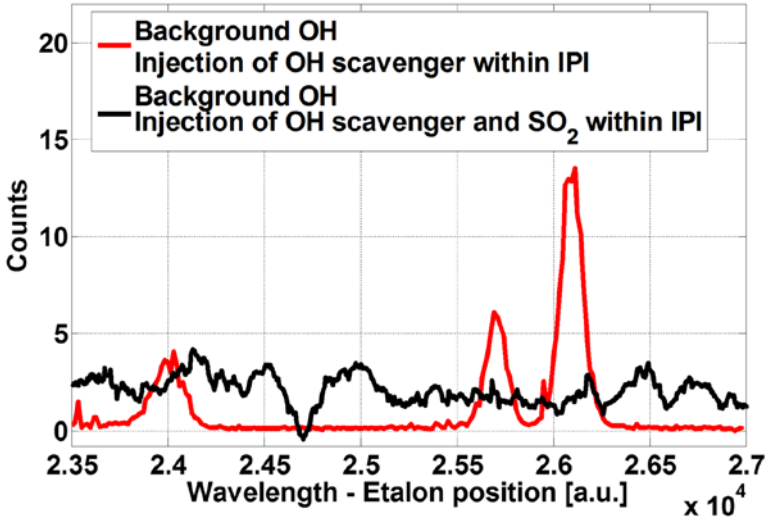

Figure 4.11. Fluorescence spectra at around 308 nm during injection of propane (2.5 x 10^{15} molecules cm^{-3}) within IPI (red line) and injection of propane and SO_2 (1 x 10^{13} molecules cm^{-3}) simultaneously.

4.5 SCI as a source of background OH

During the HUMPPA-COPEC 2010 campaign the background OH showed a strong correlation with temperature (R = 0.8) and with the OH reactivity (R = 0.6), which indicates correlation with BVOC, with ozone (R = 0.7), and it also correlated with the $P[H_2SO_4]_{unex}$ (R = 0.6).During the HOPE 2010 campaign the correlation observed between the OH_{bg} and temperature was worse (R = 0.5) and no correlation was observed with OH reactivity. The OH_{bg} correlated with the product of ozone and unsaturated VOC (R = 0.8) and was also scavenged by the addition with SO_2.

The evidence presented indicate that the OH_{bg} originates from a species formed during the ozonolysis of unsaturated VOC that decompose into OH, is removable by SO_2 and, if in a concentration high enough, has an impact on the H_2SO_4 production. We are not aware of any chemical species, apart from SCI, that are known to oxidise SO_2 at a fast enough rate and also decompose forming OH. In addition, HORUS was shown to be sensitive to the OH formed after unimolecular decomposition of SCI in the low pressure region of the instrument

(Novelli et al., 2014b) in controlled laboratory studies. During the HUMPPA-COPEC 2010 campaign, the correlation with the OH reactivity improved when considering only the night time, the period during which a higher fraction of the production rate of OH could not be accounted for (Hens et al., 2014). Indeed, during night the recycling via HO_2+NO is inhibited due to the low NO concentration, therefore a different path of formation of OH is necessary. One likely path could be the formation of OH from excited and stabilised CI formed from ozonolysis of unsaturated compounds.

The considerations above are all consistent with the hypothesis that OH_{bg} originates from unimolecular decomposition of SCI in the field as well as in the laboratory. Still, we cannot completely exclude that the OH_{bg} could be caused by another species, or by more than one chemical species. Such species would have to match the observation listed above, i.e. decompose in OH, oxidize SO_2 to H_2SO_4, react very slowly with alkanes, correlate with temperature as terpenes emissions do in a Boreal forest and correlate with the product of unsaturated VOC and ozone on a German hill. It is not clear at the moment which non-SCI species could account for all these observations simultaneously.

4.6 Absolute concentration of SCI from the background OH

Starting from four different approaches: missing H_2SO_4 oxidant, measured VOC, unidentified OH reactivity and unidentified production rate of OH, we estimated the concentration of SCI to be between ~ 10^4 to ~ 10^6 molecules cm^{-3}.

It has been shown that, with our current knowledge, the best candidate for the species causing the OH_{bg} measured within our IPI-LIF-FAGE instrument are SCI. More challenging is the determination of an absolute concentration of SCI starting from our OH_{bg}. At this moment, no method is available to produce and quantify a known concentration of a specific SCI conformer, yet this is necessary to obtain a calibration factor for such a species. *A priori*, it seems unlikely that the IPI-LIF-FAGE instrument calibration factor for ambient OH, i.e. sampled from the outside through the nozzle, is identical to the sensitivity for OH generated on the inside. The transmission factor through our nozzle pinhole is currently not known for either OH radicals or SCI; the calibration factor used for ambient OH accounts for this transmission as well as for e.g. OH losses on the walls, alignment of the white cell, transmission optics, and response of the MCP. These last three factors affect the OH

generated from the SCI similarly, while wall losses and transmission through the pinhole are different and possibly also differ between SCI conformers. Additionally, different SCI vary in their unimolecular decomposition rates and hence affect calibration by a different time-specific OH yield. For example, theoretical studies (Vereecken and Francisco, 2012) indicate that acetone oxide will decompose faster than *syn*-acetaldehyde oxide causing the formation of a different amount of OH, which in turn will be also affected by different losses in the low pressure segment of the instrument. Thus, it is not possible to convert the internal OH to an absolute SCI concentration in case of an unknown mixture of SCI. At best one could obtain an "average" sensitivity factor, if one knew the OH_{bg} formed from a series of reference SCI conformers, and if the ambient SCI speciation was known and not too dependent on reaction conditions. To further illustrate the need of a SCI-specific calibration, we try to naively calculate the external [SCI] from the internal OH_{bg} signal strength, calibrated based on the combined experimental and modelling study by (Novelli et al., 2014b). For a SCI mixture that behaves identical to syn-CH_3CHOO, the OH_{bg} from the HUMPPA-COPEC 2010 campaign would then indicate an external [SCI] $\geq 2 \times 10^7$ molecules cm^{-3}, well above the estimates presented in section 4.3. Even worse, the observed OH_{bg} signal interpreted in this way would imply an ambient OH production exceeding 4×10^8 molecules cm^{-3} s^{-1}, clearly in disagreement with established chemistry. If we assume a faster decomposition rate for the SCI of 200 s^{-1}, a higher fraction of the SCI decomposes in the low-pressure region, i.e. 80% compared to 25% for $k_{uni} = 20$ s^{-1}. This leads to a higher OH signal per SCI, and from this a [SCI] of 4×10^6 molecules cm^{-3}, though the implied OH production would remain significantly too high. Thus, the conversion of the OH signal to an absolute concentration of ambient SCI cannot be done unambiguously without full SCI speciation, and knowledge of their chemical kinetics. Note that these [SCI] estimates represent a lower limit as we only observe SCI that decompose to OH, whereas e.g. anti-SCI convert to acids/esters.

In an effort to work towards SCI-specific calibration, we probed the transmission of OH and syn-CH_3CHOO through nozzle and low-pressure region in the instrument, with preliminary laboratory tests using a traditional nozzle and a molecular beam skimmer nozzle. The difference between these two nozzles is shown in figure 4.12: the traditional nozzle, with a pinhole drilled through the tip of a cone, is characterized by quick gas expansion in the area immediately below the pinhole, contacting the wall surface of the bore. During ambient

measurement, deposition of matter in the position A from figure 4.12 has been observed, further illustrating the prevalence of wall contact.

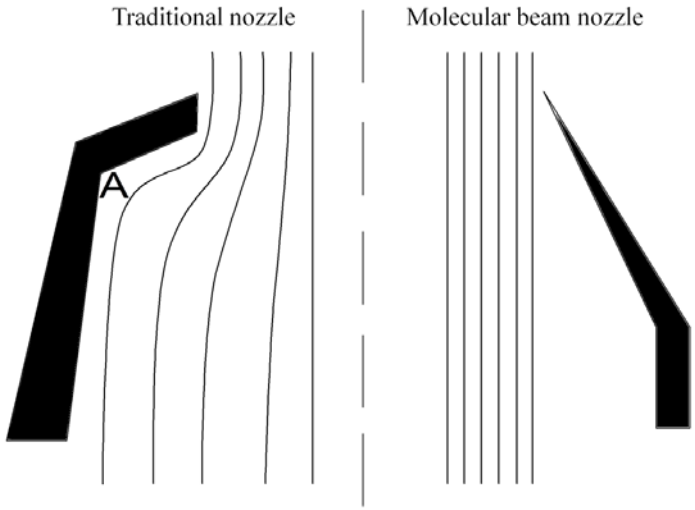

Figure 4.12. Schematic representation of the flow patterns in the traditional and molecular beam nozzles. A represent the area where deposit of particles is observed.

The molecular beam skimmer nozzle, on the other hand, has much thinner sidewalls and a significantly narrower gas expansion, strongly reducing wall contact. The laboratory test showed that the OH radical has a 23 % higher transmission through the molecular beam nozzle compared to the traditional nozzle. The *syn*-acetaldehyde oxide did not show any statistical difference in the transmission between the two nozzles. This indicates that (a) SCI and OH have a different transmission and most likely have different wall losses, underlining that the OH calibration factor is not applicable to SCI for ambient measurements, and (b) that the calibration factor for OH obtained for ambient OH does not alone allow the quantification of the absolute OH concentration in the low-pressure section of the FAGE instrument. This is the fundamental reason why the earlier naive estimate of [SCI] and OH production led to highly over-estimated values.

In addition to the above effects, one should also consider that OH-production from SCI in the low-pressure section might be catalysed to proceed at rates beyond their ambient counterpart, biasing our interpretation of their ambient fate. The catalysis might involve wall-induced isomerisation of the higher-energy *anti*-SCI to the more stable, OH-producing *syn*-SCI,

which would artificially increase the *syn*:*anti* ratio. Another possibility is the evaporation of clusters stabilizing the SCI, as it is known that SCI form strong complexes with many compounds, including water, acids, alcohols, hydroperoxides, HO_x radicals, etc. (Vereecken and Francisco, 2012). Redissociation of secondary ozonides (SOZ) seems less important, except perhaps the SOZ formed with CO_2 (Aplincourt and Ruiz-López, 2000) which has no alternative accessible unimolecular channels. At this time, insufficient information is available to assess the impact, if any, of such catalysis.

4.7 Conclusions

The estimate of a steady state concentration of SCI was done for the HUMPPA-COPEC 2010 and the HOPE 2012 campaigns based on a large array of available data. Starting from four different approaches, i.e. missing H_2SO_4 oxidant, measured VOC concentrations, unidentified OH reactivity and unidentified production rate of OH, we estimated the concentration of SCI to be between ~ 10^4 to ~ 10^6 molecules cm^{-3}. At such concentrations, SCI have an impact on the H_2SO_4 chemistry during the HUMPPA-COPEC 2010 campaign while during the HOPE 2012 campaign their impact is small to negligible. Additionally, it was shown that, with the yields and unimolecular decomposition rate chosen in this study, SCI do not have a large impact on the OH production compared to the impact of prompt OH generated from ozonolysis of unsaturated VOC. During both campaigns described in this study, the IPI-LIF-FAGE instrument detected an OH background signal that originates from decomposition of one or more species inside the low pressure region of the instrument. The source compound of the OH_{bg} was shown to oxidize SO_2 and a correlation had been found with the missing H_2SO_4 production rate. It correlates with temperature in the same way as the emission of terpenes and with the product of unsaturated VOC and ozone as well as with the OH reactivity. These observations are consistent with known SCI chemistry, suggesting that the source of the OH_{bg} are stabilized Criegee intermediates, and that an observable amount of such SCI is present in ambient conditions. The lack of a calibration factor for SCI does not currently allow the quantification of the steady state concentration of SCI in the atmosphere based on the observed OH_{bg} signal alone.

Although still affected by large uncertainties, the overall conclusion emerges that stabilized Criegee intermediates are acting consistently across the different aspects of tropospheric

chemistry, in full agreement with our current understanding of their chemistry, and thus present a strong case in favour of SCI as an actor in the atmosphere even if it has not yet been observed directly.

5 Summary and conclusions

An inlet pre-injector (IPI) has been developed and deployed to separate interfering signals from the atmospheric OH signal measured with our LIF-FAGE instrument. IPI allows for a periodic injection of an OH scavenger to the ambient air before it is sampled by the instrument. During periods with no injection of the OH scavenger the instrument measures a total OH signal (OH_{tot}); during the injection of the OH scavenger the instrument measures a background OH signal (OH_{bg}) caused by interfering species. Subtracting these two signals yields the OH radical concentration in ambient air (OH_{atm}). The IPI-LIF-FAGE instrument was used during three field campaigns: HUMPPA-COPEC 2010 (Boreal forest, Finland), DOMINO HO_x (Mediterranean forest, Spain) and HOPE 2012 (rural Europe, Germany). During daytime the OH_{bg} was found to contribute up to 80 % of the OH_{tot} signal within the canopy in the Boreal forest and on average only up to 30 % of the OH_{tot} signal in Germany. During night time, for all three sites, the OH_{bg} represented up to 100 % of the total OH signal and a very small concentration of atmospheric OH was measured in agreement with the known nocturnal chemistry of OH radicals. The atmospheric OH radical concentration measured by the IPI-LIF-FAGE was compared with two CIMS instruments during HUMPPA-COPEC 2010 and HOPE 2012 campaigns. Only with the implementation of IPI a reasonable agreement (R^2 = 0.4) was found in HUMMPA-COPEC-2010 and a good agreement (R^2 = 0.8) in HOPE, indicating the necessity of such a technique for our LIF-FAGE instrument. The OH_{bg} was found not to be laser or instrumental generated and its abundance seems to be related to the typology of VOC (biogenic vs. anthropogenic) and their absolute concentration.

Laboratory tests on the IPI-LIF-FAGE were performed to identify the species causing the OH_{bg} signal while measuring in the field. As no bimolecular reaction happens at a competitive rate within the low pressure region of the instrument and the signal is not laser generated, attention is focused on species able to generate OH radicals via unimolecular decomposition. The foremost candidates are Criegee intermediates (CI), also known as carbonyl oxides, which are formed in the atmosphere via ozonolysis of unsaturated volatile organic compounds. The CI exists mainly as excited CI and stabilised CI (SCI), and depending on their structure they can undergo unimolecular decomposition forming OH. To

test if the IPI-LIF-FAGE is sensitive to the detection of the OH formed from SCI, ozonolysis tests of propene and (E)-2-butene were performed in a flowtube at ambient pressure directly connected to the inlet of the instrument. The experiments were completed at ambient pressure and the OH radicals formed in the flowtube were scavenged with propane. The scavenger was added in a concentration such as to remove a large fraction of the OH formed at ambient pressure as the focus was on a possible OH signal observed from the unimolecular decomposition of SCI within the low pressure region of the instrument. Laboratory tests showed that even when injecting an OH scavenger concentration large enough to remove 99 % of the OH formed at ambient pressure, the IPI-LIF-FAGE instrument still detects quite a large OH signal. As the ozonolysis is totally suppressed in the low pressure, the signal has to come from the unimolecular decomposition of a species formed during the ozonolysis of the alkenes tested. To confirm that such a species is SCI, scavenging experiments with known SCI scavengers (water vapour, SO_2 and acetic acid) were done and the OH signal disappeared. This confirmed that the OH signal observed originated from SCI. To better understand where inside the instrument the OH was formed, the residence time of the SCI inside the low pressure region was varied and a temporal profile of OH within the instrument was measured for the *syn*-CH_3CHOO SCI conformer. Comparison between the experimental data and an upgraded version of the Master Chemical Mechanism including the most up-to-date chemistry for the SCI, permitted the determination of the unimolecular decomposition rate of the *syn*-CH_3CHOO ($k = 20 \pm 10\ s^{-1}$).

With this newly acquired knowledge, the OH_{bg} observed during field campaigns was investigated to understand if it could be caused by unimolecular decomposition of SCI as observed in the laboratory experiments. Firstly, the steady state concentration of SCI ($[SCI]_{ss}$) was estimated from available data for the HUMPPA-COPEC 2010 and HOPE 2012 campaigns. It was calculated starting from four different approaches: unexplained H_2SO_4 production rate, measured VOC, unknown OH reactivity and unknown production rate of OH. The $[SCI]_{ss}$ concentration obtained ranged between ~10^4 to ~10^6 molecules cm^{-3}. Once it was demonstrated that the SCI can be found in the atmosphere, the OH_{bg} was analysed together with the many traces gases measured during the HUMPPA-COPEC 2010 and HOPE 2012 campaigns to understand if the hypothesis about its origin could be confirmed. The source compound of the OH_{bg} was inferred to oxidize SO_2 to H_2SO_4, correlates with temperature and OH reactivity during the HUMPPA-COPEC 2010 campaign and also

correlates with the product of measured unsaturated VOC and ozone during the HOPE 2012 campaign. Additionally, during the HOPE 2012 campaign the OH_{bg} signal was scavenged with SO_2 providing additional confirmation of its reactivity with SO_2. These observations are consistent with known SCI chemistry, suggesting that the source of the OH_{bg} are stabilized Criegee intermediates, and that an observable amount of SCI is present in ambient conditions. The lack of a calibration factor for SCI does not currently allow the quantification of the steady state concentration of SCI in the atmosphere based on the observed OH_{bg} signal.

The main question surrounding Criegee intermediates is: "are SCI observable and do they have any impact in the troposphere?" The results described in this thesis show that they have an impact in the H_2SO_4 formation for both of the environments studied. Even when considering the lower limit of 1 x 10^4 molecules cm^{-3} for the $[SCI]_{ss}$ concentration calculated from the unexplained H_2SO_4 production rate, they appear to be the main chemical removal process for organic acids due to the very fast rate coefficient. In the Boreal forest, the majority of organic acid is removed by wet and dry deposition, but SCI contribute substantial proportion, up to 30 %, of the organic acid removal. It is not clear yet what products are formed after this reaction, but because of the very large number of oxygen atoms involved, it has been hypothesized that the products will have low volatility and be likely to contribute to particle formation. Therefore SCI would seem to play an active role in aerosol formation. If the SCI steady state concentration lies in the order of 10^4 molecules cm^{-3}, they will not have any impact in removal of CO or NO_2 and they will not impact the NO_3 production rate. In addition, they do not have a large impact on the production rate of OH when compared to the formation of prompt OH from ozonolysis of unsaturated VOC. Therefore, in a first approximation, they could be ignored in models investigating the OH radical concentration.

The large uncertainties in estimations of the steady state concentration of SCI clearly shows that further work is needed toward a reliable, direct or indirect, technique to measure their concentration in the atmosphere. Even without such a measurement, additional information concerning the rate coefficient of a larger number of SCI conformers with water and water dimers, and also less uncertain rate coefficients for reaction with OH, HO_2, RO_2 and alcohols are necessary. These would allow a better understanding of their behavior in ambient and improve our knowledge on the oxidation capacity of a certain environment.

6 Appendix

6.1 Direct observation of OH formation from stabilised Criegee intermediates, supplementary information.

6.1.1 Residence time

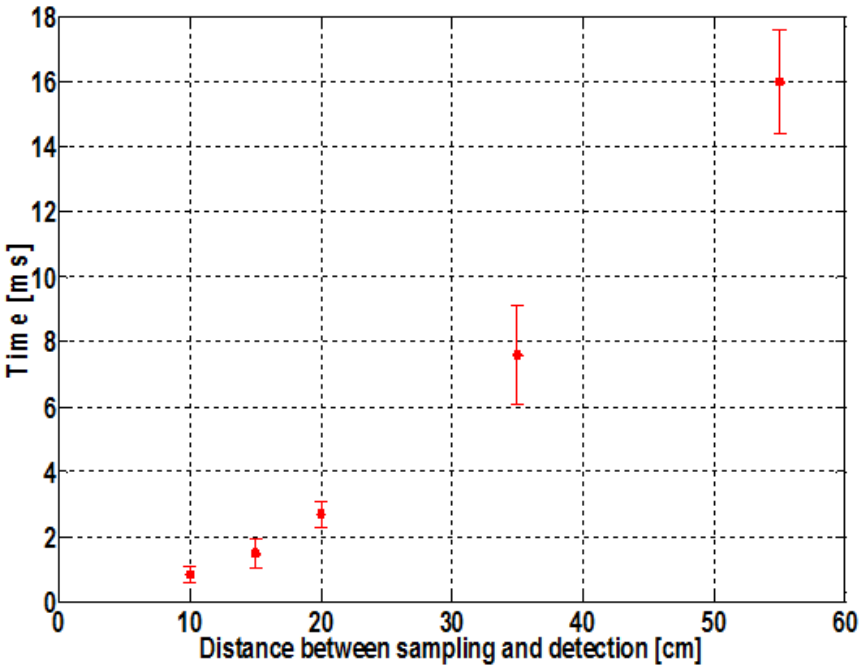

Figure 6.1. Residence time between the sampling point and the detection of OH radicals for five different inlet lengths.

6.1.2 HO_x losses

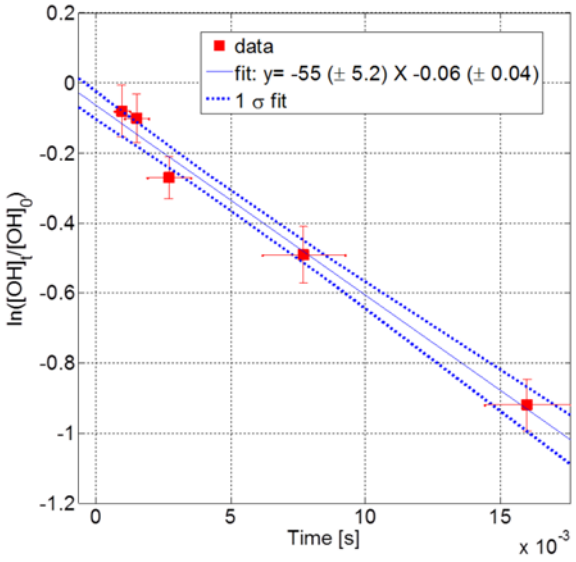

Figure 6.2. Wall loss of OH with residence time in the low-pressure segment of the LIF-FAGE instrument.

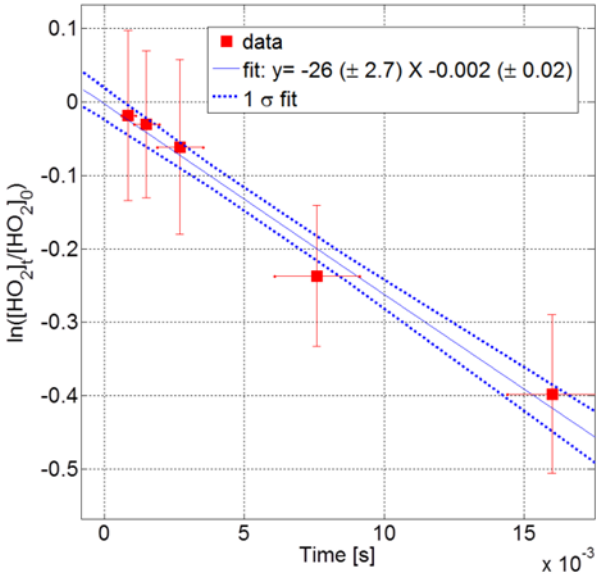

Figure 6.3. Wall loss of HO_2 with residence time in the low-pressure segment of the LIF-FAGE instrument.

6.1.3 Propene + Ozone – Additional figures and table

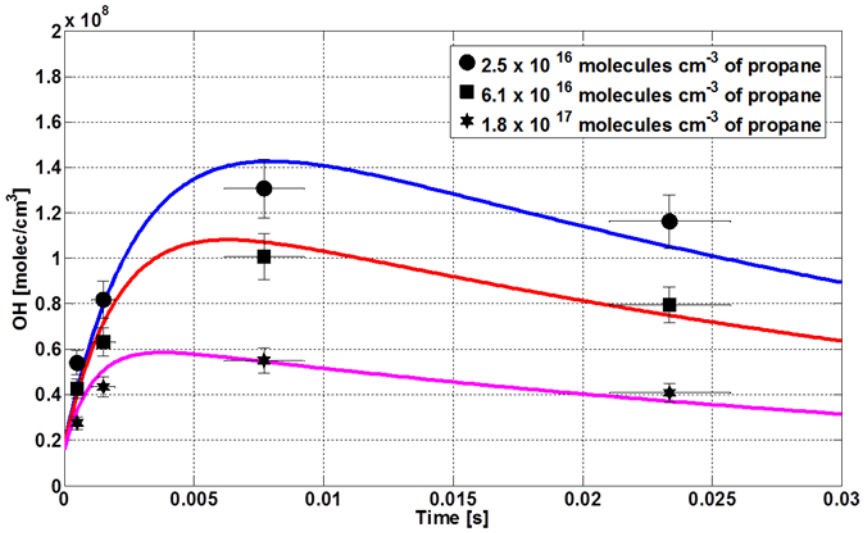

Figure 6.4. Temporal profiles of the OH signal (solid symbols) inside the detection cell of the LIF-FAGE instrument for the ozonolysis reaction of propene (3.5 x 10^{15} molecules cm^{-3}) and model simulations (lines) for three different concentrations of propane.

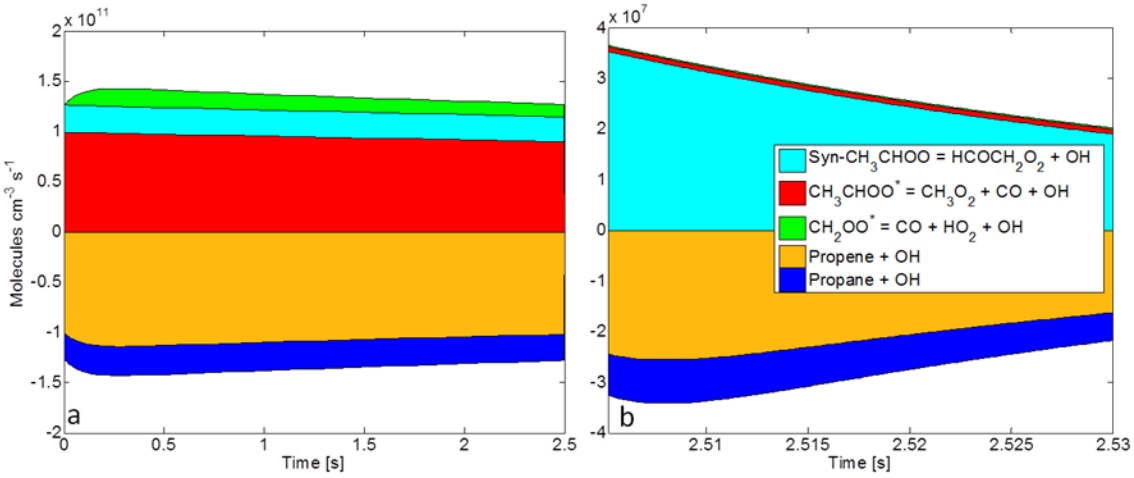

Figure 6.5. a, cumulative formation (positive contribution) and loss (negative contribution) pathways of OH in the flow tube at ambient pressure and b, formation and loss path of OH in the instrument inlet at ~ 3.5 hPa during the ozonolysis of propene.

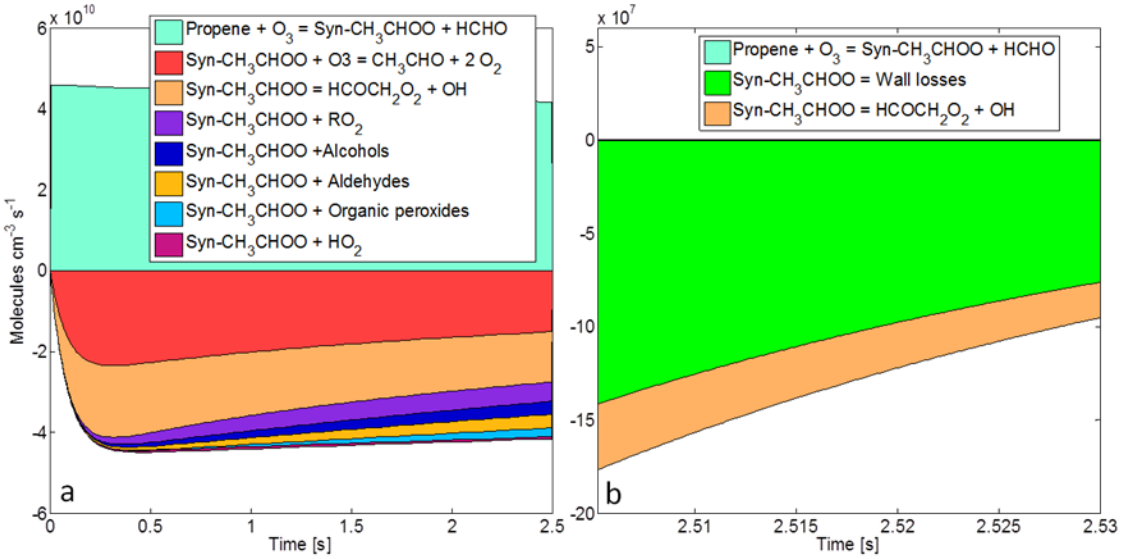

Figure 6.6. a, cumulative formation (positive contribution) and loss (negative contribution) pathway of *syn*-CH_3CHOO in the flow tube at ambient pressure and b, formation and loss path of *syn*-CH_3CHOO in the instrument inlet at ~ 3.5 hPa during the ozonolysis of propene.

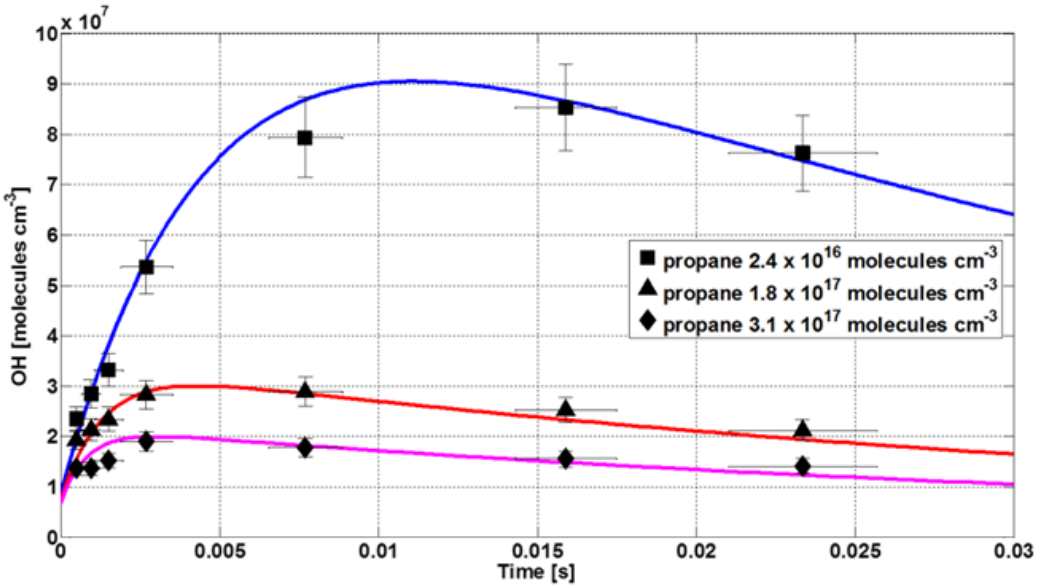

Figure 6.7. Temporal profiles of the OH signal (solid symbols) inside the detection cell of the LIF-FAGE instrument for the ozonolysis reaction of propene (1.8 x 10^{15} molecules cm^{-3}) and model simulations (lines) for three different concentrations of propane.

Table 6.1. Concentrations (molecules cm^{-3}) of SCIs at the sampling point together with the peak OH concentration observed during the ozonolysis experiments.

Propene	**Propane**	***Syn*-CH_3CHOO**	***Anti*-CH_3CHOO**	**CH_2OO**	**OH**
3.5×10^{15}	2.5×10^{16}	1.8×10^{9}	2.5×10^{8}	4.1×10^{9}	1.3×10^{8}
	6.1×10^{16}	1.8×10^{9}	2.5×10^{8}	4.2×10^{9}	1.0×10^{8}
	1.8×10^{17}	1.6×10^{9}	2.5×10^{8}	4.2×10^{9}	5.7×10^{7}
1.8×10^{15}	2.5×10^{16}	9.3×10^{8}	1.6×10^{8}	1.3×10^{9}	8.5×10^{7}
	1.8×10^{17}	9.3×10^{8}	1.6×10^{8}	1.3×10^{8}	3.0×10^{7}
	3.0×10^{17}	9.3×10^{8}	1.6×10^{8}	1.3×10^{8}	2.0×10^{7}

6.1.4 (E)-2-butene + Ozone – Additional figures and table

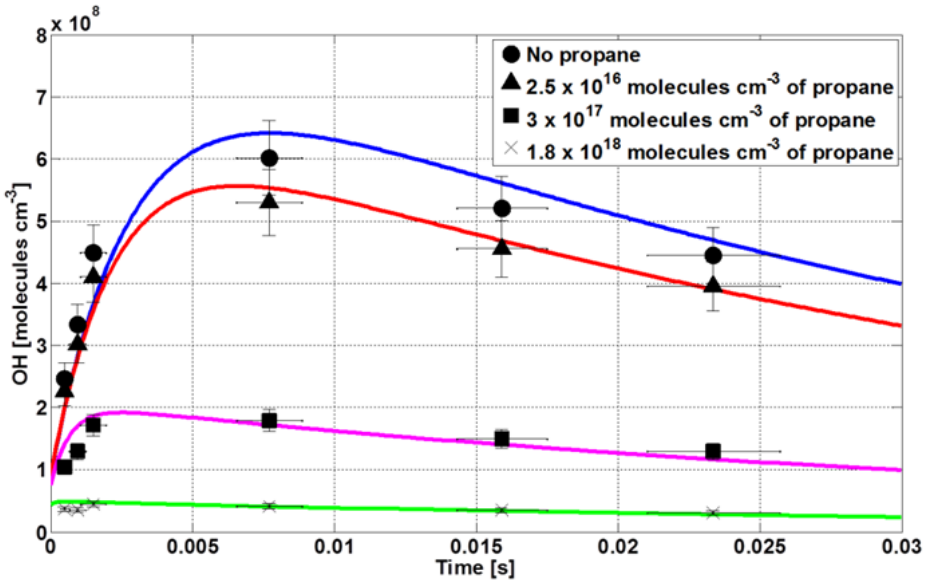

Figure 6.8. Temporal profiles of the OH signal (solid symbols) inside the detection cell of the LIF-FAGE instrument for the ozonolysis reaction of (E)-2-butene (1.4 x 10^{15} molecules cm^{-3}) and model simulations (lines) for four different concentrations of propane.

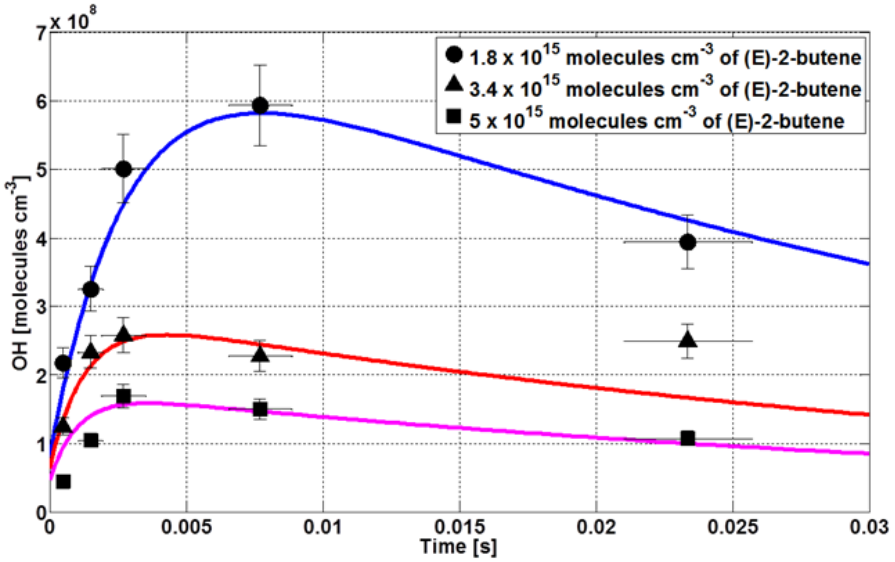

Figure 6.9. Temporal profiles of the OH signal (solid symbols) inside the detection cell of the LIF-FAGE instrument for the ozonolysis reaction of (E)-2-butene and model simulations (lines) for three different concentrations of (E)-2-butene at a constant concentration of propane of 2.5 x 10^{16} molecules cm^{-3}.

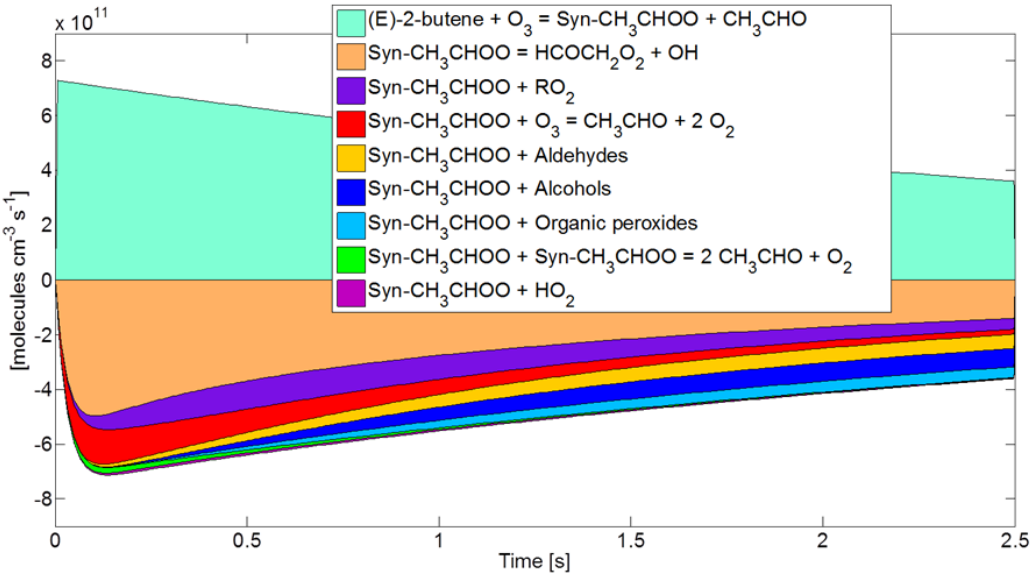

Figure 6.10. Cumulative formation (positive contribution) and loss path (negative contribution) of *syn*-CH_3CHOO in the flow tube at ambient pressure and b, formation and loss path of *syn*-CH_3CHOO in the instrument inlet at ~ 3.5 hPa during the ozonolysis of (E)-2-butene.

Table 6.2. Concentrations (molecules cm^{-3}) of SCIs at the sampling point together with the peak OH concentration observed during the ozonolysis experiments.

(E)-2-butene	**Propane**	***Syn*-CH_3CHOO**	***Anti*-CH_3CHOO**	**OH**
1.4×10^{15}	0	9.2×10^{9}	2.2×10^{9}	6.0×10^{8}
	2.5×10^{16}	9.0×10^{9}	2.2×10^{9}	5.3×10^{8}
	3.0×10^{17}	9.5×10^{9}	2.4×10^{9}	2.9×10^{8}
	1.8×10^{18}	9.7×10^{9}	2.4×10^{9}	5.8×10^{8}
1.8×10^{15}	2.5×10^{16}	9.2×10^{9}	9.0×10^{9}	5.9×10^{8}
3.4×10^{15}		9.0×10^{9}	6.8×10^{9}	2.5×10^{8}
5.0×10^{15}		9.5×10^{9}	4.4×10^{9}	1.8×10^{8}

6.1.5 Ethene + Ozone – Additional figures

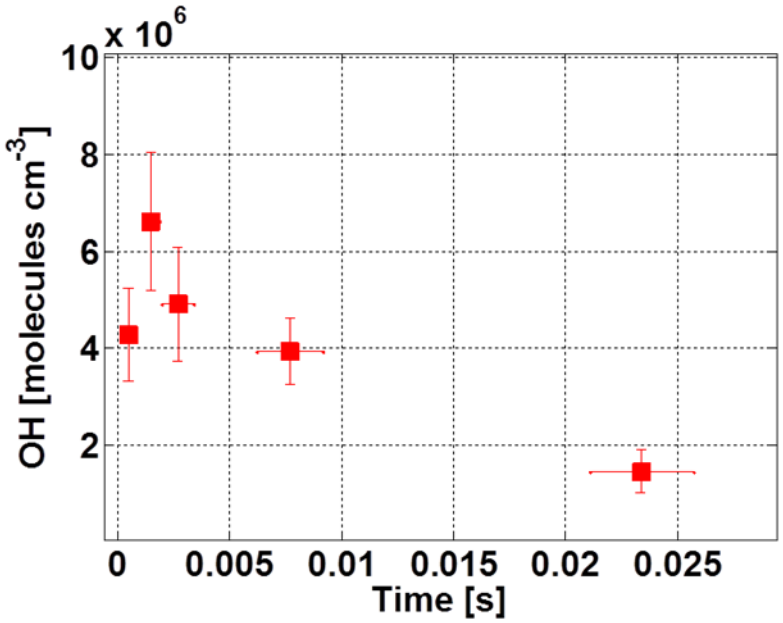

Figure 6.11. Temporal profile of the OH signal (red squares) inside the detection cell of the LIF-FAGE instrument for the ozonolysis reaction of ethene.

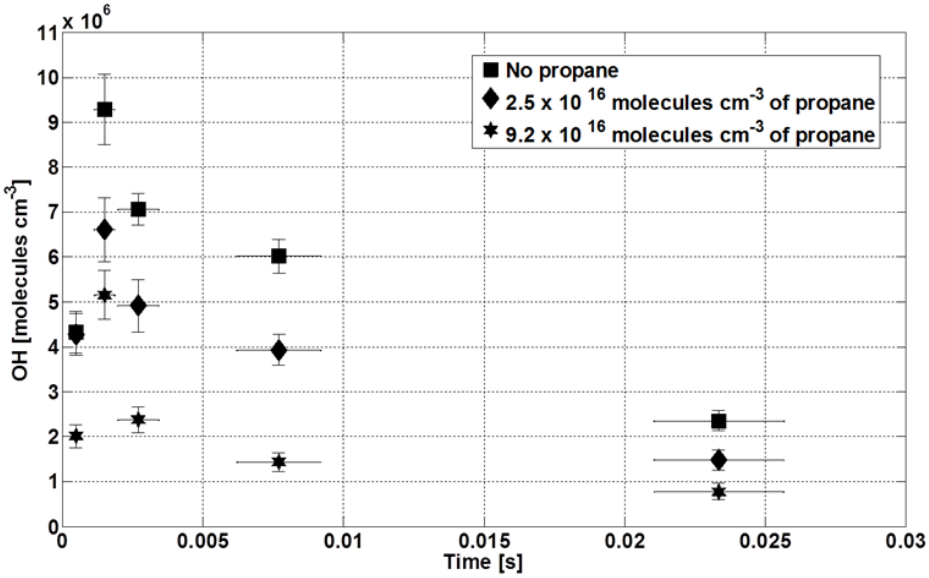

Figure 6.12. Temporal profiles of the OH signal (solid symbols) inside the detection cell of the LIF-FAGE instrument for the ozonolysis reaction of ethene (1.1 x 10^{16} molecules cm^{-3}) for three different concentrations of propane.

6.1.6 Scavenging experiment with water vapor

Figure 6.13 presents model simulations for three assumed rate coefficients of the reaction between *syn*-CH_3CHOO and water monomers and dimers. In these simulations, the ratio of $k(H_2O)$ and $k((H_2O)_2)$ is maintained as derived from Ryzhkov and Ariya (2004) as detailed in the main text, while the ratio $[(H_2O)_2]/[H_2O]$ is obtained by the equilibrium constant for dimerization.(Vereecken and Francisco, 2012) The best agreement is obtained for a rate coefficient between *syn*-CH_3CHOO and H_2O of ~ 3 x 10^{-17} cm^3 $molecule^{-1}$ s^{-1}, in agreement with the upper limit of 4 x 10^{-15} cm^3 $molecule^{-1}$ s^{-1} measured by Taatjes et al. (2013) The last experimental point at the highest humidity level (RH 46%) is not reproduced by the model simulation suggesting that the rate coefficient used for the *syn*-CH_3CHOO + $(H_2O)_2$ is too high, i.e. that the acceleration factor of 1.6 x 10^5 compared to the rate coefficient with water monomers (based on Ryzhkov and Ariya (2004)), could be overestimated.

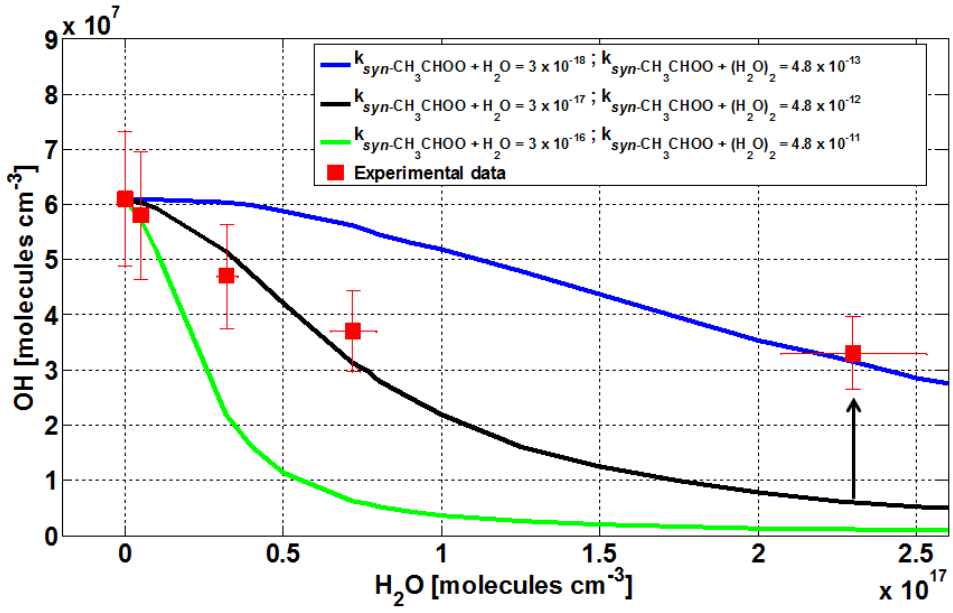

Figure 6.13. OH concentration observed at 2.4 ms as a function of water vapour (red square) together with model simulations (lines) for three different rate coefficients (cm^3 $molecule^{-1}$ s^{-1}) between *syn*-CH_3CHOO and water monomers and dimers.

6.1.7 Scavenging experiment with SO_2

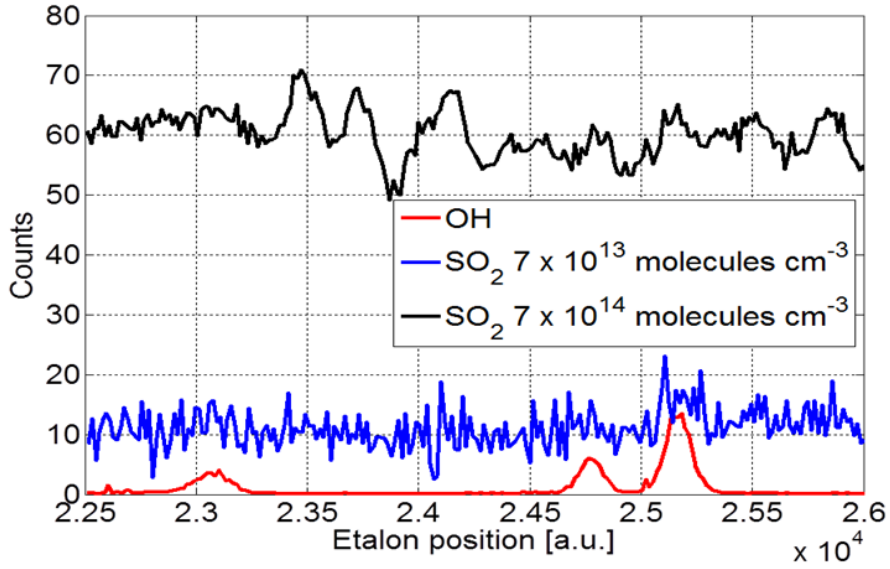

Figure 6.14. Fluorescence spectra at around 308 nm during ozonolysis of alkenes (red line), with the addition of 7 x 10^{13} molecules cm^{-3} (blue line) and 7 x 10^{14} molecules cm^{-3} (black line) of SO_2.

From Figure 6.14, it follows that the impact of SO_2 on the OH measurements cannot be easily subtracted. The measurement of the OH concentration is performed by tuning the excitation laser on and off resonance with the transition line at 308 nm (the high red peak in figure 6.14), thus allowing removal of the spectral background from the pure OH signal.

With SO_2 added, the signal differences between the on-resonance and off-resonance frequencies are not a straightforward superposition of an OH signal and a linearly increasing spectral background caused by SO_2, other compounds, and instrumental noise. In particular, the overall spectrum changes qualitatively with increasing [SO_2], i.e. the position and shape of the peaks changes as the contribution to the signal from each of the components changes with changing SO_2. As such, the spectral background measured off-resonance is not necessarily equal to the background signal underneath the on-resonance OH peak, nor can it be reduced to a fixed ratio between the two wavelengths employed. This occurs to a significant extent even for the lowest SO_2 concentrations we used. As such, the subtracted signals obtained in these conditions are not a true measure of the OH concentration.

What can be observed from the spectra is that the OH peak is significantly reduced or even removed entirely even at the lowest SO_2 concentrations, i.e. the peak signal at 308 nm should be clearly visible above the noisy spectral background for [SO_2] = 7 x 10^{-13} molecules cm^{-3} if

the OH concentration would remain unaffected. This loss of OH is corroborated by the model predictions which, using a rate coefficient k(*syn*-$CH_3CHOO+SO_2$) = 2.4 x 10^{-11} cm^3 $molecule^{-1}$ s^{-1},(Taatjes et al., 2013) predict a 100-fold decrease in *syn*-CH_3CHOO and concomitant OH decrease, i.e. at these SO_2 concentration the OH peak is expected to be near-vanishing in the spectrum, contributing only 1% of the signal for [SO_2] = 7 x 10^{-13} molecules cm^{-3} (blue curve, SI-14). Note that SO_2 does not react with OH directly, either in the high- or low-pressure regimes, and the lack of OH peak is thus directly related to removal of *syn*-CH_3CHOO by SO_2 in the high-pressure flow tube, removing the *syn*-CH_3CHOO decomposition as the OH source in the low-pressure cell.

A quantitative analysis might be possible using significantly lower concentrations of SO_2, provided a concentration range can be found where the spectral background caused by SO_2 remains negligible, while the *syn*-CH_3CHOO is still sufficiently scavenged to cause a measurable reduction in OH signal.

6.1.8 Scavenging experiment with acetic acid

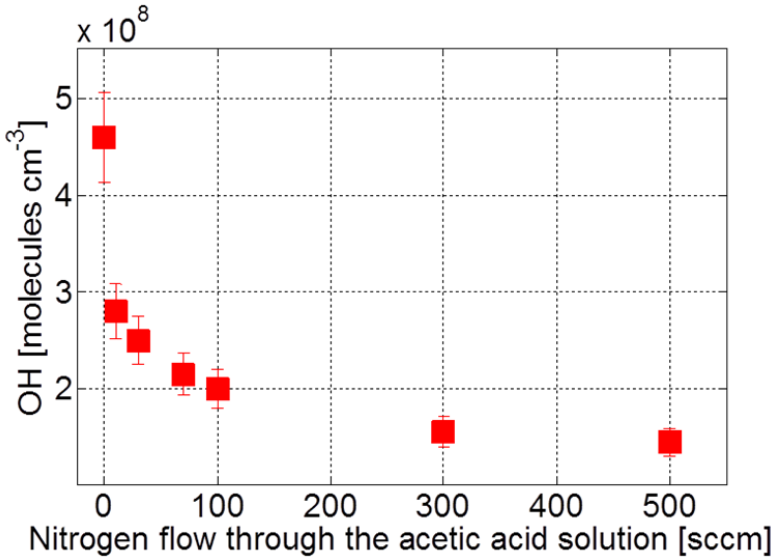

Figure 6.15. OH concentration observed at 2.4 ms as a function of acetic acid vapor.

6.1.9 Flow Tube Experiment – Kinetic Models

6.1.9.1 Ethene

Kinetic model added to the MCM chemistry to describe the CI chemistry in ethene ozonolysis, in Facsimile format. The MCM uses container species, i.e. class-specific-species that contain the sum of all individual species in this class, to describe certain reaction, e.g. for RO2. We have defined some additional container species to easily describe the generic reactions of CI with aldehyde, ketone, hydroxy, carboxylic acid and organic peroxide-compounds. These were calculated using the following MCM species names:

Ketones = CH3COCH3 + HCOCO3H + HCOCO2H + ACETOL + HYPERACET + IPROPOLPER + MGLYOX + CH3CO3H + GLYOX + HOC2H4CO3H + HOCH2CO3H + CH3CO2H + C2H5CO3 + CH3CHOHCO3 + CH3COCH2O + CO23C3CHO + HOC2H4CO3 + CH3COCH2O2;

Aldehydes = HCHO + CH3CHO + C2H5CHO + CH3CHOHCHO + HOCH2CHO + HOC2H4CHO + HCOCH2O + HCOCH2O2 + HCOCH2OOH;

Alcohols = CH3OH + C2H5OH + NPROPOL + IPROPOL + HOC2H4CO2H + ETHGLY + HYETHO2H + IPROPOLPER + IPROPOLO2H + HOC2H4CO3H + PROPGLY + CH3CHOHCHO + HOCH2CO2H + HO1C3OOH + HOC3H6OH + HOCH2CHO + C4ME22OH + HOC2H4CHO + HYPROPO2H + C4ME2OHOOH + ACETOL + HOCH2CO3H + CH3CHOHCO3 + HO1C3O + HO1C3O2 + HO1C3OOH + HOC2H4CO3 + HOCH2CH2O + HOCH2CH2O2 + HOCH2CO3 + HYPROPO2 + ETHGLY + HYPROPO + IPROPOLO2;

Acids = HCOOH + CH3CO2H + PROPACID + HOC2H4CO2H + HCOCO2H + HOCH2CO2H + HCOCO3H + PERPROACID;

Organic peroxides = HYPERACET + IPROPOLPER + CH3CO3H + HYETHO2H + IPROPOLO2H + HOC2H4CO3H + HO1C3OOH + HYPROPO2H + C4ME2OHOOH + HOCH2CO3H + C2H5OOH + CH3OOH + H2O2 + HCOCH2OOH + HO1C3OOH + IC3H7OOH;

For some of the CI reactions, the fate of the products was not explicitly modeled, as they didn't accumulate to a sufficiently high concentration to affect the kinetics. Future work will include the secondary chemistry explicitly; in many cases, the CI reactions lead to oxygenated compounds that should be part of the RO2, Aldehydes, Ketones, Alcohols, Acids or Organic Peroxides container species.
Finally, to merge the model below with the MCM, some reactions need to be removed from the original MCM model, as they are redefined or altered in our more explicit model: C2H4 + O3, all CH2OOA reactions, all CH2OO reactions.

```
* ------------------------------------------------------------------------------------------------------
-- ;
* Novelli, Vereecken, Lelieveld and Harder, “Direct observation of OH formation from ;
* stabilised Criegee intermediates” PCCP, submitted 2014 ;
* ------------------------------------------------------------------------------------------------------
---;
```

```
* Ozonolysis reaction yields excited CI (reactions as per the MCM) ;
* or forms stabilized CI ;
* YCH2 = fraction of CI stabilized  ;

YCH2 = 0.4; * The fraction of SCI formed during ozonolysis;

% 9.1D-15*EXP(-2580/TEMP)*(1-YCH2E) : C2H4 + O3 = HCHO + CH2OOA ;
% 9.1D-15*EXP(-2580/TEMP) : C2H4 + O3 = HCHO + CH2OO ;

* The chemistry of the excited Criegee intermediates, CH2OOA ;
* is taken from the MCM;

% KDEC*0.54/(1-YCH2) : CH2OOA = CO ;
% KDEC*0.10/(1-YCH2) : CH2OOA = HO2 + CO + OH ;

* Rate coefficients for the reaction of CI are discussed in the main paper ;

KEth      = 1;
KSO2      = 4D-11;
KAcids    = 2D-10;
KRO2      = 5D-12;
KHO2      = 5D-12;
KKeton    = 2.3D-13;
KAlde     = 1D-12;
KPerox    = 3D-12;
KOH       = 5D-12;
KAlco     = 5D-12;
KCO       = 4D-14;
KH2O      = 2D-16;
KAlke     = 6D-16;
KCriegee  = 4D-10;
KOzone    = 4D-13;
KDime     = 7D-11;
KNO2      = 2D-12;
KWall     = 22;

* Where feasible, the MCM products are specified. For other reactions, we define product
sinks;
* whose secondary chemistry is not considered further at this stage, (i.e. SOZ, Oligomers
;
* Product1/2/3/4/5), as in our conditions they do not accumulate to relevant concentrations.
;

% KEth :    CH2OO              = Dioxirane;
% KCO:      CH2OO + CO         = HCHO + CO2;
% KH2O:     CH2OO + H2O        = HOCH2OOH;
% KSO2 :    CH2OO + SO2        = SO3 ;
% KKeton :  CH2OO + Ketones    = SOZ;
```

% KAlde : CH2OO + Aldehydes = SOZ;
% KPerox : CH2OO + Peroxides = Oligomers;
% KAlco : CH2OO + Alcohols = Product1;
% KHO2 : CH2OO + HO2 = Oligomers;
% KRO2 : CH2OO + RO2 = Oligomers;
% KAcids : CH2OO + Acids = Product2;
% KOH : CH2OO + OH = Product3;
% KAlke : CH2OO + C2H4 = Product4;
% KCriegee : CH2OO + CH2OO = CH2O + CH2O + O2 ;
% KOzone : CH2OO + O3 = CH2O + O2 + O2 ;
% KWall : CH2OO = Product5;
% KDime : CH2OO + Dime = Product6;
% KNO2 : CH2OO + NO2 = CH3CHO + NO3 ;

* For completeness, we also added two ozone reactions, with rate ;
* coefficients from IUPAC ;
% 2D-15 : HO2 + O3 = OH + O2;
% 7.3D-14 : OH + O3 = HO2 + O2;
* ---------- ;

6.1.9.2 Propene

Kinetic model added to the MCM chemistry to describe the CI chemistry in propene ozonolysis, in Facsimile format. The MCM uses container species, i.e. class-specific-species that contain the sum of all individual species in this class, to describe certain reaction, e.g. for RO2. We have defined some additional container species to easily describe the generic reactions of CI with aldehyde, ketone, hydroxy, carboxylic acid and organic peroxide-compounds. These were calculated using the following MCM species names:

Ketones = CH3COCH3 + HCOCO3H + HCOCO2H + ACETOL + HYPERACET + IPROPOLPER + MGLYOX + CH3CO3H + GLYOX + HOC2H4CO3H + HOCH2CO3H + BIACET + BIACETO2 + BIACETOH + BIACETOOH + BUT2OLO +C2H5CO3 + CH3CHOHCO3 + CH3COCH2O + CO23C3CHO + HOC2H4CO3 + PERPROACID;
Aldehydes = HCHO + CH3CHO + C2H5CHO + CH3CHOHCHO + HOCH2CHO + HOC2H4CHO + HCOCH2O + HCOCH2O2 + HCOCH2OOH + PROPALO;
Alcohols = CH3OH + C2H5OH + NPROPOL + IPROPOL + HOC2H4CO2H + ETHGLY + HYETHO2H + IPROPOLPER + IPROPOLO2H + HOC2H4CO3H + PROPGLY + CH3CHOHCHO + HOCH2CO2H + HO1C3OOH + HOC3H6OH + HOCH2CHO + C4ME22OH + HOC2H4CHO + HYPROPO2H + C4ME2OHOOH + ACETOL + HOCH2CO3H + BIACETOH + BUT2OLAO + BUT2OLO + BUT2OLO + BUT2OLOH + BUT2OLOOH + CH3CHOHCO3 + HO1C3O + HO1C3O2 + HO1C3OOH + HOC2H4CO3 + HOCH2CH2O + HOCH2CH2O2 + HOCH2CO3 + HYPROPO2 + IPROPOLO + IPROPOLO2;
Acids = HCOOH + CH3CO2H + PROPACID + HOC2H4CO2H + HCOCO2H + HOCH2CO2H + HCOCO3H;

Organic peroxides = HYPERACET + IPROPOLPER + CH3CO3H + HYETHO2H + IPROPOLO2H + HOC2H4CO3H + HO1C3OOH + HYPROPO2H + C4ME2OHOOH + HOCH2CO3H + BIACETOOH + C2H5OOH + CH3OOH + H2O2 + HCOCH2OOH + HO1C3OOH + IC3H7OOH + PERPROACID;

For some of the CI reactions, the fate of the products was not explicitly modeled, as they didn't accumulate to a sufficiently high concentration to affect the kinetics. Future work will include the secondary chemistry explicitly; in many cases, the CI reactions lead to oxygenated compounds that should be part of the RO2, Aldehydes, Ketones, Alcohols, Acids or Organic Peroxides container species.
Finally, to merge the model below with the MCM, some reactions need to be removed from the original MCM model, as they are redefined or altered in our more explicit model: C3H6 + O3, all CH2OOB reactions, all CH2OO reactions, all CH3CHOOA reactions, all CH3CHOO.

```
* ------------------------------------------------------------------------------------------------------
--;
* Novelli, Vereecken, Lelieveld and Harder, “Direct observation of OH formation from;
* stabilised Criegee intermediates” PCCP, submitted 2014 ;
* ------------------------------------------------------------------------------------------------------
--;
* Ozonolysis reaction yields excited CI (reactions as per the MCM) ;
* or forms stabilized syn-CI or stabilized anti-CI ;
* YPropSCI = fraction of CI stabilized ;
* YPropSS = fraction of syn-CI in the CI formed ;

YPropSCI = 0.24;   * The fraction of SCI formed during ozonolysis;
YPropSS   = 0.4;     * The fraction of syn or anti in the SCI;

% (5.5D-15*EXP(-1880/TEMP)*(1-YPropSCI)*0.5) : O3 + C3H6 =
CH3CHOOB + HCHO ;
% (5.5D-15*EXP(-1880/TEMP)*(1-YPropSCI)*0.5) : O3 + C3H6 =
CH2OOB + CH3CHO ;
% (5.5D-15*EXP(-1880/TEMP)*(YPropSCI)*(YPropSS)) : O3 + C3H6 =
CH3CHOOS + HCHO ;
% (5.5D-15*EXP(-1880/TEMP)*(YPropSCI)*(0.5-YPropSS)) : O3 + C3H6 =
CH3CHOOA + HCHO ;
% (5.5D-15*EXP(-1880/TEMP)*(YPropSCI)*0.5) : O3 + C3H6 =
CH2OO + CH3CHO ;


* The chemistry of the excited Criegee intermediates, CH3CHOOB ;
* and CH2OOB is taken from the MCM;

% KDEC*0.3/(1-YPropSCI) : CH3CHOOB     = CH3O2 + CO + OH;
% KDEC*0.125/(1-YPropSCI) : CH3CHOOB = CH3O2 + HO2;
% KDEC*0.125/(1-YPropSCI) : CH3CHOOB = CH4;
```

```
% KDEC*0.57/(1-YPropSCI) : CH2OOB        = CO ;
% KDEC*0.10/(1-YPropSCI) : CH2OOB        = HO2 + CO + OH ;

* Rate coefficients for the reaction of CI are discussed in the main paper ;
* Some rate coefficients are specific for CH2OO or syn or anti-CH3CHOO, as indicated ;
* by suffix E/S/A ;

KSCIS     = 3;
KSCIA     = 3;
KSO2E     = 4D-11;
KSO2S     = 2D-11;
KSO2A     = 7D-11;
KAcids    = 2.5D-10;
KRO2      = 5D-12;
KHO2      = 5D-12;
KOH       = 9D-12;
KKeton    = 2D-13;
KAlde     = 1D-12;
KPerox    = 3D-12;
KAlco     = 5D-12;
KCO       = 4D-14;
KH2OE     = 2D-16;
KH2OS     = 2D-19;
KH2OA     = 1D-14;
KAlkeE    = 2D-15;
KalkeS    = 2D-18;
KAlkeA    = 9D-15;
KCriegee  = 2.7D-11;
KCriegeeE = 4D-10;
KOzone    = 3.8D-13;
KDimeS    = 3.2D-14;
KDimeA    = 5.1D-11;
KDimeE    = 7D-11;
KNO2      = 2D-12;
KWall     = 22;

* Syn- and anti-CI-specific chemistry. Where feasible, the MCM ;
* products are specified. For other reactions, we define product sinks;
* whose secondary chemistry is not considered further at this stage, ;
*(i.e. SOZ, Oligomers, Product1/2/3/4/5/6), as in our conditions they do;
* not accumulate to relevant concentrations. ;

% KEth :    CH2OO                 = Dioxirane;
% KCO:      CH2OO + CO            = HCHO + CO2;
% KH2OE:    CH2OO + H2O           = HOCH2OOH;
% KSO2E :   CH2OO + SO2           = SO3 ;
% KKeton :  CH2OO + Ketones       = SOZ;
% KAlde :   CH2OO + Aldehydes     = SOZ;
```

```
% KPerox : CH2OO + Peroxides          = Oligomers;
% KAlco : CH2OO + Alcohols            = Product1;
% KHO2 : CH2OO + HO2                  = Oligomers;
% KRO2 : CH2OO + RO2                  = Oligomers;
% KAcids : CH2OO + Acids              = Product2;
% KOH : CH2OO + OH                    = Product3;
% KAlkeE : CH2OO + C3H6               = Product4;
% KCriegeeE : CH2OO + CH2OO           = CH2O + CH2O + O2 ;
% KCriegee : CH2OO + CH3CHOOS         = CH2O + CH3CHO + O2 ;
% KCriegee : CH2OO + CH3CHOOA         = CH2O + CH3CHO + O2  ;
% KOzone : CH2OO + O3                 = CH2O + O2 + O2 ;
% KWall : CH2OO                       = Product5;
% KDimeE : CH2OO + Dime               = Product6;
% KNO2 : CH2OO + NO2                  = CH3CHO + NO3 ;

% KSCIS :    CH3CHOOS                 = OH + HCOCH2O2;
% KCO :      CH3CHOOS + CO            = CH3CHO + CO2;
% KH2OS :    CH3CHOOS + H2O           = HOCH3CHOOH;
% KSO2S :    CH3CHOOS + SO2           = SO3 ;
% KAlco :    CH3CHOOS + Alcohols      = Product1;
% KKeton :   CH3CHOOS + Ketones       = SOZ;
% KAlde :    CH3CHOOS + Aldehydes     = SOZ;
% KPerox :   CH3CHOOS + Peroxides     = Oligomers;
% KHO2 :     CH3CHOOS + HO2           = Oligomers;
% KRO2 :     CH3CHOOS + RO2           = Oligomers;
% KAcids :   CH3CHOOS + Acids         = Product2;
% KOH :      CH3CHOOS + OH            = Product3;
% KAlkeS :   CH3CHOOS + C3H6          = Product4;
% KCriegee : CH3CHOOS + CH3CHOOS      = CH3CHO + CH3CHO + O2;
% KCriegee : CH3CHOOS + CH3CHOOA      = CH3CHO + CH3CHO + O2;
% KOzone :   CH3CHOOS + O3            = CH3CHO + O2 + O2;
% KWall :    CH3CHOOS                 = Product5;
% KDimeS :   CH3CHOOS + Dime          = Product6;
% KNO2 :     CH3CHOOS + NO2           = CH3CHO + NO3 ;

% KSCIA :    CH3CHOOA                 = Dioxirane;
% KCO :      CH3CHOOA + CO            = CH3CHO + CO2;
% KH2OA :    CH3CHOOA + H2O           = HOCH3CHOOH;
% KSO2A :    CH3CHOOA + SO2           = SO3 ;
% KAlco :    CH3CHOOA + Alcohols      = Product1;
% KKeton :   CH3CHOOA + Ketones       = SOZ;
% KAlde :    CH3CHOOA + Aldehydes     = SOZ;
% KPerox :   CH3CHOOA + Peroxides     = Oligomers;
% KHO2 :     CH3CHOOA + HO2           = Oligomers;
% KRO2 :     CH3CHOOA + RO2           = Oligomers;
% KAcids :   CH3CHOOA + Acids         = Product2;
% KOH :      CH3CHOOA + OH            = Product3;
% KAlkeA :   CH3CHOOA + C3H6          = Product4;
```

% KCriegee : CH3CHOOA + CH3CHOOA = CH3CHO + CH3CHO + O2;
% KOzone : CH3CHOOA + O3 = CH3CHO;
% KWall : CH3CHOOA = Product5;
% KDimeA : CH3CHOOA + Dime = Product6;
% KNO2 : CH3CHOOA + NO2 = CH3CHO + NO3 ;

* For completeness, we also added two ozone reactions, with rate ;
* coefficients from IUPAC ;
% 2D-15 : HO2 + O3 = OH + O2;
% 7.3D-14 : OH + O3 = HO2 + O2;
* ---------- ;

6.1.9.3 (E)-2-butene

Kinetic model added to the MCM chemistry to describe the CI chemistry in (E)-2-butene ozonolysis, in Facsimile format. The MCM uses container species, i.e. class-specific-species that contain the sum of all individual species in this class, to describe certain reaction, e.g. for RO2. We have defined some additional container species to easily describe the generic reactions of CI with aldehyde, ketone, hydroxy, carboxylic acid and organic peroxide-compounds. These were calculated using the following MCM species names:

Ketones = CH3COCH3 + HCOCO3H + HCOCO2H + ACETOL + HYPERACET + IPROPOLPER + MGLYOX + CH3CO3H + GLYOX + HOC2H4CO3H + HOCH2CO3H + BIACET + BIACETO2 + BIACETOH + BIACETOOH + BUT2OLO + C2H5CO3 + CH3CHOHCO3 + CH3COCH2O + CO23C3CHO + HOC2H4CO3;
Aldehydes = HCHO + CH3CHO + C2H5CHO + CH3CHOHCHO + HOCH2CHO + HOC2H4CHO + HCOCH2O + HCOCH2O2 + HCOCH2OOH;
Alcohols = CH3OH + C2H5OH + NPROPOL + IPROPOL + HOC2H4CO2H + ETHGLY + HYETHO2H + IPROPOLPER + IPROPOLO2H + HOC2H4CO3H + PROPGLY + CH3CHOHCHO + HOCH2CO2H + HO1C3OOH + HOC3H6OH + HOCH2CHO + C4ME22OH + HOC2H4CHO + HYPROPO2H + C4ME2OHOOH + ACETOL + HOCH2CO3H + BIACETOH + BUT2OLAO + BUT2OLO + BUT2OLO + BUT2OLOH + BUT2OLOOH + CH3CHOHCO3 + HO1C3O + HO1C3O2 + HO1C3OOH + HOC2H4CO3 + HOCH2CH2O + HOCH2CH2O2 + HOCH2CO3 + HYPROPO2;
Acids = , CH3CO2H + PROPACID + HOC2H4CO2H + HCOCO2H + HOCH2CO2H + HCOCO3H;
Organic peroxides = HYPERACET + IPROPOLPER + CH3CO3H + HYETHO2H + IPROPOLO2H + HOC2H4CO3H + HO1C3OOH + HYPROPO2H + C4ME2OHOOH + HOCH2CO3H + BIACETOOH + C2H5OOH + CH3OOH + H2O2 + HCOCH2OOH + HO1C3OOH + IC3H7OOH;

For some of the CI reactions, the fate of the products was not explicitly modeled, as they didn't accumulate to a sufficiently high concentration to affect the kinetics. Future work will

include the secondary chemistry explicitly; in many cases, the CI reactions lead to oxygenated compounds that should be part of the RO2, Aldehydes, Ketones, Alcohols, Acids or Organic Peroxides container species.
Finally, to merge the model below with the MCM, some reactions need to be removed from the original MCM model, as they are redefined or altered in our more explicit model:
TBUT2ENE + O3, all CH3CHOO reactions, all CH3CHOOB reactions.

```
* ------------------------------------------------------------------------------------------------------
-- ;
* Novelli, Vereecken, Lelieveld and Harder, “Direct observation of OH formation from ;
* stabilised Criegee intermediates” PCCP, submitted 2014 ;
* ------------------------------------------------------------------------------------------------------
---;
* Ozonolysis reaction yields excited CI (reactions as per the MCM), ;
* or forms stabilized syn-CI or stabilized anti-CI ;
* YButSCI = fraction of CI stabilized ;
* YButSS = fraction of syn-CI in the CI formed ;

YButSCI = 0.18; * The fraction of SCI formed during ozonolysis;
YButSS = 0.8; * The fraction of syn or anti in the SCI;

% 6.64D-15*EXP(-1059/TEMP)*(1-YButSCI) : TBUT2ENE + O3
= CH3CHO + CH3CHOOB ;
% 6.64D-15*EXP(-1059/TEMP)*(YButSCI*YButSS) : TBUT2ENE + O3
 = CH3CHO + CH3CHOOS ;
% 6.64D-15*EXP(-1059/TEMP)*(YButSCI*(1-YButSS)) : TBUT2ENE + O3
= CH3CHO + CH3CHOOA ;

* The chemistry of the excited Criegee intermediates, CH3CHOOB ;
* is taken from the MCM ;

% KDEC*0.3/(1-YButSCI) :    CH3CHOOB  = CH3O2 + CO + OH;
% KDEC*0.125/(1-YButSCI) : CH3CHOOB = CH3O2 + HO2;
% KDEC*0.125/(1-YButSCI) : CH3CHOOB = CH4;



* Rate coefficients for the reaction of CI are discussed in the main ;
* paper. Some rate coefficients are specific for syn or anti-CI, as ;
* indicated by suffix S/A ;

KSCIS        = 3;
KSCIA        = 3;
KAlkeS       = 1.7D-19;
KH2OS        = 2D-19;
KAlkeA       = 1.4D-15;
KH2OA        = 1D-14;
KAcids       = 2.5D-10;
```

KRO2 = 5D-12;
KHO2 = 5D-12;
KOH = 5D-12;
KKeton = 2D-13;
KAlde = 1D-12;
KPerox = 3D-12;
KAlco = 5D-12;
KCO = 4D-14;
KCriegee = 3D-11;
KOzone = 3.8D-13;
KDimeS = 3.2D-14;
KDimeA = 5.1D-11;
KSO2S = 2D-11;
KSO2A = 7D-11;
KNO2 = 2D-12;
KWall = 22;

* Syn- and anti-CI-specific chemistry. Where feasible, the MCM ;
* products are specified. For other reactions, we define product sinks;
* whose secondary chemistry is not considered further at this stage, ;
*(i.e. SOZ, Oligomers, Product1/2/3/4/5), as in our conditions they do;
* not accumulate to relevant concentrations. ;

% KSCIS : CH3CHOOS = OH + HCOCH2O2;
% KCO : CH3CHOOS + CO = CH3CHO + CO2;
% KH2OS : CH3CHOOS + H2O = HOCH3CHOOH;
% KSO2S: CH3CHOOS + SO2 = SO3 ;
% KAlco : CH3CHOOS + Alco = Product1;
% KKeton : CH3CHOOS + Keton = SOZ;
% KAlde : CH3CHOOS + Alde = SOZ;
% KPerox : CH3CHOOS + Perox = Oligomers;
% KHO2 : CH3CHOOS + HO2 = Oligomers;
% KRO2 : CH3CHOOS + RO2 = Oligomers;
% KAcids : CH3CHOOS + Acids = Product2;
% KOH : CH3CHOOS + OH = Product3;
% KAlkeS : CH3CHOOS + TBUT2ENE = Product4;
% KCriegee : CH3CHOOS + CH3CHOOS = CH3CHO + CH3CHO + O2;
% KCriegee : CH3CHOOS + CH3CHOOA = CH3CHO + CH3CHO + O2;
% KOzone : CH3CHOOS + O3 = CH3CHO + O2 + O2;
% KWall : CH3CHOOS = Product5;
% KDimeS : CH3CHOOS + Dime = Product6;
% KNO2 : CH3CHOOS + NO2 = CH3CHO + NO3 ;

% KSCIA : CH3CHOOA = Dioxirane;
% KCO : CH3CHOOA + CO = CH3CHO + CO2;
% KH2OA : CH3CHOOA + H2O = HOCH3CHOOH;
% KSO2A: CH3CHOOA + SO2 = SO3 ;
% KAlco : CH3CHOOA + Alcohols = Product1;

```
% KKeton :    CH3CHOOA + Ketones          = SOZ;
% KAlde :     CH3CHOOA + Aldehydes        = SOZ;
% KPerox :    CH3CHOOA + Peroxides        = Oligomers;
% KHO2 :      CH3CHOOA + HO2              = Oligomers;
% KRO2 :      CH3CHOOA + RO2              = Oligomers;
% KAcids :    CH3CHOOA + Acids            = Product2;
% KOH :       CH3CHOOA + OH               = Product3;
% KAlkeA :    CH3CHOOA + TBUT2ENE         = Product4;
% KCriegee : CH3CHOOA + CH3CHOOA          = CH3CHO + CH3CHO + O2;
% KOzone :    CH3CHOOA + O3               = CH3CHO;
% Kwall :     CH3CHOOA                    = Product5;
% KDimeA : CH3CHOOA + Dime                = Product6;
% KNO2 :     CH3CHOOA + NO2               = CH3CHO + NO3 ;

* For completeness, we also added two ozone reactions, with rate ;
* coefficients from IUPAC ;
% 2D-15 : HO2 + O3  = OH + O2;
% 7.3D-14 : OH + O3 = HO2 + O2;
* ---------------------------------------------------------------- ;
```

6.2 Identification of Criegee intermediates as potential oxidants in the troposphere, supplementary information.

6.2.1 Additional figures

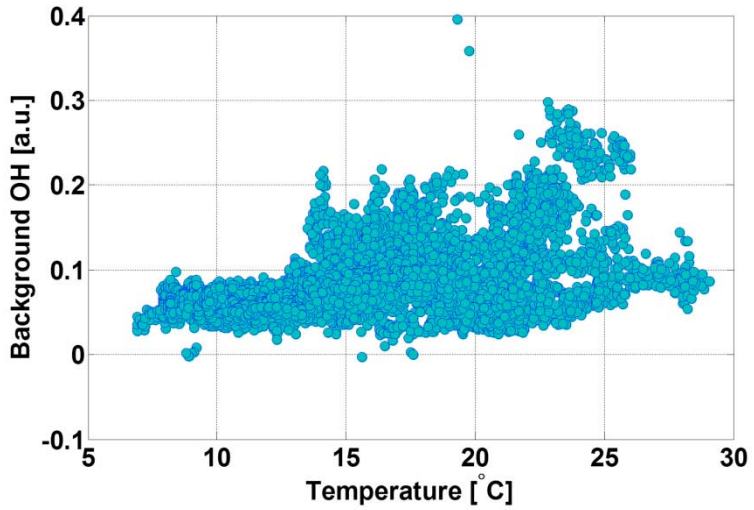

Figure 6.16. Correlation between the background OH signal and temperature during the HOPE 2012 campaign.

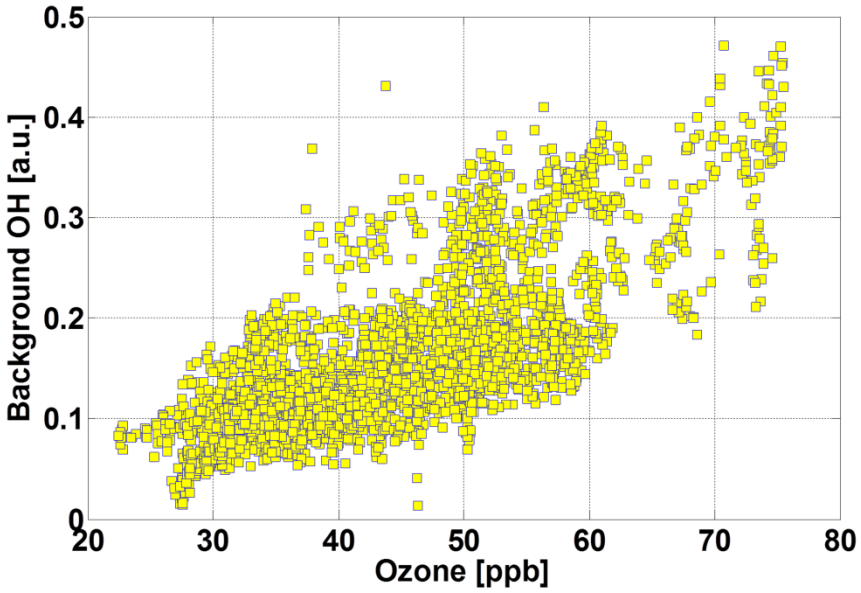

Figure 6.17. Correlation between the background OH signal and the ozone concentration during the HUMPPA-COPEC 2010 campaign.

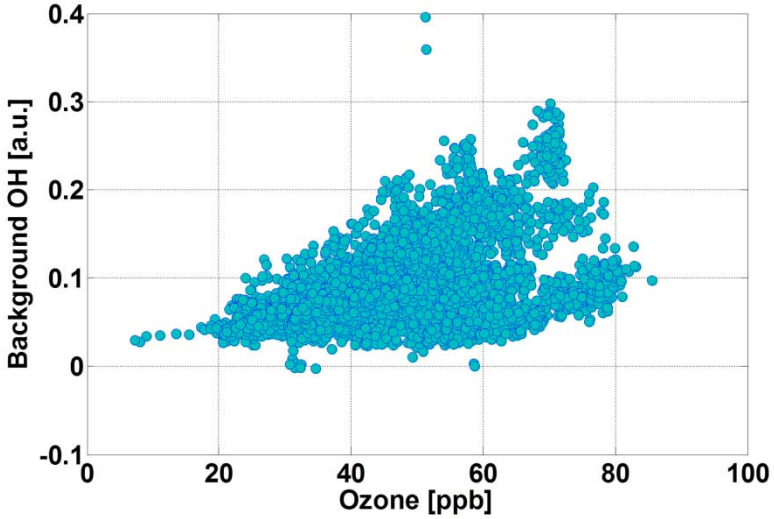

Figure 6.18. Correlation between the background OH signal and the ozone concentration during the HOPE 2012 campaign.

7 References

Aalto, P., HÄMeri, K., Becker, E. D. O., Weber, R., Salm, J., MÄKelÄ, J. M., Hoell, C., O'Dowd, C. D., Karlsson, H., Hansson, H.-C., VÄKevÄ, M., Koponen, I. K., Buzorius, G., and Kulmala, M.: Physical characterization of aerosol particles during nucleation events, Tellus B, 53, 344-358, 2001.

Ahrens, J., Carlsson, P. T., Hertl, N., Olzmann, M., Pfeifle, M., Wolf, J. L., and Zeuch, T.: Infrared detection of Criegee intermediates formed during the ozonolysis of beta-pinene and their reactivity towards sulfur dioxide, Angew Chem Int Ed Engl, 53, 715-719, 2014.

Anglada, J. M., Aplincourt, P., Bofill, J. M., and Cremer, D.: Atmospheric Formation of OH Radicals and H_2O_2 from Alkene Ozonolysis under Humid Conditions, Chemphyschem, 3, 215-221, 2002.

Anglada, J. M., Bofill, J. M., Olivella, S., and Solé, A.: Unimolecular Isomerizations and Oxygen Atom Loss in Formaldehyde and Acetaldehyde Carbonyl Oxides. A Theoretical Investigation, J Am Chem Soc, 118, 4636-4647, 1996.

Anglada, J. M., Gonzalez, J., and Torrent-Sucarrat, M.: Effects of the substituents on the reactivity of carbonyl oxides. A theoretical study on the reaction of substituted carbonyl oxides with water, Phys Chem Chem Phys, 13, 13034-13045, 2011.

Aplincourt, P. and Ruiz-López, M. F.: Theoretical Investigation of Reaction Mechanisms for Carboxylic Acid Formation in the Atmosphere, J Am Chem Soc, 122, 8990-8997, 2000.

Atkinson, R. and Arey, J.: Atmospheric Degradation of Volatile Organic Compounds, Chemical Reviews, 103, 4605-4638, 2003.

Atkinson, R., Baulch, D. L., Cox, R. A., Crowley, J. N., Hampson, R. F., Hynes, R. G., Jenkin, M. E., Rossi, M. J., and Troe, J.: Evaluated kinetic and photochemical data for atmospheric chemistry: Volume I - gas phase reactions of Ox, HOx, NOx and SOx species, Atmos. Chem. Phys., 4, 1461-1738, 2004.

Atkinson, R., Baulch, D. L., Cox, R. A., Crowley, J. N., Hampson, R. F., Hynes, R. G., Jenkin, M. E., Rossi, M. J., Troe, J., and Subcommittee, I.: Evaluated kinetic and photochemical data for atmospheric chemistry: Volume II - gas phase reactions of organic species, Atmos. Chem. Phys., 6, 3625-4055, 2006.

Beames, J. M., Liu, F., Lu, L., and Lester, M. I.: UV spectroscopic characterization of an alkyl substituted Criegee intermediate CH_3CHOO, J Chem Phys, 138, 244307, 2013.

Berndt, T., Jokinen, T., Mauldin, R. L., Petaja, T., Herrmann, H., Junninen, H., Paasonen, P., Worsnop, D. R., and Sipila, M.: Gas-Phase Ozonolysis of Selected Olefins: The Yield of Stabilized Criegee Intermediate and the Reactivity toward SO_2, J. Phys. Chem. Lett., 3, 2892-2896, 2012.

Berndt, T., Jokinen, T., Sipilä, M., Mauldin Iii, R. L., Herrmann, H., Stratmann, F., Junninen, H., and Kulmala, M.: H_2SO_4 formation from the gas-phase reaction of stabilized Criegee Intermediates with SO_2: Influence of water vapour content and temperature, Atmos Environ, 89, 603-612, 2014a.

Berndt, T., Junninen, H., Roy, L. M. I., Herrmann, H., Kulmala, M., and Sipilä, M.: Competitive reaction of CH_2OO with SO_2 and water vapour and the thermal lifetime of CH_2OO at 293 K, Geophysical Research Abstracts 16, 2014b.

Berndt, T., Voigtlander, J., Stratmann, F., Junninen, H., Mauldin Iii, R. L., Sipila, M., Kulmala, M., and Herrmann, H.: Competing atmospheric reactions of CH_2OO with SO_2 and water vapour, Phys Chem Chem Phys, 16, 19130-19136, 2014c.

Berresheim, H., Elste, T., Plass-Dülmer, C., Eisele, F. L., and Tanner, D. J.: Chemical ionization mass spectrometer for long-term measurements of atmospheric OH and H_2SO_4, International Journal of Mass Spectrometry, 202, 91-109, 2000.

Birmili, W., Berresheim, H., Plass-Dülmer, C., Elste, T., Gilge, S., Wiedensohler, A., and Uhrner, U.: The Hohenpeissenberg aerosol formation experiment (HAFEX): a long-term study including size-resolved aerosol, H_2SO_4, OH, and monoterpenes measurements, Atmos. Chem. Phys., 3, 361-376, 2003.

Boy, M., Mogensen, D., Smolander, S., Zhou, L., Nieminen, T., Paasonen, P., Plass-Dülmer, C., Sipilä, M., Petäjä, T., Mauldin, L., Berresheim, H., and Kulmala, M.: Oxidation of SO_2 by stabilized Criegee intermediate (sCI) radicals as a crucial source for atmospheric sulfuric acid concentrations, Atmos. Chem. Phys., 13, 3865-3879, 2013.

Buras, Z. J., Elsamra, R. M., Jalan, A., Middaugh, J. E., and Green, W. H.: Direct kinetic measurements of reactions between the simplest Criegee intermediate CH_2OO and alkenes, J Phys Chem A, 118, 1997-2006, 2014.

C. D. Rathman, W., A. Claxton, T., R. Rickard, A., and Marston, G.: A theoretical investigation of OH formation in the gas-phase ozonolysis of E-but-2-ene and Z-but-2-ene, Phys Chem Chem Phys, 1, 3981-3985, 1999.

Carlsson, P. T. M., Keunecke, C., Kruger, B. C., Maa, and Zeuch, T.: Sulfur dioxide oxidation induced mechanistic branching and particle formation during the ozonolysis of [small beta]-pinene and 2-butene, Phys Chem Chem Phys, 14, 15637-15640, 2012.

Case Hanks, A. T.: Formaldehyde Instrument Development and Boundary Layer Sulfuric Acid: Implications for Photochemistry, Doctor of Philosophy, Earth & Atmospheric Sciences, Georgia Institute of technology, 2008.

Chuong, B., Zhang, J., and Donahue, N. M.: Cycloalkene Ozonolysis: Collisionally Mediated Mechanistic Branching, J Am Chem Soc, 126, 12363-12373, 2004.

Criegee, R.: Mechanism of Ozonolysis, Angew. Chem.-Int. Edit. Engl., 14, 745-752, 1975.

Crounse, J. D., Paulot, F., Kjaergaard, H. G., and Wennberg, P. O.: Peroxy radical isomerization in the oxidation of isoprene, Phys Chem Chem Phys, 13, 13607-13613, 2011.

Crowley, J. N., Thieser, J., Tang, M. J., Schuster, G., Bozem, H., Beygi, Z. H., Fischer, H., Diesch, J. M., Drewnick, F., Borrmann, S., Song, W., Yassaa, N., Williams, J., Pöhler, D., Platt, U., and Lelieveld, J.:

Variable lifetimes and loss mechanisms for NO_3 and N_2O_5 during the DOMINO campaign: contrasts between marine, urban and continental air, Atmos. Chem. Phys., 11, 10853-10870, 2011.

Curtis, A. R. and Sweetenham, W. P.: Facsimile / CHeckmat User's Manual, Harwell Laboratory, Oxfordshire, 1987. 1987.

da Silva, G.: Hydroxyl radical regeneration in the photochemical oxidation of glyoxal: kinetics and mechanism of the HC(O)CO + O_2 reaction, Phys Chem Chem Phys, 12, 6698-6705, 2010a.

da Silva, G.: Kinetics and Mechanism of the Glyoxal + HO_2 Reaction: Conversion of HO_2 to OH by Carbonyls, The Journal of Physical Chemistry A, 115, 291-297, 2010b.

da Silva, G.: Oxidation of Carboxylic Acids Regenerates Hydroxyl Radicals in the Unpolluted and Nighttime Troposphere, The Journal of Physical Chemistry A, 114, 6861-6869, 2010c.

Di Carlo, P., Brune, W. H., Martinez, M., Harder, H., Lesher, R., Ren, X. R., Thornberry, T., Carroll, M. A., Young, V., Shepson, P. B., Riemer, D., Apel, E., and Campbell, C.: Missing OH reactivity in a forest: Evidence for unknown reactive biogenic VOCs, Science, 304, 722-725, 2004.

Dillon, T. J. and Crowley, J. N.: Direct detection of OH formation in the reactions of HO_2 with $CH_3C(O)O_2$ and other substituted peroxy radicals, Atmos. Chem. Phys., 8, 4877-4889, 2008.

Donahue, N. M., Drozd, G. T., Epstein, S. A., Presto, A. A., and Kroll, J. H.: Adventures in ozoneland: down the rabbit-hole, Phys Chem Chem Phys, 13, 10848-10857, 2011.

Drozd, G. T. and Donahue, N. M.: Pressure Dependence of Stabilized Criegee Intermediate Formation from a Sequence of Alkenes, J Phys Chem A, 115, 4381-4387, 2011.

Drozd, G. T., Kroll, J., and Donahue, N. M.: 2,3-Dimethyl-2-butene (TME) Ozonolysis: Pressure Dependence of Stabilized Criegee Intermediates and Evidence of Stabilized Vinyl Hydroperoxides, J Phys Chem A, 115, 161-166, 2011.

Duhl, T. R., Helmig, D., and Guenther, A.: Sesquiterpene emissions from vegetation: a review, Biogeosciences, 5, 761-777, 2008.

Edwards, P. M., Evans, M. J., Furneaux, K. L., Hopkins, J., Ingham, T., Jones, C., Lee, J. D., Lewis, A. C., Moller, S. J., Stone, D., Whalley, L. K., and Heard, D. E.: OH reactivity in a South East Asian tropical rainforest during the Oxidant and Particle Photochemical Processes (OP3) project, Atmos. Chem. Phys., 13, 9497-9514, 2013.

Eisele, F. L., Mauldin, R. L., Tanner, D. J., Cantrell, C., Kosciuch, E., Nowak, J. B., Brune, B., Faloona, I., Tan, D., Davis, D. D., Wang, L., and Chen, G.: Relationship between OH measurements on two different NASA aircraft during PEM Tropics B, Journal of Geophysical Research: Atmospheres, 106, 32683-32689, 2001.

Eisele, F. L., Mauldin, R. L., Tanner, D. J., Fox, J. R., Mouch, T., and Scully, T.: An inlet/sampling duct for airborne OR and sulfuric acid measurements, J Geophys Res-Atmos, 102, 27993-28001, 1997.

Eisele, F. L. and Tanner, D. J.: Ion-assisted tropospheric OH measurements, Journal of Geophysical Research: Atmospheres, 96, 9295-9308, 1991.

Epstein, S. A. and Donahue, N. M.: Ozonolysis of Cyclic Alkenes as Surrogates for Biogenic Terpenes: Primary Ozonide Formation and Decomposition, The Journal of Physical Chemistry A, 114, 7509-7515, 2010.

Faloona, I., Tan, D., Brune, W., Hurst, J., Barket, D., Couch, T. L., Shepson, P., Apel, E., Riemer, D., Thornberry, T., Carroll, M. A., Sillman, S., Keeler, G. J., Sagady, J., Hooper, D., and Paterson, K.: Nighttime observations of anomalously high levels of hydroxyl radicals above a deciduous forest canopy, Journal of Geophysical Research: Atmospheres, 106, 24315-24333, 2001.

Faloona, I., Tan, D., Lesher, R., Hazen, N., Frame, C., Simpas, J., Harder, H., Martinez, M., Di Carlo, P., Ren, X., and Brune, W.: A Laser-induced Fluorescence Instrument for Detecting Tropospheric OH and HO_2: Characteristics and Calibration, J. Atmos. Chem., 47, 139-167, 2004.

Fenske, J. D., Hasson, A. S., Ho, A. W., and Paulson, S. E.: Measurement of Absolute Unimolecular and Bimolecular Rate Constants for CH_3CHOO Generated by the trans-2-Butene Reaction with Ozone in the Gas Phase, The Journal of Physical Chemistry A, 104, 9921-9932, 2000a.

Fenske, J. D., Kuwata, K. T., Houk, K. N., and Paulson, S. E.: OH Radical Yields from the Ozone Reaction with Cycloalkenes, The Journal of Physical Chemistry A, 104, 7246-7254, 2000b.

Fortner, E. C., Zheng, J., Zhang, R., Berk Knighton, W., Volkamer, R. M., Sheehy, P., Molina, L., and André, M.: Measurements of Volatile Organic Compounds Using Proton Transfer Reaction – Mass Spectrometry during the MILAGRO 2006 Campaign, Atmos. Chem. Phys., 9, 467-481, 2009.

Fuchs, H., Hofzumahaus, A., Rohrer, F., Bohn, B., Brauers, T., Dorn, H. P., Haseler, R., Holland, F., Kaminski, M., Li, X., Lu, K., Nehr, S., Tillmann, R., Wegener, R., and Wahner, A.: Experimental evidence for efficient hydroxyl radical regeneration in isoprene oxidation, Nature Geosci, advance online publication, 2013.

Gilge, S., Plass-Dülmer, C., Fricke, W., Kaiser, A., Ries, L., Buchmann, B., and Steinbacher, M.: Ozone, carbon monoxide and nitrogen oxides time series at four alpine GAW mountain stations in central Europe, Atmos. Chem. Phys., 10, 12295-12316, 2010.

Grossmann, D., Moortgat, G. K., Kibler, M., Schlomski, S., Bächmann, K., Alicke, B., Geyer, A., Platt, U., Hammer, M. U., Vogel, B., Mihelcic, D., Hofzumahaus, A., Holland, F., and Volz-Thomas, A.: Hydrogen peroxide, organic peroxides, carbonyl compounds, and organic acids measured at Pabstthum during BERLIOZ, J. Geophys. Res., 108, 8250, 2003.

Gutbrod, R., Kraka, E., Schindler, R. N., and Cremer, D.: Kinetic and Theoretical Investigation of the Gas-Phase Ozonolysis of Isoprene: Carbony l Oxides as an Important Source for OH Radicals in the Atmosphere, J Am Chem Soc, 119, 7330-7342, 1997.

Hakola, H., Tarvainen, V., Laurila, T., Hiltunen, V., Hellén, H., and Keronen, P.: Seasonal variation of VOC concentrations above a boreal coniferous forest, Atmos Environ, 37, 1623-1634, 2003.

Handisides, G. M., Plass-Dülmer, C., Gilge, S., Bingemer, H., and Berresheim, H.: Hohenpeissenberg Photochemical Experiment (HOPE 2000): Measurements and photostationary state calculations of OH and peroxy radicals, Atmos. Chem. Phys., 3, 1565-1588, 2003.

Hard, T. M., O'Brien, R. J., Chan, C. Y., and Mehrabzadeh, A. A.: Tropospheric free radical determination by fluorescence assay with gas expansion, Environ Sci Technol, 18, 768-777, 1984.

Harrison, R. M., Yin, J., Tilling, R. M., Cai, X., Seakins, P. W., Hopkins, J. R., Lansley, D. L., Lewis, A. C., Hunter, M. C., Heard, D. E., Carpenter, L. J., Creasey, D. J., Lee, J. D., Pilling, M. J., Carslaw, N., Emmerson, K. M., Redington, A., Derwent, R. G., Ryall, D., Mills, G., and Penkett, S. A.: Measurement and modelling of air pollution and atmospheric chemistry in the U.K. West Midlands conurbation: Overview of the PUMA Consortium project, Sci. Total Environ., 360, 5-25, 2006.

Hasson, A. S., Ho, A. W., Kuwata, K. T., and Paulson, S. E.: Production of stabilized Criegee intermediates and peroxides in the gas phase ozonolysis of alkenes: 2. Asymmetric and biogenic alkenes, Journal of Geophysical Research: Atmospheres, 106, 34143-34153, 2001.

Hatakeyama, S., Kobayashi, H., Lin, Z. Y., Takagi, H., and Akimoto, H.: Mechanism for the reaction of CH_2OO with SO_2, J. Phys. Chem., 90, 4131-4135, 1986.

Heard, D. E. and Pilling, M. J.: Measurement of OH and HO_2 in the Troposphere, Chemical Reviews, 103, 5163-5198, 2003.

Hens, K., Novelli, A., Martinez, M., Auld, J., Axinte, R., Bohn, B., Fischer, H., Keronen, P., Kubistin, D., Nölscher, A. C., Oswald, R., Paasonen, P., Petäjä, T., Regelin, E., Sander, R., Sinha, V., Sipilä, M., Taraborrelli, D., Tatum Ernest, C., Williams, J., Lelieveld, J., and Harder, H.: Observation and modelling of HOx radicals in a boreal forest, Atmos. Chem. Phys., 14, 8723-8747, 2014.

Hoerger, C. C., Werner, A., Plass-Duelmer, C., Reimann, S., Eckart, E., Steinbrecher, R., Aalto, J., Arduini, J., Bonnaire, N., Cape, J. N., Colomb, A., Connolly, R., Diskova, J., Dumitrean, P., Ehlers, C., Gros, V., Hakola, H., Hill, M., Hopkins, J. R., Jäger, J., Junek, R., Kajos, M. K., Klemp, D., Leuchner, M., Lewis, A. C., Locoge, N., Maione, M., Martin, D., Michl, K., Nemitz, E., O'Doherty, S., Pérez Ballesta, P., Ruuskanen, T. M., Sauvage, S., Schmidbauer, N., Spain, T. G., Straube, E., Vana, M., Vollmer, M. K., Wegener, R., and Wenger, A.: ACTRIS non-methane hydrocarbon intercomparison experiment in Europe to support WMO-GAW and EMEP observation networks, Atmos. Meas. Tech. Discuss., 7, 10423-10485, 2014.

Hofzumahaus, A., Aschmutat, U., Brandenburger, U., Brauers, T., Dorn, H. P., Hausmann, M., Heßling, M., Holland, F., Plass-Dülmer, C., and Ehhalt, D. H.: Intercomparison of Tropospheric OH Measurements by Different Laser Techniques during the POPCORN Campaign 1994, J. Atmos. Chem., 31, 227-246, 1998.

Hofzumahaus, A., Rohrer, F., Lu, K., Bohn, B., Brauers, T., Chang, C.-C., Fuchs, H., Holland, F., Kita, K., Kondo, Y., Li, X., Lou, S., Shao, M., Zeng, L., Wahner, A., and Zhang, Y.: Amplified Trace Gas Removal in the Troposphere, Science, 324, 1702-1704, 2009.

Holland, F. and Hessling, M.: In situ measurement of tropospheric OH radicals by laser-induced fluorescence, Journal of the Atmospheric Sciences, 52, 3393, 1995.

Horie, O. and Moortgat, G. K.: Decomposition pathways of the excited Criegee intermediates in the ozonolysis of simple alkenes, Atmospheric Environment. Part A. General Topics, 25, 1881-1896, 1991.

Horie, O., Neeb, P., and Moortgat, G. K.: The reactions of the Criegee intermediate CH_3CHOO in the gas-phase ozonolysis of 2-butene isomers, Int J Chem Kinet, 29, 461-468, 1997.

Horie, O., Schäfer, C., and Moortgat, G. K.: High reactivity of hexafluoroacetone toward criegee intermediates in the gas-phase ozonolysis of simple alkenes, Int J Chem Kinet, 31, 261-269, 1999.

Hosaynali Beygi, Z., Fischer, H., Harder, H. D., Martinez, M., Sander, R., Williams, J., Brookes, D. M., Monks, P. S., and Lelieveld, J.: Oxidation photochemistry in the Southern Atlantic boundary layer: unexpected deviations of photochemical steady state, Atmos. Chem. Phys., 11, 8497-8513, 2011.

Jenkin, M. E., Saunders, S. M., and Pilling, M. J.: The tropospheric degradation of volatile organic compounds: a protocol for mechanism development, Atmos Environ, 31, 81-104, 1997.

Jiang, L., Xu, Y.-s., and Ding, A.-z.: Reaction of Stabilized Criegee Intermediates from Ozonolysis of Limonene with Sulfur Dioxide: Ab Initio and DFT Study, The Journal of Physical Chemistry A, 114, 12452-12461, 2010.

Johnson, D., Lewin, A. G., and Marston, G.: The Effect of Criegee-Intermediate Scavengers on the OH Yield from the Reaction of Ozone with 2-methylbut-2-ene, The Journal of Physical Chemistry A, 105, 2933-2935, 2001.

Johnson, D. and Marston, G.: The gas-phase ozonolysis of unsaturated volatile organic compounds in the troposphere, Chemical Society Reviews, 37, 699-716, 2008.

Junkermann, W., Platt, U., and Volz-Thomas, A.: A photoelectric detector for the measurement of photolysis frequencies of ozone and other atmospheric molecules, J. Atmos. Chem., 8, 203-227, 1989.

Junninen, H., Lauri, A., Keronen, P., Aalto, P., Hiltunen, V., Hari, P., and Kulmala, M.: Smart-SMEAR: on-line data exploration and visualization tool for SMEAR stations, Boreal Env. Res., 14, 447-457, 2009.

Kjaergaard, H. G., Kurten, T., Nielsen, L. B., Jorgensen, S., and Wennberg, P. O.: Criegee Intermediates React with Ozone, J. Phys. Chem. Lett., 4, 2525-2529, 2013.

Kroll, J. H., Donahue, N. M., Cee, V. J., Demerjian, K. L., and Anderson, J. G.: Gas-Phase Ozonolysis of Alkenes: Formation of OH from Anti Carbonyl Oxides, J Am Chem Soc, 124, 8518-8519, 2002.

Kroll, J. H., Sahay, S. R., Anderson, J. G., Demerjian, K. L., and Donahue, N. M.: Mechanism of HOx Formation in the Gas-Phase Ozone-Alkene Reaction. 2. Prompt versus Thermal Dissociation of Carbonyl Oxides to Form OH, The Journal of Physical Chemistry A, 105, 4446-4457, 2001.

Kubistin, D.: OH und HO_2 Radikale uber dem tropischen Regenwald, 2009. Physics, Johannes Gutenberg Univeristät, Germany, Mainz, 2009.

Kubistin, D., Harder, H., Martinez, M., Rudolf, M., Sander, R., Bozem, H., Eerdekens, G., Fischer, H., Gurk, C., Klupfel, T., Konigstedt, R., Parchatka, U., Schiller, C. L., Stickler, A., Taraborrelli, D., Williams, J., and Lelieveld, J.: Hydroxyl radicals in the tropical troposphere over the Suriname rainforest: comparison of measurements with the box model MECCA, Atmospheric Chemistry and Physics, 10, 9705-9728, 2010.

Kulmala, M., Arola, A., Nieminen, T., Riuttanen, L., Sogacheva, L., de Leeuw, G., Kerminen, V. M., and Lehtinen, K. E. J.: The first estimates of global nucleation mode aerosol concentrations based on satellite measurements, Atmospheric Chemistry and Physics, 11, 10791-10801, 2011.

Kurtén, T., Lane, J. R., Jørgensen, S., and Kjaergaard, H. G.: A Computational Study of the Oxidation of SO2 to SO3 by Gas-Phase Organic Oxidants, The Journal of Physical Chemistry A, 115, 8669-8681, 2011.

Kuwata, K. T., Hermes, M. R., Carlson, M. J., and Zogg, C. K.: Computational studies of the isomerization and hydration reactions of acetaldehyde oxide and methyl vinyl carbonyl oxide, J Phys Chem A, 114, 9192-9204, 2010.

Kuwata, K. T., Valin, L. C., and Converse, A. D.: Quantum Chemical and Master Equation Studies of the Methyl Vinyl Carbonyl Oxides Formed in Isoprene Ozonolysis, The Journal of Physical Chemistry A, 109, 10710-10725, 2005.

Lelieveld, J., Butler, T. M., Crowley, J. N., Dillon, T. J., Fischer, H., Ganzeveld, L., Harder, H., Lawrence, M. G., Martinez, M., Taraborrelli, D., and Williams, J.: Atmospheric oxidation capacity sustained by a tropical forest, Nature, 452, 737-740, 2008.

Levy, H.: Normal Atmosphere - Large radical and formaldehyde concentrations predicted, Science, 173, 141-&, 1971.

Levy, H.: Photochemistry of the Troposphere. In: Advances in Photochemistry, John Wiley & Sons, Inc., 1974.

Limón-Sánchez, M. T., Arriaga-Colina, J. L., Escalona-Segura, S., and Ruíz-Suárez, L. G.: Observations of formic and acetic acids at three sites of Mexico City, Sci. Total Environ., 287, 203-212, 2002.

Liu, F., Beames, J. M., Green, A. M., and Lester, M. I.: UV spectroscopic characterization of dimethyl- and ethyl-substituted carbonyl oxides, J Phys Chem A, 118, 2298-2306, 2014a.

Liu, Y., Bayes, K. D., and Sander, S. P.: Measuring rate constants for reactions of the simplest Criegee intermediate (CH_2OO) by monitoring the OH radical, J Phys Chem A, 118, 741-747, 2014b.

Lu, L., Beames, J. M., and Lester, M. I.: Early time detection of OH radical products from energized Criegee intermediates CH_2OO and CH_3CHOO, Chemical Physics Letters, 598, 23-27, 2014.

Mansergas, A. and Anglada, J. M.: Reaction Mechanism between Carbonyl Oxide and Hydroxyl Radical: A Theoretical Study, The Journal of Physical Chemistry A, 110, 4001-4011, 2006.

Mao, J., Ren, X., Zhang, L., Van Duin, D. M., Cohen, R. C., Park, J. H., Goldstein, A. H., Paulot, F., Beaver, M. R., Crounse, J. D., Wennberg, P. O., DiGangi, J. P., Henry, S. B., Keutsch, F. N., Park, C.,

Schade, G. W., Wolfe, G. M., Thornton, J. A., and Brune, W. H.: Insights into hydroxyl measurements and atmospheric oxidation in a California forest, Atmos. Chem. Phys., 12, 8009-8020, 2012.

Martinez, M., Harder, H., Kubistin, D., Rudolf, M., Bozem, H., Eerdekens, G., Fischer, H., Klupfel, T., Gurk, C., Konigstedt, R., Parchatka, U., Schiller, C. L., Stickler, A., Williams, J., and Lelieveld, J.: Hydroxyl radicals in the tropical troposphere over the Suriname rainforest: airborne measurements, Atmospheric Chemistry and Physics, 10, 3759-3773, 2010.

Martinez, M., Harder, H., Ren, X., Lesher, R. L., and Brune, W. H.: Measuring atmospheric naphthalene with laser-induced fluorescence, Atmos. Chem. Phys., 4, 563-569, 2004.

Mauldin III, R. L., Berndt, T., Sipila, M., Paasonen, P., Petaja, T., Kim, S., Kurten, T., Stratmann, F., Kerminen, V. M., and Kulmala, M.: A new atmospherically relevant oxidant of sulphur dioxide, Nature, 488, 193-196, 2012.

Nakajima, M. and Endo, Y.: Communication: spectroscopic characterization of an alkyl substituted Criegee intermediate syn-CH(3)CHOO through pure rotational transitions, J Chem Phys, 140, 011101, 2014.

Neeb, P. and Moortgat, G. K.: Formation of OH radicals in the gas-phase reaction of propene, isobutene, and isoprene with O_3: Yields and mechanistic implications, J Phys Chem A, 103, 9003-9012, 1999.

Nguyen, T. L., Peeters, J., and Vereecken, L.: Theoretical study of the gas-phase ozonolysis of beta-pinene (C(10)H(16)), Phys Chem Chem Phys, 11, 5643-5656, 2009a.

Nguyen, T. L., Winterhalter, R., Moortgat, G., Kanawati, B., Peeters, J., and Vereecken, L.: The gas-phase ozonolysis of [small beta]-caryophyllene (C15H24). Part II: A theoretical study, Phys Chem Chem Phys, 11, 4173-4183, 2009b.

Niki, H., Maker, P. D., Savage, C. M., and Breitenbach, L. P.: A FT IR study of a transitory product in the gas-phase ozone-ethylene reaction, The Journal of Physical Chemistry, 85, 1024-1027, 1981.

Nölscher, A. C., Williams, J., Sinha, V., Custer, T., Song, W., Johnson, A. M., Axinte, R., Bozem, H., Fischer, H., Pouvesle, N., Phillips, G., Crowley, J. N., Rantala, P., Rinne, J., Kulmala, M., Gonzales, D., Valverde-Canossa, J., Vogel, A., Hoffmann, T., Ouwersloot, H. G., Vilà-Guerau de Arellano, J., and Lelieveld, J.: Summertime total OH reactivity measurements from boreal forest during HUMPPA-COPEC 2010, Atmos. Chem. Phys., 12, 8257-8270, 2012.

Novelli, A., Hens, K., Tatum Ernest, C., Kubistin, D., Regelin, E., Elste, T., Plass-Dülmer, C., Martinez, M., Lelieveld, J., and Harder, H.: Characterisation of an inlet pre-injector laser-induced fluorescence instrument for the measurement of atmospheric hydroxyl radicals, Atmos. Meas. Tech., 7, 3413-3430, 2014a.

Novelli, A., Vereecken, L., Lelieveld, J., and Harder, H.: Direct observation of OH formation from stabilised Criegee intermediates, Phys Chem Chem Phys, 16, 19941-19951, 2014b.

Ouyang, B., McLeod, M. W., Jones, R. L., and Bloss, W. J.: NO_3 radical production from the reaction between the Criegee intermediate CH_2OO and NO_2, Phys Chem Chem Phys, 15, 17070-17075, 2013.

Paulson, S. E., Chung, M. Y., and Hasson, A. S.: OH Radical Formation from the Gas-Phase Reaction of Ozone with Terminal Alkenes and the Relationship between Structure and Mechanism, The Journal of Physical Chemistry A, 103, 8125-8138, 1999.

Peeters, J. and Müller, J.-F.: HO_x radical regeneration in isoprene oxidation via peroxy radical isomerisations. II: experimental evidence and global impact, Phys Chem Chem Phys, 12, 14227-14235, 2010.

Peeters, J., Müller, J.-F., Stavrakou, T., and Nguyen, V. S.: Hydroxyl Radical Recycling in Isoprene Oxidation Driven by Hydrogen Bonding and Hydrogen Tunneling: The Upgraded LIM1 Mechanism, The Journal of Physical Chemistry A, doi: 10.1021/jp5033146, 2014. 2014.

Peeters, J., Nguyen, T. L., and Vereecken, L.: HO_x radical regeneration in the oxidation of isoprene, Phys Chem Chem Phys, 11, 5935-5939, 2009.

Percival, C. J., Welz, O., Eskola, A. J., Savee, J. D., Osborn, D. L., Topping, D. O., Lowe, D., Utembe, S. R., Bacak, A., McFiggans, G., Cooke, M. C., Xiao, P., Archibald, A. T., Jenkin, M. E., Derwent, R. G., Riipinen, I., Mok, D. W., Lee, E. P., Dyke, J. M., Taatjes, C. A., and Shallcross, D. E.: Regional and global impacts of Criegee intermediates on atmospheric sulphuric acid concentrations and first steps of aerosol formation, Faraday Discuss, 165, 45-73, 2013.

Perner, D., Platt, U., Trainer, M., Hübler, G., Drummond, J., Junkermann, W., Rudolph, J., Schubert, B., Volz, A., Ehhalt, D. H., Rumpel, K. J., and Helas, G.: Measurements of tropospheric OH concentrations: A comparison of field data with model predictions, J. Atmos. Chem., 5, 185-216, 1987.

Petäjä, T., Mauldin, R. L., Kosciuch, E., McGrath, J., Nieminen, T., Paasonen, P., Boy, M., Adamov, A., Kotiaho, T., and Kulmala, M.: Sulfuric acid and OH concentrations in a boreal forest site, Atmospheric Chemistry and Physics, 9, 7435-7448, 2009.

Pierce, J. R., Evans, M. J., Scott, C. E., D'Andrea, S. D., Farmer, D. K., Swietlicki, E., and Spracklen, D. V.: Weak global sensitivity of cloud condensation nuclei and the aerosol indirect effect to Criegee + SO_2 chemistry, Atmos. Chem. Phys., 13, 3163-3176, 2013.

Plass-Dülmer, C., Michl, K., Ruf, R., and Berresheim, H.: C2–C8 Hydrocarbon measurement and quality control procedures at the Global Atmosphere Watch Observatory Hohenpeissenberg, Journal of Chromatography A, 953, 175-197, 2002.

Regelin, E., Harder, H., Martinez, M., Kubistin, D., Tatum Ernest, C., Bozem, H., Klippel, T., Hosaynali-Beygi, Z., Fischer, H., Sander, R., Jöckel, P., Königstedt, R., and Lelieveld, J.: HO_x measurements in the summertime upper troposphere over Europe: a comparison of observations to a box model and a 3-D model, Atmos. Chem. Phys., 13, 10703-10720, 2013.

Ren, X., Harder, H., Martinez, M., Faloona, I., Tan, D., Lesher, R., Di Carlo, P., Simpas, J., and Brune, W.: Interference Testing for Atmospheric HO_x Measurements by Laser-induced Fluorescence, J. Atmos. Chem., 47, 169-190, 2004.

Ren, X., Mao, J., Brune, W. H., Cantrell, C. A., Mauldin III, R. L., Hornbrook, R. S., Kosciuch, E., Olson, J. R., Crawford, J. H., Chen, G., and Singh, H. B.: Airborne intercomparison of HO_x measurements using

laser-induced fluorescence and chemical ionization mass spectrometry during ARCTAS, Atmos. Meas. Tech., 5, 2025-2037, 2012.

Ren, X., Olson, J. R., Crawford, J. H., Brune, W. H., Mao, J., Long, R. B., Chen, Z., Chen, G., Avery, M. A., Sachse, G. W., Barrick, J. D., Diskin, G. S., Huey, L. G., Fried, A., Cohen, R. C., Heikes, B., Wennberg, P. O., Singh, H. B., Blake, D. R., and Shetter, R. E.: HO_x chemistry during INTEX-A 2004: Observation, model calculation, and comparison with previous studies, Journal of Geophysical Research: Atmospheres, 113, D05310, 2008.

Rickard, A. R., Johnson, D., McGill, C. D., and Marston, G.: OH Yields in the Gas-Phase Reactions of Ozone with Alkenes, The Journal of Physical Chemistry A, 103, 7656-7664, 1999.

Rivera-Rios, J. C., Nguyen, T. B., Crounse, J. D., Jud, W., St. Clair, J. M., Mikoviny, T., Gilman, J. B., Lerner, B. M., Kaiser, J. B., de Gouw, J., Wisthaler, A., Hansel, A., Wennberg, P. O., Seinfeld, J. H., and Keutsch, F. N.: Conversion of hydroperoxides to carbonyls in field and laboratory instrumentation: observational bias in diagnosing pristine versus anthropogenically-controlled atmospheric chemistry, Geophys Res Lett, doi: 10.1002/2014gl061919, 2014. 2014GL061919, 2014.

Ryzhkov, A. B. and Ariya, P. A.: The importance of water clusters (H2O), (n=2,...,4) in the reaction of Criegee intermediate with water in the atmosphere, Chemical Physics Letters, 419, 479-485, 2006.

Ryzhkov, A. B. and Ariya, P. A.: A theoretical study of the reactions of carbonyl oxide with water in atmosphere: the role of water dimer, Chemical Physics Letters, 367, 423-429, 2003.

Ryzhkov, A. B. and Ariya, P. A.: A theoretical study of the reactions of parent and substituted Criegee intermediates with water and the water dimer, Phys Chem Chem Phys, 6, 5042-5050, 2004.

Sander, S. P., Abbatt, J., Barker, J. R., Burkholder, J. B., Friedl, R. R., Golden, D. M., Huie, R. E., Kolb, C. E., Kurylo, M. J., Moortgat, G. K., Orkin, V. L., and Wine, P. H.: Chemical Kinetics and Photochemical Data for Use in Atmospheric Studies, Evaluation No. 17, JPL Publication 10-6 Jet Propulsion Laboratory Pasadena, California, 2011, 2011.

Sarwar, G., Fahey, K., Kwok, R., Gilliam, R. C., Roselle, S. J., Mathur, R., Xue, J., Yu, J., and Carter, W. P. L.: Potential impacts of two SO_2 oxidation pathways on regional sulfate concentrations: Aqueous-phase oxidation by NO_2 and gas-phase oxidation by Stabilized Criegee Intermediates, Atmos Environ, 68, 186-197, 2013.

Sarwar, G., Simon, H., Fahey, K., Mathur, R., Goliff, W. S., and Stockwell, W. R.: Impact of sulfur dioxide oxidation by Stabilized Criegee Intermediate on sulfate, Atmos Environ, 85, 204-214, 2014.

Saunders, S. M., Jenkin, M. E., Derwent, R. G., and Pilling, M. J.: Protocol for the development of the Master Chemical Mechanism, MCM v3 (Part A): tropospheric degradation of non-aromatic volatile organic compounds, Atmos. Chem. Phys., 3, 161-180, 2003.

Schlosser, E., Bohn, B., Brauers, T., Dorn, H.-P., Fuchs, H., Häseler, R., Hofzumahaus, A., Holland, F., Rohrer, F., Rupp, L., Siese, M., Tillmann, R., and Wahner, A.: Intercomparison of Two Hydroxyl Radical Measurement Techniques at the Atmosphere Simulation Chamber SAPHIR, J. Atmos. Chem., 56, 187-205, 2007.

Schlosser, E., Brauers, T., Dorn, H. P., Fuchs, H., Häseler, R., Hofzumahaus, A., Holland, F., Wahner, A., Kanaya, Y., Kajii, Y., Miyamoto, K., Nishida, S., Watanabe, K., Yoshino, A., Kubistin, D., Martinez, M., Rudolf, M., Harder, H., Berresheim, H., Elste, T., Plass-Dülmer, C., Stange, G., and Schurath, U.: Technical Note: Formal blind intercomparison of OH measurements: results from the international campaign HOxComp, Atmos. Chem. Phys., 9, 7923-7948, 2009.

Seinfeld, J. H. and Pandis, S. N.: Atmospheric Chemistry and Physics - From Air Pollution to Climate Change (2nd Edition), John Wiley and Sons, 2006. 2006.

Shallcross, D. E., Taatjes, C. A., and Percival, C. J.: Criegee intermediates in the indoor environment: new insights, Indoor Air, doi: 10.1111/ina.12102, 2014. n/a-n/a, 2014.

Sheps, L., Scully, A. M., and Au, K.: UV absorption probing of the conformer-dependent reactivity of a Criegee intermediate CH_3CHOO, Phys Chem Chem Phys, doi: 10.1039/c4cp04408h, 2014. 2014.

Shirley, T. R., Brune, W. H., Ren, X., Mao, J., Lesher, R., Cardenas, B., Volkamer, R., Molina, L. T., Molina, M. J., Lamb, B., Velasco, E., Jobson, T., and Alexander, M.: Atmospheric oxidation in the Mexico City Metropolitan Area (MCMA) during April 2003, Atmos. Chem. Phys., 6, 2753-2765, 2006.

Sinha, V., Williams, J., Crowley, J. N., and Lelieveld, J.: The Comparative Reactivity Method – a new tool to measure total OH Reactivity in ambient air, Atmos. Chem. Phys., 8, 2213-2227, 2008.

Sinha, V., Williams, J., Diesch, J. M., Drewnick, F., Martinez, M., Harder, H., Regelin, E., Kubistin, D., Bozem, H., Hosaynali-Beygi, Z., Fischer, H., Andrés-Hernández, M. D., Kartal, D., Adame, J. A., and Lelieveld, J.: OH reactivity measurements in a coastal location in Southwestern Spain during DOMINO, Atmos. Chem. Phys. Discuss., 12, 4979-5014, 2012.

Song, W., Williams, J., Yassaa, N., Martinez, M., Carnero, J., Hidalgo, P., Bozem, H., and Lelieveld, J.: Winter and summer characterization of biogenic enantiomeric monoterpenes and anthropogenic BTEX compounds at a Mediterranean Stone Pine forest site, J. Atmos. Chem., 68, 233-250, 2011.

Stone, D., Blitz, M., Daubney, L., Howes, N. U., and Seakins, P.: Kinetics of CH_2OO reactions with SO_2, NO_2, NO, H_2O and CH_3CHO as a function of pressure, Phys Chem Chem Phys, 16, 1139-1149, 2014.

Stone, D., Whalley, L. K., and Heard, D. E.: Tropospheric OH and HO_2 radicals: field measurements and model comparisons, Chemical Society Reviews, 41, 6348-6404, 2012.

Su, Y. T., Lin, H. Y., Putikam, R., Matsui, H., Lin, M. C., and Lee, Y. P.: Extremely rapid self-reaction of the simplest Criegee intermediate CH_2OO and its implications in atmospheric chemistry, Nat Chem, 6, 477-483, 2014.

Taatjes, C. A., Shallcross, D. E., and Percival, C. J.: Research frontiers in the chemistry of Criegee intermediates and tropospheric ozonolysis, Phys Chem Chem Phys, 16, 1704-1718, 2014.

Taatjes, C. A., Welz, O., Eskola, A. J., Savee, J. D., Osborn, D. L., Lee, E. P. F., Dyke, J. M., Mok, D. W. K., Shallcross, D. E., and Percival, C. J.: Direct measurement of Criegee intermediate (CH2OO) reactions with acetone, acetaldehyde, and hexafluoroacetone, Phys Chem Chem Phys, 14, 10391-10400, 2012.

Taatjes, C. A., Welz, O., Eskola, A. J., Savee, J. D., Scheer, A. M., Shallcross, D. E., Rotavera, B., Lee, E. P., Dyke, J. M., Mok, D. K., Osborn, D. L., and Percival, C. J.: Direct measurements of conformer-dependent reactivity of the Criegee intermediate CH_3CHOO, Science, 340, 177-180, 2013.

Taraborrelli, D., Lawrence, M. G., Crowley, J. N., Dillon, T. J., Gromov, S., Groß, C. B. M., Vereecken, L., and Lelieveld, J.: Hydroxyl radical buffered by isoprene oxidation over tropical forests, Nature Geosci, 5, 190-193, 2012.

Tobias, H. J. and Ziemann, P. J.: Kinetics of the Gas-Phase Reactions of Alcohols, Aldehydes, Carboxylic Acids, and Water with the C13 Stabilized Criegee Intermediate Formed from Ozonolysis of 1-Tetradecene, The Journal of Physical Chemistry A, 105, 6129-6135, 2001.

Vereecken, L. and Francisco, J. S.: Theoretical studies of atmospheric reaction mechanisms in the troposphere, Chemical Society Reviews, 41, 6259-6293, 2012.

Vereecken, L., Harder, H., and Novelli, A.: The reaction of Criegee intermediates with NO, RO_2, and SO_2, and their fate in the atmosphere, Phys Chem Chem Phys, 14, 14682-14695, 2012.

Vereecken, L., Harder, H., and Novelli, A.: The reactions of Criegee intermediates with alkenes, ozone, and carbonyl oxides, Phys Chem Chem Phys, 16, 4039-4049, 2014a.

Vereecken, L., Harder, H., and Novelli, A.: Reactions of stabilized Criegee Intermediates, Geophysical Research Abstracts 16, EGU2014-3788, 2014b.

Wayne, R. P.: Chemistry of Atmosphere, Oxford University Press: Oxford, 2000. 2000.

Welz, O., Eskola, A. J., Sheps, L., Rotavera, B., Savee, J. D., Scheer, A. M., Osborn, D. L., Lowe, D., Murray Booth, A., Xiao, P., Anwar H. Khan, M., Percival, C. J., Shallcross, D. E., and Taatjes, C. A.: Rate Coefficients of C1 and C2 Criegee Intermediate Reactions with Formic and Acetic Acid Near the Collision Limit: Direct Kinetics Measurements and Atmospheric Implications, Angewandte Chemie, 126, 4635-4638, 2014.

Welz, O., Savee, J. D., Osborn, D. L., Vasu, S. S., Percival, C. J., Shallcross, D. E., and Taatjes, C. A.: Direct Kinetic Measurements of Criegee Intermediate (CH_2OO) Formed by Reaction of CH_2I with O_2, Science, 335, 204-207, 2012.

Wennberg, P. O., Cohen, R. C., Hazen, N. L., Lapson, L. B., Allen, N. T., Hanisco, T. F., Oliver, J. F., Lanham, N. W., Demusz, J. N., and Anderson, J. G.: Aircraft-borne, laser-induced fluorescence instrument for the in situ detection of hydroxyl and hydroperoxyl radicals, Review of Scientific Instruments, 65, 1858-1876, 1994.

Whalley, L. K., Edwards, P. M., Furneaux, K. L., Goddard, A., Ingham, T., Evans, M. J., Stone, D., Hopkins, J. R., Jones, C. E., Karunaharan, A., Lee, J. D., Lewis, A. C., Monks, P. S., Moller, S. J., and Heard, D. E.: Quantifying the magnitude of a missing hydroxyl radical source in a tropical rainforest, Atmospheric Chemistry and Physics, 11, 7223-7233, 2011.

White, J. U.: Long optical paths of large aperture, J. Opt. Soc. Am., 32, 285-288, 1942.

Williams, J., Crowley, J., Fischer, H., Harder, H., Martinez, M., Petäjä, T., Rinne, J., Bäck, J., Boy, M., Dal Maso, M., Hakala, J., Kajos, M., Keronen, P., Rantala, P., Aalto, J., Aaltonen, H., Paatero, J., Vesala, T., Hakola, H., Levula, J., Pohja, T., Herrmann, F., Auld, J., Mesarchaki, E., Song, W., Yassaa, N., Nölscher, A., Johnson, A. M., Custer, T., Sinha, V., Thieser, J., Pouvesle, N., Taraborrelli, D., Tang, M. J., Bozem, H., Hosaynali-Beygi, Z., Axinte, R., Oswald, R., Novelli, A., Kubistin, D., Hens, K., Javed, U., Trawny, K., Breitenberger, C., Hidalgo, P. J., Ebben, C. J., Geiger, F. M., Corrigan, A. L., Russell, L. M., Ouwersloot, H. G., Vilà-Guerau de Arellano, J., Ganzeveld, L., Vogel, A., Beck, M., Bayerle, A., Kampf, C. J., Bertelmann, M., Köllner, F., Hoffmann, T., Valverde, J., González, D., Riekkola, M. L., Kulmala, M., and Lelieveld, J.: The summertime Boreal forest field measurement intensive (HUMPPA-COPEC-2010): an overview of meteorological and chemical influences, Atmos. Chem. Phys., 11, 10599-10618, 2011.

Wood, E. C., Herndon, S. C., Onasch, T. B., Kroll, J. H., Canagaratna, M. R., Kolb, C. E., Worsnop, D. R., Neuman, J. A., Seila, R., Zavala, M., and Knighton, W. B.: A case study of ozone production, nitrogen oxides, and the radical budget in Mexico City, Atmos. Chem. Phys., 9, 2499-2516, 2009.

Yassaa, N., Song, W., Lelieveld, J., Vanhatalo, A., Back, J., and Williams, J.: Diel cycles of isoprenoids in the emissions of Norway spruce, four Scots pine chemotypes, and in Boreal forest ambient air during HUMPPA-COPEC-2010, Atmospheric Chemistry and Physics, 12, 7215-7229, 2012.

York, D., Evensen, N. M., Martínez, M. L., and De Basabe Delgado, J.: Unified equations for the slope, intercept, and standard errors of the best straight line, American Journal of Physics, 72, 367-375, 2004.

Zhang, D. and Zhang, R.: Mechanism of OH Formation from Ozonolysis of Isoprene: A Quantum - Chemical Study, J Am Chem Soc, 124, 2692-2703, 2002.

Anna Novelli

Education and Research Experience

2015 **PhD**
Measurements of Criegee Intermediates by LIF-FAGE
University of Mainz and Max Planck Institute for Chemistry, Mainz
Atmospheric Chemistry Department
Radical measurements group
Field measurements and laboratory investigations of stabilised Criegee intermediates chemistry and their role as atmospheric oxidants

2009 **Master of Environmental Chemistry and Chemistry of Cultural Heritage**
University of Turin, Faculty of Mathematics, Physics and Natural Sciences
Thesis: The role of photosensitisers in the transformation of organic contaminants in marine water.

2007 **Bachelor of Chemistry**
University of Turin, Faculty of Mathematics, Physics and Natural Sciences
Thesis: A new tetradentate ligand for the synthesis of ruthenium complexes.

2006 **Research internship in analytical chemistry**
Experimental Zooprophylactic Institute of Piemonte

Publications

A comparison of HONO budgets for two measurement heights at a field station within the boreal forest in Finland
R. Oswald, M. Ermel, K. Hens, A. Novelli, H.G. Ouwersloot, P. Paasonen, T. Petäjä, M. Sipilä, P. Keronen, J. Bäck, R. Königstedt, Y. Hosaznali Beygi, H. Fischer, B. Bohn, D. Kubistin, H. Harder, M. Martinez, J. Williams, T. Hoffmann, I. Trebs and M. Sörgel.
Atmos. Chem. Phys., 15, 799-813, DOI: 10.5194/acp-15-799-2015, 2015.

Characterization of an inlet pre-injector laser induced fluorescence instrument for the measurement of ambient hydroxyl radical.
A. Novelli, K. Hens, C. Tatum Ernest, T. Elste, C. Plass-Duelmer, M. Martinez, J. Lelieveld and H. Harder.
Atmos. Meas. Tech., 7, 3413-3430, DOI:10.5194/amt-7-3413-2014, 2014.

Observation and modelling of HO_x radicals in a boreal forest.
K. Hens, A. Novelli, M. Martinez, J. Auld, R. Axinte, B. Bohn, H. Fischer, P. Keronen, D. Kubistin, A. C. Nölscher, R. Oswald, P. Paasonen, T. Petäjä, E. Regelin, R. Sander, V. Sinha, M. Sipilä, D. Taraborrelli, C. Tatum Ernest, J. Williams, J. Lelieveld, and H. Harder.
Atmos. Chem. Phys., 14, 8723-8747, DOI:10.5194/acp-14-8723-2014, 2014.

Direct observation of OH formation from stabilised Criegee intermediates.
A. Novelli, L. Vereecken, J. Lelieveld, H. Harder.
Phys Chem Chem Phys, 16 (37), 19941 – 19951, DOI: 10.1039/c4cp02719a, 2014.

The reactions of Criegee intermediates with alkenes, ozone, and carbonyl oxides.
L. Vereecken, H. Harder and A. Novelli.
Phys. Chem. Chem. Phys., 16, 4039-4049, DOI: 10.1039/C3CP54514H, 2014.

The role of nitrite and nitrate ions as photosensitizers in the phototransformation of phenolic compounds in seawater.
P. Calza, D. Vione, A. Novelli, E. Pellizzetti, C. Minero.
Sci. Total Environ., 439, 67-75, DOI: 10.1016/j.scitotenv.2012.09.009, 2012.

The reaction of Criegee intermediates with NO, RO_2, and SO_2, and their fate in the atmosphere.
L. Vereecken, H. Harder and A. Novelli.
Phys. Chem. Chem. Phys., 14, 14682-14695, DOI: 10.1039/C2CP42300F, 2012.

The summertime Boreal forest field measurement intensive (HUMPPA-COPEC-2010): an overview of meteorological and chemical influences.
J.Williams, J. Crowley, H. Fischer, H. Harder, M. Martinez, T. Petäjä, J. Rinne, J. Bäck, M. Boy,M. Dal Maso, J. Hakala, M. Kajos, P. Keronen, P. Rantala, J. Aalto, H. Aaltonen, J. Paatero, T. Vesala, H. Hakola, J. Levula, T. Pohja, F. Herrmann, J. Auld, E. Mesarchaki, W. Song, N. Yassaa, A. Nölscher, A. M. Johnson, T. Custer, V. Sinha, J. Thieser, N. Pouvesle, D. Taraborrelli, M. J. Tang, H. Bozem, Z. Hosaynali-Beygi, R. Axinte, R. Oswald, A. Novelli, D. Kubistin, K. Hens, U. Javed, K. Trawny, C. Breitenberger, P. J. Hidalgo, C. J. Ebben, F. M. Geiger, A. L. Corrigan, L. M. Russell, H. G. Ouwersloot, J. Vilà-Guerau de Arellano, L. Ganzeveld, A. Vogel, M. Beck, A. Bayerle, C. J. Kampf, M. Bertelmann, F. Köllner, T. Hoffmann, J. Valverde, D. Gonzàlez, M.-L. Riekkola, M. Kulmala and J. Lelieveld.
Atmos. Chem. Phys., 11, 10599-10618, DOI:10.5194/acp-11-10599-2011, 2011.

Conference Abstracts

Direct observation of OH formation from stabilised Criegee intermediates
A. Novelli, L. Vereecken, J. Lelieveld, H. Harder.
Atmospheric Chemical Mechanisms Conference, UC Davis, CA, USA, December 10-12, 20124. (Poster)

OH, recycling and reactivity in a boreal forest during HUMPPA.
A. Novelli, K. Hens, C. Tatum Ernest, P. Paasonen, M. Sipilä, T. Petäjä, A. Nölscher, P. Keronen, K. Trawny, D. Kubistin, R. Oswald, R. Axinte, Z. Hosaynali Beygi, J. Auld, T. Klüpfel, E. Mesarchaki, W. Song, J. Valverde Canossa, D. González Orozco, B. Bohn, D. Taraborrelli, R. Sander, H. Fischer, J. Williams, J. Crowley, M. Martinez, H. Harder.
OH Reactivity Specialists Uniting Meeting (ORSUM), Mainz, Germany, 13 -15 October 2014. (Oral presentation)

Direct observation of OH formation from stabilised Criegee intermediates.
A. Novelli, K. Hens, C. Tatum Ernest, P. Paasonen, M. Sipilä, T. Petäjä, P. Keronen, J. Lelieveld, L. Vereecken, M. Martinez, H. Harder.
OH Reactivity Specialists Uniting Meeting (ORSUM), Mainz, Germany, 13-15 October 2014. (Poster)

Reactions of Stabilized Criegee intermediates
L. Vereecken, H. Harder, A. Novelli.
European Geosciences Union General Assembly, Vienna, Austria, April 27-May 2 2014 (Poster). Geophysical Research Abstracts Vol. 16, EGU2014-3788, 2014.

Reactions of Stabilized Criegee intermediates
L. Vereecken, H. Harder, A. Novelli.
European Geosciences Union General Assembly, Vienna, Austria, April 07-12 2013 (Poster). Geophysical Research Abstracts Vol. 15, EGU2013-11234.

Assessment of the Role of Stabilized Criegee Intermediates in OH Radical Measurements by LIF
A. Novelli, K. Hens, C. Tatum Ernest, K. Trawny, M. Rudolf, D. Kubistin, Z. Hosaynali Beygi, H. Fischer, J. Williams, P. Paasonen, M. Sipilä, P. Keronen, T. Petäjä, T. Elste, C. Plass-Duelmer, L. Vereecken, M. Martinez, J. Lelieveld and H. Harder.
TOXCA Meeting, Bremen, Germany, 16-18 January 2013. (Oral presentation)

Assessment of the Role of Stabilized Criegee Intermediates in OH Radical Measurements by LIF
A. Novelli, K. Hens, C. Tatum Ernest, K. Trawny, M. Rudolf, D. Kubistin, Z. Hosaynali Beygi, H. Fischer, J. Williams, P. Paasonen, M. Sipilä, P. Keronen, T. Petäjä, T. Elste, C. Plass-Duelmer, L. Vereecken, M. Martinez, J. Lelieveld and H. Harder.
Atmospheric Chemical Mechanisms Conference, UC Davis, CA, USA, December 10-13, 2012. (Oral presentation)

OH and HO_2 Measurements in a Rural Mid-Latitude Environment during HOPE2012
C.Tatum Ernest, A. Novelli, K. Hens, K. Trawny, M. Rudolf, T. Elste, A. Werner, J. Englert, S. Gilge, C. Plass-Dülmer, J. Lelieveld, M. Martinez and H. Harder.
Atmospheric Chemical Mechanisms Conference, UC Davis, CA, USA, December 10-13, 2012. (Oral presentation)

The role of stabilised Criegee intermediate in gas phase H_2SO_4 formation
A. Novelli, K. Hens, C. Tatum Ernest, K. Trawny, M. Rudolf, D. Kubistin, Z. Hosaynali

Beygi, H. Fischer, J. Williams, P. Paasonen, M. Sipilä, P. Keronen, T. Petäjä, T. Elste, C. Plass-Duelmer, L. Vereecken, M. Martinez, J. Lelieveld and H. Harder.
Abstract A24D-04 presented at 2012 Fall Meeting, AGU, San Francisco, Calif., 3-7 Dec. (Oral presentation)

Hydroxyl radical measurements and oxidation capacity in a boreal forest environment
K. Hens, C. Tatum Ernest, A. Novelli, P. Paasonen, M. Sipilä, T. Petäjä, A. Nölscher, P. Keronen, K. Trawny, D. Kubistin, R. Oswald, R. Axinte, Z. Hosaynali Beygi, J. Auld, T. Klüpfel, E. Mesarchaki, W. Song, J. Valverde Canossa, D. González Orozco, R. Königstedt, B. Bohn, M. Rudolf, H. Fischer, J. Williams, J. Crowley , M. Martinez and H. Harder.
Abstract 33K-0299 presented at 2012 Fall Meeting, AGU, San Francisco, Calif., 3-7 Dec. (Poster)

Hydroxyl radical measurements in a boreal forest during HUMPPA-COPEC 2010
K. Hens, A. Novelli, P. Paasonen, M. Sipilä, T. Petäjä, A. Nölscher, P. Keronen, K. Trawny, D. Kubistin, R. Oswald, R. Axinte, Z. Hosaynali Beygi, J. Auld, T. Klüpfel, E. Mesarchaki, W. Song, J. Valverde Canossa, D. González Orozco, R. Königstedt, B. Bohn, D. Taraborrelli, R. Sander, M. Rudolf, H. Fischer, J. Williams, J. Crowley, M. Martinez and H. Harder.
European Geosciences Union General Assembly, Vienna, Austria, April 22-27 2012 (Oral presentation). Geophysical Research Abstracts Vol. 14, EGU2012-9051.

Assessment of the role of stabilized Criegee Intermediates in OH radical measurements by LIF
A. Novelli, K. Hens, P. Paasonen, M. Sipilä, T. Petäjä, P. Keronen, J. Auld, Z. H. Beygi, R. Axinte, K. Trawny, D. Kubistin, C. Ernest, M. Rudolf, J. Antonio Adame, H. Fischer, J. Williams, L. Veerecken, M. Martinez and H. Harder.
8 **European Geosciences Union General Assembly, Vienna, Austria, April 22-27 2012 (Poster).** Geophysical Research Abstracts Vol. 14, EGU2012-9491.

Fieldwork
Field setup, operation and maintenance of the inlet pre injector-LIF FAGE instrument for the measurement of HO_x radicals and stabilised Criegee intermediates during:
- HUMPPA-COPEC 2010 (Boreal forest, Finland)
- DOMINO HOx 2010 (Mediterranean forest, Spain)
- PARADE 2011 (Mixed forest, Germany)
- HOPE 2012 (Mixed forest, Germany)
- CYPHEX 2014 (Mediterranean Boundary layer, Cyprus)

I hereby declare that I wrote the dissertation submitted without any unauthorized external assistance and used only sources acknowledged in the work. All textual passages which are appropriated verbatim or paraphrased from published and unpublished texts as well as all information obtained from oral sources are duly indicated and listed in accordance with bibliographical rules. In carrying out this research, I complied with the rules of standard scientific practice as formulated in the statutes of Johannes Gutenberg-University Mainz to insure standard scientific practice.

Mainz, 11 January 2015